The Role of Stress Fluctuations in Seismogenic Processes:

Fluid injection-induced earthquakes and scale invariance

Dissertation
zur Erlangung des akademischen Grades

Doktor der Naturwissenschaften

am Fachbereich Geowissenschaften
der Freien Universität Berlin

vorgelegt von
Cornelius Langenbruch
April 2014

Ich erkläre hiermit an Eides statt, dass ich die vorliegende Dissertation selbstständig und nur unter Verwendung der angegebenen Quellen und Hilfsmittel angefertigt habe.

Berlin, den 25.04.2014

Referent: Prof. Dr. Serge A. Shapiro
Korreferent: Prof. Dr. Frederik Tilmann

Datum der Disputation: 12. Juni 2014

Summary

Ongoing seismogenic processes in the brittle Earth's crust are substantially driven by different aspects of stress. Thus, characterizing the role of stress during nucleation and rupturing of earthquakes is a crucial factor for understanding the physics of earthquakes. In this thesis I investigate the role of stress fluctuations in seismogenic processes. In particular, I draw inferences from the concept of scale invariance and the analysis of seismicity, induced by the injection of pressurized fluids through boreholes. This hydraulic reservoir stimulation is among others performed in order to develop enhanced geothermal systems (EGS) for sustainable power generation. The investigation of fluid-induced earthquakes is of particular importance because the basic conditions during earthquake nucleation and rupturing at fluid injection sites can be better constrained than for earthquakes on tectonic scale. Observed scale invariance of the physics of earthquakes suggests transferability of results obtained at different scales.

I quantify the perturbation of stress caused by the injection of pressurized fluids. This is done under the assumption that pore pressure diffusion in the fluid saturated pore and fracture space of rocks is the governing triggering mechanism of fluid injection-induced earthquakes. Moreover, the importance of stress changes generated by the occurrence of fluid-induced earthquakes is evaluated by analyzing the waiting times between subsequent seismic events. I show that no signatures of aftershock triggering can be identified in six analyzed seismicity catalogs gathered at EGS sites. Based on this result I demonstrate that the Poisson model can be used to compute the occurrence probability of fluid injection-induced earthquakes. This statistical model is needed in order to assess and mitigate the seismic risk, which still acts as an obstacle for efficient and risk-free use of the geothermal potential of the subsurface for sustainable power generation. The finding that stress changes caused by preceding events are only of second order importance for the seismogenesis of fluid-induced earthquakes underlines the significance of studies assuming pore pressure diffusion to be the triggering mechanism of seismic events. Based on this assumption and the consideration of a nearly critical state of stress in the Earth's crust, a physically based statistical model describing the seismicity rate of fluid-induced earthquakes during and after injection of fluids is presented. The investigation of seismicity occurring after termination of reservoir stimulation is of particular importance as the physical processes leading to the triggering of post-injection seismic events have not yet been fully understood. In addition, it has been observed that the strongest seismic events tend to occur close before or after the termination of reservoir stimulation. I show that the decay rate of seismicity after reservoir

stimulation can be approximated by a modification of Omori's law, describing the decay of aftershock activity succeeding tectonic main shocks. Moreover, I demonstrate that in the case of fluid injection-induced seismicity the power law exponent of Omori's law depends on the criticality of stress in rocks.

Furthermore, I investigate the impact of elastic rock heterogeneity on the distribution of stress in the brittle Earth's crust. The results provide fundamental insights into the nature of seismogenic processes. My findings suggest that the scale invariance of earthquakes originates from scale-invariant fluctuations of stress in rocks. These fluctuations occur naturally because of the universal fractal nature of elastic rock heterogeneity in the Earth's crust. Scientific evidence for the universal fractal nature of elastic rock heterogeneity is given by measurements along boreholes at various drilling sites in different regions. As a consequence, fault planes and correspondingly magnitudes of earthquakes scale according to a universal power law. This explains the emergence of the Gutenberg-Richter relation characterized by a universal b-value of $b = 1$ and implies the scale invariance of the magnitude scaling of earthquakes. My findings suggest that the observed stress dependency of the two fundamental power laws of statistical seismology occurs due to characteristic scales of seismogenic processes. Each characteristic scale involved in a process causes a limitation or change of fractal scaling. Moreover, the heterogeneous nature of critical stress changes in rocks, observed in various studies, can be physically explained by the influence of elastic rock heterogeneity. I show that stress changes in the range of 10^3 to 10^7 Pa are capable of triggering brittle failure and associated seismicity in rocks of the Earth's crust. This result validates the concept of a nearly critical state of stress in the Earth's crust and suggests that already stress changes just above perturbations caused by tidal forces ($\approx 10^3 Pa$) are sufficient to trigger rupturing in the most critically stressed parts of rocks.

Zusammenfassung

Seismogene Prozesse in der spröden Erdkruste werden maßgeblich durch verschiedene Aspekte von Spannung gelenkt. Deshalb ist es entscheidend, die Bedeutung von Spannungen für die Entstehung und das Auftreten von Erdbeben zu bestimmen. In dieser Arbeit untersuche ich die Rolle von Spannungsfluktuationen in seismogenen Prozessen. Im Besonderen ziehe ich Rückschlüsse aus dem Konzept der Skaleninvarianz und der Analyse fluid-induzierter Erdbeben, die durch das Einpressen unter Druck gesetzter Fluide in Bohrlöcher ausgelöst werden. Diese Methode der hydraulischen Reservoirstimulation wird unter anderem zur Entwicklung sogenannter Enhanced Geothermal Systems (EGS) im kristallinen Grundgebirge für eine nachhaltige Stromerzeugung durchgeführt. Die Untersuchung fluid-induzierter seismischer Ereignisse ist von besonderer Bedeutung, weil die grundlegenden Rahmenbedingungen während der Bildung und dem Auftreten der seismischen Ereignisse besser zugänglich sind als für Erdbeben auf tektonischer Größenordnung. Die beobachtete Skaleninvarianz der Physik der Erdbeben weist auf eine Übertragbarkeit der Ergebnisse hin, die auf einer anderen Größenskala erlangt wurden.

Ich quantifiziere die Störung des Spannungszustandes, der durch das Einpressen von Fluiden während hydraulischen Reservoir Stimulationen hervorgerufen wird. Hierbei wird angenommen, dass die seismischen Ereignisse durch Porendruckdiffusion im Poren- und Kluftraum von Gesteinen ausgelöst werden. Des Weiteren wird die Bedeutung von Spannungsänderungen, welche durch das Auftreten fluid-induzierter seismischer Ereignisse bedingt sind, anhand einer Analyse der Wartezeiten zwischen aufeinander folgenden Ereignissen ausgewertet. Meine Ergebnisse zeigen, dass innerhalb sechs betrachteter Kataloge fluid-induzierter Seismizität an EGS Standorten, keine Nachbebensignaturen identifizierbar sind. Basierend auf diesem Ergebnis zeige ich, dass das Poisson Model zur Berechnung der Auftrittswahrscheinlichkeit fluid-induzierter Erdbeben herangezogen werden kann. Die Entwicklung dieses statistischen Models ist von großer Bedeutung, weil das seismische Risiko immer noch ein Hindernis für eine effiziente und risikofreie Nutzung des geothermischen Potenzials des Untergrundes für die nachhaltige Stromerzeugung darstellt. Die Erkenntnis, dass Spannungsänderungen, die durch das Auftreten vorangegangener seismischer Ereignisse entstehen, im Vergleich zu Spannungsänderungen, welche direkt durch das Einpressen von Fluid verursacht sind, für die Seismogenese fluid-induzierter Erdbeben von vernachlässigbarer Bedeutung sind unterstreicht die Aussagekraft der Studien, die Porendruckdiffusion als den auslösenden Prozess seismischer

Ereignisse betrachten. Unter genau dieser Annahme und dem Gesichtspunkt eines nahe kritischen Spannungszustands in der Erdkruste entwickle ich ein physikalisch basiertes statistisches Model zur Bestimmung der Seismizitätsrate während und nach hydraulischen Reservoirstimulationen. Die Untersuchung von nach Stimulationsabschluss auftretender fluid-induzierter Seismizität ist von besonderer Bedeutung da das Verständnis der physikalischen Prozesse, die zum Auftreten der Seismizität nach Abschluss von Fuidverpressungen führen, noch nicht vollständig ist. Außerdem wurde beobachtet, dass die stärksten seismischen Ereignisse häufig kurz vor oder nach dem Abschluss der Reservoirstimulation auftreten. Ich zeige, dass die Abklingrate fluid-induzierter Erdbeben nach dem Abschluss von Reservoirstimulationen näherungsweise durch eine Modifikation des Omori Gesetzes bestimmt werden kann. Das Omori Gesetz beschreibt ursprünglich das zeitliche Abklingen der Nachbebenaktivität nach tektonischen Erdbeben. Meine Untersuchungen zeigen, dass der Potenzgesetz Exponent des Omori Gesetzes im Falle fluid-induzierter Seismizität vom Spannungszustand im Reservoirgestein abhängt.

Ich bestimme den Einfluss elastischer Gesteinsheterogenität auf die Spannungsverteilung in Gesteinen der spröden Erdkruste. Die Ergebnisse meiner Studie geben einen grundlegenden Einblick in die Beschaffenheit seismogener Prozesse. Meine Resultate weisen darauf hin, dass die beobachtete Skaleninvarianz von Erbeben seine Ursache in skaleninvarianten Spannungsfluktuationen in Gesteinen hat. Diese Spannungsfluktuationen treten von Natur aus aufgrund der universalen fraktalen Beschaffenheit elastischer Geteinsheterogenität auf. Wissenschaftliche Nachweise für die universale fraktale Natur elastischer Gesteinsheterogenität sind durch Bohrlochmessungen an verschiedenen Bohrplätzen in unterschiedlichen Regionen gegeben. Die Universalität der natürlich entstehenden Spannungsfluktutionen in der Erdkruste hat zur Folge, dass die Bruchflächen und dementsprechend die Magnituden auftretender Erdbeben entsprechend eines universalen Potenzgesetzes skalieren. Diese Gegebenheit gibt eine physikalische Erklärung für das Entstehen des Gutenberg-Richter Gesetzes mit einem universalen b-Wert von $b = 1$ und impliziert Skaleninvarianz der Erdbeben-Magnituden Verteilung. Meine Ergebnisse geben zu erkennen, dass die beobachtete Spannungsabhängigkeit der beiden grundlegenden empirisch hergeleiteten Potenzgesetzte der statistischen Seismologie durch charakteristische Größen in seismogenen Prozessen verursacht werden. Jede in einen Prozess einbezogene charakteristische Größe hat eine Einschränkung oder Änderung der fraktalen Skalierung zur Folge. Darüber hinaus liefern die durch elastische Gesteinsheterogenität hervorgerufenen Spannungsfluktuationen in der Erdkruste eine physikalische Erklärung für die beobachtete Heterogenität kritischer Spannungsänderungen in Gesteinen, die zu sprödem Gesteinsversagen und somit

zum Auftreten seismischer Ereignisse führen. Meine Untersuchungen zeigen, dass Spannungsänderungen in der Größenordnung 10^3 bis 10^7 Pa imstande sind seismische Ereignisse in Gesteinen der Erdkruste auszulösen. Diese Erkenntnis bestätigt das Konzept eines nahe kritischen Spannungszustand in der Erdkruste und legt nahe, dass bereits Spannungsänderungen knapp über den durch Gezeitenkräften bedingten Änderungen ($\approx 10^3$ Pa) ausreichend sind, um Gesteinsversagen in den am kritischsten gespannten Gesteinszonen auszulösen.

Contents

Chapter 1

General introduction

Investigating the role of stress in seismogenic processes is an important step towards understanding the physics of earthquakes. However, the potential of quantifying the significance of different aspects of stress by analyzing tectonic earthquakes, caused by large-scale motion of the Earth's plates, is limited because many unknown parameters are involved in the complex process of earthquake nucleation and rupturing. Therefore, it is crucial to understand these processes on smaller scales, at which basic conditions can be better constrained. Similarities and differences of seismogenesis at different scales can provide important insights into the governing mechanics of earthquakes. Brittle rock failure is observable on scales ranging from Acoustic Emission on grain size scale ($\approx 10^{-3}$ m) [see e.g., Lockner (1993), Sellers et al. (2003), Mayr et al. (2011)] over mining and fluid injection induced seismicity ($\approx 10^{0}$ m to 10^{2} m) [see e.g., Pearson (1982), Gibowicz and Kijko (1994), Shapiro et al. (2013)] to tectonic earthquakes which can span over the complete down-dip width of the seismogenic zone of the Earth's crust ($\approx 10^{4} - 10^{5}$ m) [see e.g., Pacheco et al. (1992)].

In order to stimulate geothermal and hydrocarbon reservoirs pressurized fluids are injected through boreholes. The occurrence of associated seismicity provides a unique opportunity to study different aspects of stress during the process of earthquake nucleation and rupturing under well-known and even adjustable conditions. The driving force, that is, mass and pressure of the injected fluid, is a known and controllable parameter. In addition, the approximate source region of possibly occurring seismic events during and after the injection of the fluid is known a priori. This allows for a highly precise design of the seismic monitoring system. The existence of boreholes at geothermal and hydrocarbon reservoirs opens up even more beneficial conditions. Firstly, in situ physical properties of the reservoir rock are accessible by borehole logging. Secondly, in situ stress directions and magnitudes can be estimated by evaluating borehole

breakouts, drilling-induced fractures and hydraulic fracturing tests [see e.g., Zoback (2010)]. The availability of these basic parameters, which are usually not accessible for large scale tectonic earthquakes, makes fluid-induced seismicity an outstanding research target to achieve a sound understanding of the role of stress in seismogenic processes. Despite these good basic conditions, the physical processes leading to the triggering of fluid injection-induced seismicity are still uncertain. Especially, processes leading to the occurrence of seismic events after the termination of hydraulic reservoir stimulation are not well-understood. In addition, statistical models to compute the occurrence probability of seismic events are lacking. These models are needed in order to assess and mitigate the seismic risk which still acts as an obstacle to the efficient and risk-free use of the geothermal potential of the subsurface for sustainable power generation [see e.g., Majer et al. (2007)]. However, advances will only be made by combining the beneficial basic conditions at fluid injection sites with knowledge gathered over decades of research in global seismology.

Several observations suggest scale-invariant physics of brittle rock failure from grain-size cracks to tectonic earthquakes [Aki (1967), Hirata (1987), Rundle (1989), Abercrombie and Brune (1994)]. This underlines the importance of investigating seismogenesis at different scales to understand the mechanics of earthquakes. Due to the complexity of seismogenic processes, it became accepted to apply empirically determined laws to approach key issues of earthquake nucleation and rupturing. In particular, Gutenberg and Richter's law of earthquake magnitude scaling [Gutenberg and Richter (1954)] and Omori's law of aftershock occurrence [Omori (1894), Utsu et al. (1995)] are frequently used in seismological studies. In general, the power law form of these empirical laws implies scale invariance. The brittle failure of rocks consistently obeys similar statistics over source dimensions ranging from large scale crustal earthquakes to laboratory grain size cracks [Lockner (1993)]. This finds its expression in validity of the two basic, empirically determined scaling laws of seismology down to fracturing processes on grain size scale in laboratory. However, the governing physical processes of these laws and the physical origin of observed scale invariance of brittle rock failure is still under discussion. Moreover, it remains unclear if the regional state of stress in the Earth's crust is governing Gutenberg and Richter's and Omori's law, as suggested by recent analyses of large seismological data catalogs [Schorlemmer et al. (2005), Narteau et al. (2009)]. To resolve these open questions, physical models have to be developed to understand the controlling mechanisms of stress fluctuations in the Earth's crust and their relation to the basic scaling laws of seismology.

In this thesis I investigate the role of different aspects of stress fluctuations in seismogenic processes. This includes a quantification of critical stress changes, capable of triggering brittle failure and associated seismicity in rocks of the Earth's crust. In addition, the stress perturbation caused by the injection of pressurized fluids is quantified and the importance of stress changes generated by the occurrence of fluid-induced earthquakes is evaluated. Moreover, I investigate the impact of scale invariant fluctuations of elastic properties in the Earth's crust on the nature and magnitudes of stress fluctuations. I relate my results to the observed scale invariance of earthquakes. Finally, the proposed stress dependency of the two fundamental power laws of statistical seismology is investigated. The main research target of this thesis is small-scale seismicity, induced by the injection of pressurized fluids. Nevertheless, my analysis contribute to the understanding of seismogenic processes in general due to the observed scale invariance of the physics of earthquakes that suggests transferability of results obtained at different scales. I utilize the beneficial basic conditions at fluid injection sites and apply methods and knowledge developed in global seismology. I demonstrate that characterizing the role of stress fluctuations in seismogenic processes is important for understanding the physics of earthquakes.

Chapter 2 provides a theoretical and empirical background for the analysis performed in the main body of this thesis. It integrates my results into the current state of research of fluid-injection induced earthquakes and scale invariance. At this point, however, I do not discuss theory and methods in detail since a theoretical and methodological introduction to specific topics is included in each of the following chapters.

The three main chapters of this thesis consist of three published research articles [Langenbruch and Shapiro (2010), Langenbruch et al. (2011), Langenbruch and Shapiro (2014a)]. Although each article presents a self-contained study, the thesis as a whole allows a deeper understanding of the role of stress fluctuations in seismogenic processes.

Chapter 3 [Langenbruch and Shapiro (2010)] presents a physically based statistical model describing the seismicity rate of fluid-induced seismicity. The focus of the study is to identify which parameters of reservoir rock and injection source control the decay rate of seismicity after terminating hydraulic reservoir stimulation. Based on the assumption that pore pressure diffusion is the governing mechanism leading to the triggering of seismic events, the spatio-temporal stress perturbation, caused by the injection of pressurized fluids, is quantified. An analytic solution for the seismicity rate during and after the injection of fluid is developed. The solution for the post-injection seismicity is compared to

Omori's law which describes the decay of aftershock activity after tectonically driven earthquakes. I verify the theoretical model by finite element modeling and application to real data, collected in case studies at Fenton Hill in the United States and Soultz-sous-Forêts in France. In addition, the relation between the state of stress in the reservoir rock and the decay characteristics of seismicity is investigated. Thereby, it is discussed if Omori's law is governed by the state of stress.

Chapter 4 [Langenbruch et al. (2011)] addresses the question if stress transfer, caused by the occurrence of preceeding fluid injection-induced earthquakes, is significant for the seismogenesis of subsequent events. The analysis aims to understand whether aftershock triggering is an important factor or if all events are directly triggered by the stress perturbation caused by the injection of pressurized fluid. To answer this question, the distribution of waiting times between subsequent fluid-induced earthquakes caused by hydraulic stimulation of geothermal reservoirs is analyzed. One objective of the study is the characterization of the statistical process describing the distribution of fluid injection-induced events in time. I develop a statistical model to compute the occurrence probability of fluid-induced seismicity. This model can help to assess the seismic risk associated with hydraulic reservoir stimulation. Six real data catalogs of fluid injection-induced earthquakes, collected at Soultz-sous-Forêts and Basel, are analyzed. In addition, the analysis includes a comparison to a synthetic seismicity catalog, simulated according to the Epidemic Type Aftershock Sequence (ETAS) model which is frequently used in statistical seismology.

Chapter 5 [Langenbruch and Shapiro (2014a)] analyzes the fundamental importance of elastic rock heterogeneity for observed scale invariance of earthquakes. Relations between elastic rock heterogeneity, stress fluctuations, and the Gutenberg-Richter b-value, describing the ratio between small- and large-magnitude earthquakes, are investigated. Based on measurements along boreholes, a representative model of elastic rock heterogeneity is constructed, a homogeneous far field stress is applied and occurring stress fluctuations are determined. Geo-mechanical considerations are used to interpret these stress fluctuations in terms of fracture strength variations. The scaling exponent of resulting fracture sizes is determined and compared to the Gutenberg-Richter b-value, describing the scaling of earthquake magnitudes. Two basic observations which argue for a non-universal b-value are discussed in the frame of the presented model. Firstly, I analyze if regional changes of elastic rock heterogeneity can explain variations of the b-value observed in different regions and in different materials in laboratory. Secondly, the observed relation between stress level and b-value is investigated. Finally, I discuss the significance

of characteristic scales in physical models and seismogenic processes in nature. The study illustrates why the b-value should show a universal value of $b = 1$.

Chapter 6 concludes the thesis with a joint interpretation and discussion of the results obtained in the three presented studies. It indicates implications of the findings and considers suggestions for further research.

Chapter 2

Integration into the current state of research of fluid-injection induced earthquakes and scale invariance

In this chapter I integrate my study into the current state of research of fluid-injection induced earthquakes and scale invariance. At this point, I do not discuss theory and methods in detail because a introduction to specific topics is included in each of the following chapters. However, this chapter aims to allow all readers to place my results into the larger and coherent framework of the current state of research.

2.1 Fluid injection-induced earthquakes

If the state of stress in the Earth's crust is just marginally perturbed, brittle failure of rocks and associated seismic events can occur. Evidence is given by occurrence of mining and reservoir-induced seismicity [see, e.g., Gibowicz and Kijko (1994), Talwani (1997)], aftershock triggering by static and dynamic stress changes [see, e.g., King et al. (1994), Kilb et al. (2002), Gomberg and Johnson (2005)], earthquake swarms triggered by magma intrusions and eruptions [see, e.g., Toda et al. (2002)] or ascending crustal fluids [see, e.g., Parotidis et al. (2003)] and rainfall-triggered seismicity [see, Hainzl et al. (2006)]. These observations show that the state of stress in the Earth's crust can be close to critical, causing brittle failure of rocks even in great distances to large scale tectonic plate boundaries. However, the most demonstrative indicator of a nearly critical state of stress in the brittle Earth's crust is given by seismicity triggered by the injection of pressurized fluids in order to stimulate geothermal and hydrocarbon reservoirs [see, e.g., Dinske and Shapiro (2013)], to dispose waste-water [see, e.g., Horton

(2012)] and to geologically store carbon dioxide [see, e.g., Bohnhoff and Zoback (2010), Zoback and Gorelick (2012)].

In general, the hydraulic energy, added to the system by the injection of pressurized fluids, results in an increase of pore pressure in the connected, fluid-saturated pore space of rocks [see, e.g., Pearson (1981), Talwani and Acree (1984), Zoback and Harjes (1997), Shapiro et al. (1997)]. In turn, this causes a decrease of the effective normal stress and a destabilization of the rock in consequence. If the frictional strength of pre-existing fractures or the tensile strength of the intact rock is exceeded, brittle rock failure and associated seismic events occur. Seismicity induced by fluid injections at any location will fall somewhere between these two end member causes, namely shear reactivation and tensile opening [Shapiro and Dinske (2009)]. Shear reactivation of pre-existing fractures usually occurs due to fluid injections at geothermal locations, aiming to create Enhanced Geothermal Systems (EGS) in the crystalline basement. During this type of hydraulic stimulation, the injection pressure stays below the minimum effective principal stress at the depth of injection. Because no new macroscopic fractures can be opened under compressive stress, the fluid rock interaction is approximately linear. Although most events observed during hydraulic stimulation at EGS sites show double-couple source mechanisms, corresponding to shear motion on planar faults, tensile events have been identified, by the inversion of moment tensors [see, e.g., Zhao et al. (2014)] which mathematically represent the movement on a fault during an earthquake.

The analysis presented in chapter 5 investigates stress fluctuations caused by elastic rock heterogeneity. The obtained results suggest that observed tensile events may correspond to small-scale hydraulic fracturing which can occur due to the highly heterogeneous stress state in rocks. Thus, close to the injection source where the pore pressure is significantly increased, the minimum effective principal stress may locally become tensile. Hence an opening of small-scale fractures can occur, although the pressure of injection stays below the large-scale minimum effective principal stress at the injection location. Non-double-couple source mechanisms of earthquakes have been observed in many other environments, including particularly volcanic and geothermal areas, mines, and deep subduction zones [Miller et al. (1998)].

During the hydraulic fracturing of hydrocarbon reservoirs in low permeable sedimentary rocks, the injection pressure usually exceeds the large-scale minimum effective stress, and macroscopic tensile fractures are opened. This results in a significant increase of the rocks' permeability and for this reason in a highly non-linear fluid rock interaction [see, e.g., Hummel and Shapiro (2012)].

However, because stress changes leading to shear reactivations can be much lower than stress changes leading to the opening of new fractures, the seismic event cloud extends into the rock, beyond the opened hydraulic fracture lengths and widths [Evans et al. (1999)].

In any case, the behavior of seismicity triggering in space and time is controlled by relaxation of the stress and pore pressure perturbation, initially created at the injection source. Shapiro and Dinske (2009) show that spatio-temporal dynamics of seismic clouds, corresponding to both end member types of seismicity, can be explained by a general non-linear diffusion equation, describing the pore pressure perturbation caused by the injection of fluids. The pore pressure relaxation can be approximately described by two differential equations, namely the continuity equation, expressing the conservation of mass, and Darcy's law, expressing the balance between the viscous friction force and the pore pressure perturbation [Shapiro and Dinske (2009)]. The authors demonstrate that both a linear pressure relaxation, describing the situation at EGS sites, and a strongly non-linear relaxation, corresponding to hydraulic fracturing at hydrocarbon reservoirs, can be obtained as special limiting cases of the resulting general diffusion equation. Apart from seismicity induced by the injection of pressurized fluids, pore pressure diffusion has been discussed as a possible triggering mechanism for Acoustic Emission (AE) in laboratory [Mayr et al. (2011)], seismicity induced by filling of reservoir lakes [Talwani and Acree (1984)], aftershock occurrence [Nur and Booker (1972)], and swarms of earthquakes for which a clear main shock is not existent [Parotidis et al. (2003)].

The knowledge about the physical processes leading to the triggering of seismic events during and after the injection of fluids can be used to estimate parameters of the reservoir rock by analyzing spatio-temporal characteristics of seismic clouds. In particular, the temporal evolution of the maximum triggering distance from the injection source, namely the triggering front [Shapiro et al. (1997)], can be used to estimate the hydraulic diffusivity of the reservoir rock [Shapiro et al. (2002), Hummel and Shapiro (2012)]. The hydraulic diffusivity is directly proportional to the permeability. In addition, the spatio-temporal evolution of seismic quiescence after the termination of injection is also controlled by the hydraulic diffusivity [Parotidis and Shapiro (2004)]. Moreover, the geometry and volume of the opened hydraulic fracture at hydrocarbon reservoirs can be estimated through the analysis of spatio-temporal signatures of the registered and located cloud of seismic events [Dinske et al. (2010)].

Because the pressure of the injected fluid and the location of the injection source are known, it is possible to quantify the criticality of stress in the Earth's

crust [see, Rothert and Shapiro (2007)]. Based on the spatio temporal pore pressure perturbation, computed according to solutions of the diffusion equation [see, Carslaw and Jaeger (1959)], the effective normal stress perturbation at the occurrence time and location of the seismic events can be determined. A reconstruction of pore pressure changes triggering seismicity during fluid injections in sedimentary and crystalline rocks suggests that the reduction of the effective normal stress from $10^3 Pa$ to $10^6 Pa$ triggered observed seismicity [Rothert and Shapiro (2007)]. In general, this supports the concept of a critically stressed crust and suggests that stress perturbations above tidal-induced stress changes, which are in the order of $10^3 Pa$ [see, e.g., Vidale et al. (1998)], are already capable of triggering brittle rock failure and associated seismic events. Mukuhira et al. (2013) estimate critical stress changes based on focal mechanisms of fluid-induced seismic events, assuming a homogeneous stress distribution in rocks. The authors conclude that a pore pressure increase of approximately 5 MPa is necessary to induce shear failure in crystalline rocks. Physical models, explaining these high values of effective stress decrease far away from the injection source or long time after the termination of injection, have not been developed yet. However, all studies characterizing critical changes of stress have one finding in common. They suggest that critical stress changes, capable of triggering brittle failure, are highly heterogeneously distributed in rocks. Nevertheless, a physical model explaining the heterogeneity of critical stress in rocks is still missing.

In chapter 5, I show that stress fluctuations caused by elastic rock heterogeneity can explain the range of critical stress changes (10^3 to 10^6 Pa) reported by Rothert and Shapiro (2007). The results support the finding that already stress perturbations above tidal-induced stress changes are sufficient to trigger brittle failure in the most critically stressed parts of rocks. Moreover, the range of stress fluctuations resulting from elastic rock heterogeneity suggest that the high critical stress changes reported by Mukuhira et al. (2013) result from neglecting the heterogeneous nature of stress in rocks.

In most studies dealing with seismicity induced by the injection of pressurized fluids, it is assumed that all events are directly triggered through the relaxation of the stress and pore pressure perturbation initially created at the injection source. This assumption is consistent with the observation of a proportionality between the cumulative number of events and the cumulative injected fluid volume [see, Shapiro and Dinske (2009), Dinske and Shapiro (2013)]. However, the occurrence of each event should alter the state of stress in the rock volume surrounding its fault plane. If sufficiently large, this change could result in a triggering of aftershocks.

In chapter 4, I address the aforementioned problem and analyze if signatures of aftershock triggering can be identified in the spatio-temporal distribution of seismicity, induced during the hydraulic stimulation at EGS sites. My results show that, even after the strongest events in the six analyzed catalogs, no signatures of aftershock triggering can be identified. Thus, stress changes resulting from the occurrence of preceding seismic events are insignificant compared to stress changes caused directly by the injection of fluids. It means that no coupling between events has to be included in statistical models describing the occurrence of fluid injection-induced earthquakes. This is an important difference to naturally triggered earthquakes, for which aftershock triggering is a crucial factor.

Some recent studies have addressed the problem of aftershock triggering during hydraulic reservoir stimulation at EGS sites through the computation of static stress changes caused by the occurrence of preceding events [Schoenball et al. (2012), Catalli et al. (2013)]. In accordance with the result obtained in chapter 4, the authors find that events occur at locations of favorable as well as unfavorable static stress changes. Only a slightly higher percentage of events occurs in regions, where static stress changes caused by preceding events promote rock failure. Nevertheless, Catalli et al. (2013) observe an increasing importance of static stress transfer with time and distance from injection. They explain this finding in accordance to the less dominant role of the pore pressure perturbation further away from the injection well and after the shut-in. In summary, the results of all studies suggest that, compared to stress and pore pressure perturbation caused by the injection of fluids, stress changes resulting from the occurrence of preceding seismic events are of second order importance. Thus, the vast majority of events is directly triggered by the stress changes caused by the injection of fluids. This finding confirms the significance of studies assuming pore pressure relaxation to be the governing triggering mechanism of seismicity.

The analysis presented in chapter 3 is based on this assumption. The main focus of the study is seismicity caused by hydraulic stimulation at EGS sites, for which the fluid-rock interaction is approximately linear. A physically based statistical model describing the seismicity rate of fluid-induced seismicity is developed. I show that the range of critical stress changes in rocks significantly influences the temporal occurrence of seismicity. In particular, the decay rate of seismicity after the termination of the hydraulic reservoir stimulation is controlled by the criticality of stress in rocks. This opens up the possibility to reconstruct the minimum effective stress changes capable of triggering seismicity. The reconstruction at two different EGS sites results in values of approximately

5000 Pa. These results confirm the concept of a critically stressed crust and the observation that even stress perturbations above tidal-induced stress changes are sufficient to trigger brittle failure in the most critically stressed parts of rocks.

Another essential aspect of fluid injection-induced earthquakes is their magnitude scaling. This point is particularly important because the seismic risk, associated with the seismic activity during and after injection of fluids, still acts as an obstacle to the efficient and risk-free use of the geothermal potential of the subsurface for sustainable power generation [see e.g., Majer et al. (2007)]. In general, it has been observed that fluid injections at geothermal sites sometimes induce events of perceptible magnitude whereas magnitudes during hydraulic fracturing operations in hydrocarbon reservoirs are usually lower. But why is the subsurface at each location reacting differently to the injection of a certain volume of fluid? Geothermal reservoirs are usually developed in hard rocks located in tectonically active regions. Hydrocarbon reservoirs are mainly located in seismically inactive regions and sedimentary rocks. This observation suggests that the seismotectonic situation in a injection region controls the intensity of seismic activity resulting from the injection of fluids. Shapiro et al. (2010) introduce a parameter, the seismogenic index, to quantify the seismotectonic situation in a injection region by analyzing fluid injection-induced seismicity. The quantification is based on the observation of a proportional increase of the number of induced earthquakes with magnitudes larger than a given one with the volume of the injected fluid [Shapiro et al. (2007), Shapiro and Dinske (2009)]. The seismogenic index combines the generally unknown site-specific seismotectonic quantities. It can be utilized to comparatively analyze the seismotectonic state of reservoir locations.

The analysis of waiting times between subsequent fluid-induced events, performed in chapter 4, shows that fluid-induced earthquakes occur independently from each other, that is, the occurrence probability of each event is independent from the occurrence of preceding events. Thus, the statistical process describing the occurrence of events is given by the Poisson process. By combining the Poisson process and the seismogenic index, it is possible to compute the occurrence probability of a given magnitude by injecting a certain volume of fluid [see Shapiro et al. (2010)]. Barth et al. (2013) combine the Poisson process and the decay rate of fluid-induced events after terminating the reservoir stimulation -developed in chapter 3- to compute the probability of exceeding a given magnitude after the termination of the hydraulic reservoir stimulation. These models can be potentially used to avoid the occurrence of large magnitude earthquakes by correspondingly planning fluid injections [Dinske and Shapiro (2013)].

Because the two basic empirically determined power laws of statistical seismology, the Gutenberg-Richter relation [Gutenberg and Richter (1954)] and the Omori law [Omori (1894), Utsu et al. (1995)], are an integral part of all following chapters, I introduce the essential research results related to these two laws in the next section. Moreover, I discuss their connection to scale invariance of earthquakes.

2.2 Scale invariance and the two basic power laws of statistical seismology

Because the accessibility of basic conditions and physical properties during nucleation and rupturing of earthquakes on tectonic scale is limited, it is crucial to understand the governing mechanisms of brittle rock failure on smaller scales. However, the question arises, if the results obtained from fracturing experiments on rock samples in laboratory and analysis of smaller scale earthquakes caused, for instance, through the injection of pressurized fluids can be transferred to other scales. Different observations, argumenting for scale invariant physics of earthquakes [Aki (1967), Hirata (1987), Rundle (1989), Abercrombie and Brune (1994)], suggest the direct transferability of results between different scales. In general, scale invariance means that a change of scales like, time or length, results only in a proportional scaling of the physical law itself. Its shape, however, remains unchanged. It means that a function $f(x)$ is scale-invariant if a rescaling of its argument x by a constant factor c results in

$$f(cx) = c^{\beta} f(x), \tag{2.1}$$

where β is a constant exponent. If relation 2.1 is valid for only a discrete set of rescaling factors c, the function is said to be self-similar. Power laws play an important role in physics because one of their fundamental characteristics is scale invariance. In the case of power law functions, the scaling exponent β is given by the power law exponent. Because power laws, characterized by the same scaling exponents, differ just by a proportional scaling, the underlying processes governing these laws should be of similar nature. Understandably, scale invariance can only arise if no characteristic scales of, for instance, length or time are existing in a process.

Both fundamental, empirically determined scaling laws of statistical seismology, namely Omori's law [Omori (1894), Utsu et al. (1995)] and the Gutenberg-Richter relation [Gutenberg and Richter (1954)], are of power law form. If the process of earthquakes occurrence is scale-invariant, the same

physical laws and scaling relations are valid independently from the scale of the considered rupture process. The validity of Gutenberg and Richter's and Omori's law has been verified on scales ranging from acoustic emission on grain scale [Lockner (1993)] over mining and fluid-induced seismicity [Gibowicz and Kijko (1994), Shapiro et al. (2007)] to large-scale tectonic earthquakes [Schorlemmer et al. (2005), Narteau et al. (2009)].

Omori's law, is given by

$$N(t) = \frac{C_1}{(C_2 + t)^p}. \tag{2.2}$$

It characterizes the temporal decay of aftershock activity following a main shock. N is the number of aftershocks. C_1, C_2 and p are empirical constants and t is the time after the main shock. The exponent p of Omori's law exhibits variability from one aftershock sequence to another, but it is typically in the range from 0.3 to 2.0 [Helmstetter and Sornette (2002)]. The variability has, among others, been attributed to variations in the state of stress, temperature, structural heterogenities, material parameters and different tectonic regimes. While the originally introduced form of Omori's law $N(t) = \frac{C_1}{t}$ [Omori (1894)] is of strict scale invariant form, the characteristic time C_2 causes a breakdown of scale invariance for a short time after the mainshock. However, it is controversial if C_2 has a physical meaning or if it is related to the incompleteness of the aftershock catalog at short times after the main shock [Lindman et al. (2006), Narteau et al. (2009)].

In chapter 3, I analyze the decay rate of fluid-induced earthquakes after the termination of the reservoir stimulation. I find that the decay rate of seismic activity after the termination of a fluid injection is very similar to Omori's law. Under the assumption that destabilizing stress changes of all magnitudes are capable of triggering seismicity, the p-value of the modified Omori law, describing the decay of seismicity after the termination of stimulation, shows values similar to the case of aftershocks sequences after tectonic main shocks. However, I find that the p-value is changing if the rock volume of the possible event occurrence is limited to a characteristic size. The limits of this seismically active rock volume are controlled by the lower limit of critical stress changes and the hydraulic diffusivity of rocks. The analysis in chapter 3 is based on the assumption of pore pressure diffusion being the governing trigger mechanism of fluid injection-induced earthquakes. Pore pressure diffusion has also been discussed as a possible triggering mechanism of aftershock sequences [Nur and Booker (1972)].

The analysis performed in chapter 4 shows that, apart from the decay of seismicity after the termination of the reservoir stimulation, which is caused by direct stress changes due to the injection of pressurized fluids, no signatures of after shock triggering can be identified in the six analyzed catalogs of fluid injection-induced seismicity at EGS sites. Even the strongest events in the catalogs do not leave any signatures according to Omori's law.

The second fundamental scaling law of seismology, the Gutenberg-Richter relation, is given by

$$log_{10}N_M = a - b\,M, \tag{2.3}$$

where N_M is the number of earthquakes greater than magnitude M. a and b are constants characterizing earthquake productivity and the ratio between small to large magnitude earthquakes in a given region. Although variations of b have been observed from one region to another, the b-value is typically close to $b = 1$ [see, e.g., Frohlich and Davis (1993), Kagan (1999)].

By considering the relations between magnitude, seismic moment M_0 and rupture area A, $M_0 \propto A^{\frac{3}{2}}$, $log_{10}(M_0) \propto \frac{3}{2}M$ [Kanamori and Anderson (1975)], the Gutenberg-Richter relation can be reformulated as follows

$$log_{10}(N_M) = a - b\,log_{10}(A). \tag{2.4}$$

This form shows that the Gutenberg-Richter relation corresponds to a power law distribution of fault areas A, where the power law exponent is given by the b-value [Aki (1981)].

The concept of fractals [Mandelbrot (1977)] quantifies the roughness of a curve, surface or volume by just one constant. This constant is named the fractal dimension and illustratively describes the change of length, area or volume of a fractal object if the scale of consideration is changed. Although classical fractals are of self-similar nature, that is, relation 2.1 is valid for only a discrete set of rescaling factors, continuous fractal distributions are characterized by the scale-invariant number size scaling of characteristic dimensions. In this case, the fractal dimension D is related to the number size scaling of objects with a characteristic linear dimension r according to [see, e.g., Turcotte (1997)]

$$N = \frac{C}{r^D}, \tag{2.5}$$

where C is a constant of proportionality. The power law form implies scale invariance and the fractal dimension D is equivalent to the scaling exponent β of

eq. 2.1. Reformulation of eq. 2.6 for the case of number size scaling of objects with a characteristic area A results in

$$N = \frac{C}{A^{\frac{D}{2}}} \quad \Leftrightarrow \quad log_{10}N = log_{10}(C) - \frac{D}{2}log(A) \tag{2.6}$$

Following this concept, the Gutenberg-Richter relation can be considered as a fractal relationship between the number of earthquakes and the characteristic size of the rupture [Aki (1981)], where the b-value is given by $b = \frac{D}{2}$ [see, Huang and Turcotte (1988)].

The basic problem, however, is to find physical models which explain the emergence of the scale invariant Gutenberg-Richter relation which can only exist if no characteristic scales are present. Most of existing models are related to the critical point theory which states that near the critical point the disappearance of characteristic scales originates in power law scaling [see, e.g., Main (1996), Bak and Tang (1989)].

In chapter 5, I propose a different approach. It has been discussed that a fractal distribution of stress in the Earth's crust should result in a scale-invariant frequency-magnitude scaling of earthquakes [Huang and Turcotte (1988)]. However, the origin of fractal fluctuations of stress in rocks has not yet been identified. Sonic borehole logging provides direct measurements of elastic heterogeneities at a specific location in the Earth's crust. Data analysis from various sites shows that elastic rock heterogeneity is of fractal scale-invariant nature. This heterogeneity of elastic properties should be directly linked to the stress distribution in rocks. I analyze elastic rock heterogeneity at various drilling sites and characterize its impact on stress fluctuations and earthquake magnitude scaling. My results show that elastic heterogeneity of the Earth's crust is of universal fractal nature and significantly impacts the stress distribution in rocks. In situ stress is mainly controlled by in situ elastic moduli. Thus, the fractal nature of elastic heterogeneity results in stress fluctuations of power law size distribution. As a consequence, fault sizes and corresponding magnitudes of earthquakes exhibit scale-invariant power law scaling according to the Gutenberg-Richter relation. Because the fractal nature of elastic rock heterogeneity, that is, the fractal dimension measured through analysis of borehole logs at various sites, is universal, the b-value resulting from elastic rock heterogeneity is universal and close to $b = 1$. My analysis shows that the universal fractal nature of elastic rock heterogeneity can be considered as the origin of the Gutenberg-Richter relation.

Although the validity of Gutenberg and Richter's and Omori's law at various length scales suggests scale-invariant physics of earthquake occurrences,

laboratory studies [Mogi (1962), Scholz (1962), Lockner and Byerlee (1977), Hirata (1987), Lockner (1993), Goebel et al. (2013)], observations [Schorlemmer et al. (2005)] and modeling [Huang and Turcotte (1988)] suggest that the power law exponents, that is, b- and p-value of these laws, are not universal. Most arguments which support non-universality are based on observations about the stress dependence of these exponents. Schorlemmer et al. (2005) connect the degree of differential stress to different tectonic stress regimes and find an inverse relation between differential stress level and b-value. Thus, high differential stress should result in a low b-value and vice versa. Based on these observations, it has been suggested to use the b-value of the Gutenberg-Richter relation as a stress meter. In a similar way, Narteau et al. (2009) analyze the influence of the faulting style of a main shock on the temporal decay of aftershocks. The authors observe a link between the temporal decay of aftershocks in dependence on the stress regime inferred from the faulting style of the main shock. They conclude that both fundamental power laws of statistical seismology are governed by the state of stress.

Many years before these observations, the influence of stress on magnitude scaling and temporal decay characteristic have been analyzed on a much smaller scale for Acoustic Emissions (AE) during laboratory experiments on samples. Various works analyze the time series of AE in laboratory [see, e.g., Lockner and Byerlee (1977), Lockner (1993), Hirata (1987), Ojala et al. (2004)]. They observe the reproduction of Omori's power law for aftershock sequences in the case of the decay characteristic of bursts of AE events. The reproduction of Omori's power law aftershock sequences of AE events suggests that the scale invariance of rock fracturing holds over a range from microfracturing to large earthquakes [Hirata (1987)]. In addition, some of the experiments reveal a slower decay of AE activity with increasing stress. This is expressed in a decrease of the p-value of Omori's law with increasing differential stress levels.

In chapter 3, I observe an increase of the p-value of the modified Omori law, describing the decay of seismicity after the termination of reservoir stimulation with increasing minimum critical stress changes capable of triggering seismicity. Because the minimum critical stress change should generally decrease with increasing differential stress level of tectonic stress in an area, this result is consistent with observations made in the laboratory.

Although the general validity of the Gutenberg-Richter relation has been observed in the case of AE during laboratory experiments on samples, Scholz (1962) notes a decrease of b-values with increasing differential stress applied to the sample. This observation has been reconfirmed by many studies [see, e.g.,

Amitrano (2003), Goebel et al. (2013)]. In general, a positive relation between b-value and the degree of rock heterogeneity as well as an inverse relation between the levels of applied differential stress is observed.

In chapter 5, I analyze the origin of b-value variations. Consistent with observations in the laboratory, I find that in theory the b-value is increasing with the degree of heterogeneity complexity expressed in the fractal dimension of elastic modulus distribution. However, as discussed above, the universal scale-invariant nature of elastic heterogeneity suggests a universal b-value of $b = 1$. Thus, the b-value variability should be related to characteristic scales of seismogenic processes which cause a change or limitation of fractal scaling. My analysis suggests that scale limitations are also the reason for observed stress dependency of the b-value. Because in all physical models as well as ongoing seismogenic processes in nature characteristic scales are involved, the b-value deviates from its universal value of $b = 1$.

One example of a characteristic length scale is the finite size of the stress perturbed volume, resulting from the injection of pressurized fluids. Although the general transferability of the Gutenberg-Richter relation has been confirmed [Shapiro et al. (2007)], deviations from a strict power law scaling of earthquake magnitudes have been observed in the case of fluid injection-induced earthquakes [Shapiro et al. (2011), Shapiro et al. (2013)]. The basic observation is a lack of larger magnitude events. This truncation of the Gutenberg-Richter relation occurs because a local injection of fluid only perturbs the state of stress in a rock volume of finite size and a certain geometry. By analysis of numerical simulations it has been shown that usually only fault planes which are almost completely embedded in the stress-perturbed rock volume will be activated [Shapiro et al. (2011)]. This means that even if the fracture sizes in rocks scale according to a power law, the finiteness of the stress-perturbed volume results in a breakdown of scale invariance because it restricts the sizes of rupturing fault planes. This finding suggests that the characteristic size of a stress perturbation controls the maximum possible magnitude of resulting earthquakes. While local man-made stress changes in the Earth's crust result in earthquakes of only small to moderate size, large-scale stress changes, caused by large scale motion of the Earth's plates, can lead to earthquake of magnitudes up to $M = 9$. However, in the tectonic case, changes and breakdowns of power law scaling of earthquake magnitudes have also been observed [see, e.g., Pacheco et al. (1992), Main (1996)].

Chapter 3

Decay rate of fluid-induced seismicity after termination of reservoir stimulations[1]

Key points:

- The seismicity rate during and after injection of fluids strongly depends on the state of stress in the reservoir rock
- The decay rate of fluid induced seismicity after termination of reservoir stimulation can be approximated by a modified Omori law
- The p-value of the modified Omori law depends on the range of critical effective stress changes, causing brittle failure of rocks
- Minimal critical stress changes are in the order of several KPa

[1]This article has been published in Geophysics: C. Langenbruch and S.A. Shapiro (2010). Decay rate of fluid-induced seismicity after termination of reservoir stimulations. http://dx.doi.org/10.1190/1.3506005. Published by the Society of Exploration Geophysicists (SEG).

GEOPHYSICS, VOL. 75, NO. 6 (NOVEMBER-DECEMBER 2010); P. MA53–MA62, 10 FIGS.
10.1190/1.3506005

Decay rate of fluid-induced seismicity after termination of reservoir stimulations

Cornelius Langenbruch[1] and Serge A. Shapiro[1]

ABSTRACT

We present a model describing the seismicity rate of fluid injection-induced seismicity. We put the focus on seismicity induced after termination of fluid injections. Here, our primary objective is the identification of parameters controlling the decay rate of seismicity. The particular importance of a theoretical model for postinjection seismicity is underlined by observations after stimulations of geothermal reservoirs at different locations. For instance, the postinjection phase is relevant for a seismic risk, which up to now has been difficult to control, because processes leading to postinjection events are not well understood. Based on the assumption of pore pressure diffusion as the governing mechanism leading to the triggering of seismic events, we develop a method to calculate the seismicity rate during and after fluid injections. We find that the decay rate of seismicity after termination of injection is very similar to the Omori law, which describes the decay rate of aftershock activity after tectonically driven earthquakes. We propose a modified Omori law for fluid-induced seismicity to estimate the decay rate in dependence on parameters of injection, reservoir rock, and the strength of preexisting fractures in a reservoir. We analyze two models of fracture-strength distribution, which represent stable and unstable preexisting fracture systems. We find that the decay rate of induced seismicity depends on the fracture strength. We present a possible application of this dependency to reservoir characterization. Furthermore, we find that the existence of unstable fractures results in a critical temporal trend of seismicity, which can enhance the occurrence probability of events with large magnitudes shortly after injection has been terminated. We verify our model by finite-element modeling and application to real data collected in case studies performed at Fenton Hill in the United States and Soultz-sous-Forêts in France.

INTRODUCTION

Fluid injections from boreholes into the surrounding reservoir rocks are performed to develop geothermal and hydrocarbon reservoirs. It is known that during these injections low-magnitude earthquakes occur in critically stressed zones of the surrounding rock (Fehler, 1989; Zoback and Harjes, 1997; Shapiro et al., 1997). A significant number of events can occur even after termination of injection. However, it is unclear which parameters of injection and reservoir control the decay rate of seismicity after hydraulic stimulations (Majer et al., 2007). In particular, seismicity induced by injections, aiming to create enhanced geothermal systems (EGS) for energy production, often is sustained for a long period of time. In this case, the events with the largest magnitudes tend to occur shortly before or shortly after termination of injection, which makes it still more difficult to control such events.

In general, the behavior of seismicity triggering in space and time is controlled by the relaxation process of stress and pore pressure perturbation that initially was created at the injection source. This relaxation process can be approximated by pressure diffusion (possibly a nonlinear one) in the pore fluid of rocks, e.g., (Hummel and Müller, 2009; Shapiro and Dinske, 2009). Also, the return to an equalized pressure state in a reservoir after termination of stimulations can be described by pressure diffusion.

At some locations in the earth's crust, the tectonic stress is close to critical, causing brittle failure of rocks. Increasing fluid pressure in a reservoir causes pressure to increase in rocks' connected pore and fracture spaces. The pore-pressure increase consequently causes a decrease of the effective normal stress, which leads to sliding along preexisting, favorably oriented, subcritically stressed cracks.

Rothert and Shapiro (2007) indicate that in the first rough approximation critical changes in pore pressure, which lead to failure of in-

Manuscript received by the Editor 16 November 2009; revised manuscript received 28 June 2010; published online 2 December 2010.
[1]Freie Universität Berlin, Fachrichtung Geophysik, Berlin, Germany. E-mail: cornelius@geophysik.fu-berlin.de; shapiro@geophysik.fu-berlin.de.

dividual preexisting fractures in rocks, are uniformly distributed between a minimal and maximal value, C_{min} and C_{max}. These values are of the order of 10^3 Pa and 10^6 Pa, respectively. Critical pore pressure values are controlled by the in situ stress state at the individual fractures in a rock and hence should depend on the tectonic setting of an injection region. The broad range of critical pressures in rocks can be explained by the existence of many fractures at all scales. Thus, the local values of in situ stress are likely to be variable, possibly highly variable (Hudson et al., 2003).

Pore pressure diffusion has been discussed as one possible triggering mechanism for aftershocks following tectonically driven earthquakes (e.g., Nur and Booker, 1972; Bosl and Nur, 2002; Helmstetter and Sornette, 2002; Gavrilenko, 2005; Lindman et al., 2006).

In comparison to hydraulic fracturing in hydrocarbon reservoirs, hydraulic stimulations of geothermal reservoirs are performed at relatively low-injection pressures. This results in an approximately linear interaction between the injected fluid and the reservoir rock. We assume in the following that linear pore pressure diffusion is the governing mechanism for triggering seismicity.

It is still an open question how the fracture strength of preexisting fractures controls the seismicity rate during and after fluid injections. Here, we develop a theoretical model to explain the temporal distribution of the seismicity rate. Our primary objective is to obtain a simple law that describes how parameters of injection source, reservoir rock, and the strength of preexisting fractures control the decay rate of fluid-induced seismicity after termination of reservoir stimulations.

Based on the assumption of linear pore pressure diffusion, we introduce a formulation to calculate the seismicity rate during and after fluid injections. We then analyze seismicity rates resulting from representative models of fracture-strength distribution. We show how the Omori law (Omori, 1894; Utsu et al., 1995), describes the decay rate of aftershock activity after tectonically driven earthquakes, can be applied to fluid-induced seismicity. In this way we develop a similar law to estimate the decay rate of seismicity after termination of reservoir stimulations. The obtained law depends on the strength of the preexisting fracture system, the hydraulic diffusivity of the reservoir rock, and the strength and duration of the fluid injection. Such dependencies can be applied to reservoir characterization.

Furthermore, we show that the existence of an unstable fracture system in a reservoir results in a critical temporal trend of seismic activity, which can enhance the occurrence probability of events with large magnitudes just before or shortly after termination of injection. We verify our theoretical model by finite-element modeling and by analyzing real data from fluid injections performed at Fenton Hill and Soultz-sous-Forêts.

THEORY

For our simple theoretical model we assume the reservoir rock to be an infinite, isotropic, homogeneous and fluid-saturated medium. The pore pressure perturbation $p(r,t)$ caused by a fluid injection then can be obtained by solving the differential equation of diffusion

$$\frac{\partial}{\partial t}p(r,t) = D\nabla^2 p(r,t), \tag{1}$$

where D represents the hydraulic diffusivity of the medium, which is directly connected to the permeability, see (Rothert and Shapiro, 2003). We approximate the pressure source by a point source and assume that pressure is liberated from this source with constant source strength q (this quantity has physical units of power) for the time t_0. Thus, t_0 is the duration of a fluid injection. The solutions $p(r,t)$ of the diffusion equation after Carslaw and Jaeger (1959) are given in Appendix A (equations A-1 and A-2). Because of a fluid injection, the pore pressure in the surrounding rock increases. This increase results in a decrease of the effective normal stress. Thus, following the Mohr-Coulomb failure criterion (Scholz, 2002) this perturbation can lead to rock failure along preexisting critically stressed cracks. Our theoretical model implements that in the following way (also see Rothert and Shapiro, (2003)): We divide the medium in N cells with elementary volume δV. Each cell represents a preexisting crack in the medium. The crack volume concentration ξ is given by $\xi = \frac{1}{\delta V}$. To simulate the fracture strength of the cracks, a criticality value C is assigned to every cell. The criticality C represents the perturbation in pore pressure that is necessary to bring the rock to failure (trigger a microseismic event) along a preexisting crack.

We presume critical pressures uniformly distributed between a minimum value C_{min} (most unstable situation) and a maximum value C_{max} (most stable situation). This situation corresponds to the reactivation of a single fracture system for which stability is characterized by C_{min} and C_{max}. The strength of a preexisting fracture system and thus the values of C_{min} and C_{max} are controlled by the individual tectonic settings of an injection region. The values of C_{min} and C_{max} hence should vary from one region to another. Even though it is likely that critical pressures can be distributed nonuniformly in nature, the analysis of our simple model will show how induced seismicity scales with the strength of a reactivated fracture system. We assume that in each cell an event can be triggered only once. This assumption is based on the fact that the specific time for tectonic stress accumulation is several orders of magnitude higher than the specific time of the pore pressure diffusion (Dieterich, 1994; Shapiro et al., 2007).

SEISMICITY RATE

Parotidis and Shapiro (2004) introduced a probability based approach to calculate the rate of seismicity triggered by linear pore pressure diffusion. Based on this approach, we calculate the temporal distribution of events induced in a given range of uniformly distributed critical pressures between C_{min} and C_{max}. Again we note that these values represent the strength of a preexisting fracture system in the reservoir rock. However, the uniform distribution of criticality values is an assumption of our model and is based on recent results obtained by Rothert and Shapiro (2007).

The probability $W(r,t)$ that in the time interval $(0,t)$ an event occurs in a cell is given by the integral of the probability density function $f(C)$ of criticality. Considering the assumption of uniformly distributed criticality values we obtain

$$W(r,t) = \int_{C_{min}}^{g(r,t)} f(C)dC = \begin{cases} 0, & \text{if } g(r,t) < C_{min} \\ \frac{1}{\Delta C}[g(r,t) - C_{min}], & \text{if } C_{min} \le g(r,t) < C_{max} \\ 1, & \text{if } g(r,t) \ge C_{max} \end{cases}, \tag{2}$$

where $f(C) = \frac{1}{\Delta C}$ and $\Delta C = C_{max} - C_{min}$. The expression $g(r,t)$ is the minimum monotonous majorant of the pressure perturbation

$p(r,t)$ and is given by the maximum pore pressure perturbation reached at a fixed distance r to the injection point in the time interval $[0,t]$. Thus, in the case of nondecreasing injection strength until the moment of termination $g(r,t) = p(r,t)$, if $\frac{\partial}{\partial t}p(r,t) \geq 0$, and $g(r,t) = p(r_{bf},t)$, if $\frac{\partial}{\partial t}p(r,t) < 0$. The expression r_{bf} is the radius of the back front, which describes the limitation of seismic activity to the domain of increasing pore pressure after termination of injection. The back front is based on the fact that a decrease in pore pressure results in an increase of the effective normal stress and thus in a strengthening of the fracture stability. By solving $\frac{\partial}{\partial t}p(r,t) = 0$ after end of injection ($t > t_0$), Parotidis et al. (2004) give the back front in 3D as

$$r_{bf} = \sqrt{6Dt\left(\frac{t}{t_0} - 1\right)ln\left(\frac{t}{t - t_0}\right)}. \tag{3}$$

The pressure $p(r_{bf},t)$ hence represents the maximum pressure perturbation value reached at a distance r to the injection point.

The seismicity rate $R_s(t)$, that is, the probability of triggering an event at a certain time t, can be calculated by considering the temporal derivative of the probability $W(r,t)$. Assuming a constant injection strength until the moment of termination we obtain

$$\begin{aligned}
&\frac{\partial}{\partial t}W(r,t) \\
&= \frac{\partial}{\partial t}\int_{C_{\min}}^{g(r,t)} f(C)dC \\
&= \begin{cases} \dfrac{1}{\Delta C}\dfrac{\partial}{\partial t}p(r,t), & if\ C_{\min} \leq p(r,t) < min\{p(r_{bf},t), C_{\max}\} \\ 0, & otherwise \end{cases}.
\end{aligned} \tag{4}$$

To calculate the seismicity rate $R_s(t)$ for the whole volume we now sum up $\frac{\partial}{\partial t}W(r,t)$ over all N cells of the medium as

$$\begin{aligned}
R_s(t) &= \sum_{i=1}^{N}\frac{\partial}{\partial t}W(r,t) \approx 4\pi\xi\int_{V_s} r^2\frac{\partial}{\partial t}W(r,t)dr \\
&= \frac{4\pi\xi}{\Delta C}\int_{max\{r_{C_{\max}}, r_{bf}\}}^{r_{C_{\min}}} r^2\frac{\partial}{\partial t}p(r,t)dr,
\end{aligned} \tag{5}$$

where V_s is the seismically active volume, that is, the volume including all cells with nonzero probability of event triggering $\left(\frac{\partial}{\partial t}W(r,t) \neq 0\right)$ at a time t. During the injection of a fluid, V_s corresponds to the volume with pressure perturbation characterized by $C_{\min} \leq p(r,t) \leq C_{\max}$. The limits of V_s therefore are given by the radii $r_{C_{\min}}$ and $r_{C_{\max}}$ of the pressure perturbation isosurfaces with values of $C_{\min}$ and $C_{\max}$. In the case of an isotropic and homogeneous medium, these isosurfaces are spherical shells propagating through the medium with time. After end of injection ($t > t_0$) the lower limit of V_s is given by the maximum of r_{bf} and $r_{C_{\max}}$. The solutions of the seismicity rate (equation 5) corresponding to the limits during and after injection are given in Appendix A (equations A-3 and A-4).

To emphasize the limits of the seismically active volume V_s and its dependence on the criticality range of the medium, we perform finite-element (FE) modeling. The pressure source is realized as a spherical source with radius a_0. Here, we define the overpressure p_0 between source and medium as a boundary condition. The source strength q then is given by $q = 4\pi D p_0 a_0$; see Rothert and Shapiro (2007). In Figure 1 the calculated event cloud for a criticality range limited by $C_{\min} = 10^3$ Pa and $C_{\max} = 10^5$ Pa is shown in the distance-time domain. Here, the distance r of a triggered event to the injection point is plotted against its occurrence time. The figure shows the limits of the seismically active volume participating in the derivation of equation 5. Following these limits, the probability to trigger an event is zero for times larger than the intersection time of r_{bf} and $r_{C_{\min}}$. In the next section we analyze the seismicity rate for three scenarios of fracture strength.

FRACTURE STRENGTH-DEPENDENT SEISMICITY RATE

Now we will analyze seismicity rates resulting from three simple, but in first approximation representative, models of fracture strength (see also Figure 2). From this analysis we will try to understand how parameters of injection source, reservoir rock and fracture-strength distribution control the decay rate of seismicity after termination of reservoir stimulations.

The reference case: Unlimited strength of preexisting fractures

We first analyze the seismicity rate resulting from the simplest model of fracture-strength distribution. We label this the reference case. The reference case corresponds to a fracture strength characterized by $C_{\min} = 0$ and $C_{\max} \geq p_0$ (see Figure 2a), where p_0 is the overpressure between source and reservoir. As a result, the seismically active volume V_s is unlimited during injection ($t \leq t_0$). To calculate the seismicity rate, we hence substitute the lower and upper integration limit in equation 5 by 0 and ∞, respectively. The integration results in the seismicity rate R_{0a} during injection

$$R_{0a} = \frac{q\xi}{C_{\max}}. \tag{6}$$

We see that the seismicity rate in the reference case is constant during injection. Its magnitude is controlled by the source strength q and the tectonic setting of the injection region, which is represented by $\frac{\xi}{C_{\max}}$.

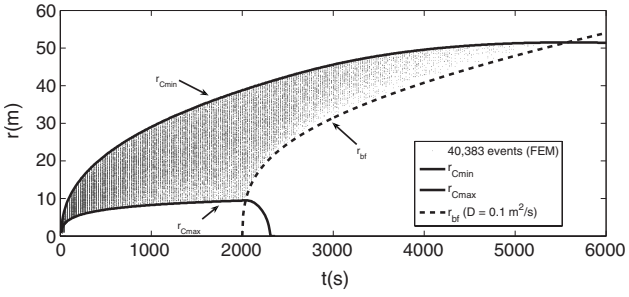

Figure 1. Limits of the seismically active volume V_s. The events are calculated using finite-element-modeling (FEM). Model parameters: $D = 0.1\ \frac{m^2}{s}$, $t_0 = 2000$ s, $C_{\min} = 10^3$ Pa, $C_{\max} = 0.1$ MPa, $p_0 = 1$ MPa. The limits of the seismically active volume are defined by: $r_{C_{\min}}$, $r_{C_{\max}}$ (distances from the injection point to the pressure isosurfaces corresponding to the value of the minimum and maximum criticality $C_{\min}$ and $C_{\max}$) and the back front (r_{bf}) of seismicity after termination of injection.

After injection, the seismically active volume is limited by the back front (see equation 3). Accordingly, the lower integration limit in equation 5 is substituted by r_{bf}. Integration results in Appendix A, equation A-6. Written in a simple form, the postinjection seismicity rate R_{0b} is hence given by $R_{0b}(\tau) = R_{0a}F(\tau)$, where R_{0a} is the constant seismicity rate during injection. The function $F(\tau)$ describes the decay rate of fluid-induced seismicity after termination of reservoir stimulations. This function depends only on $\tau = \frac{t}{t_0}$.

Can we obtain a simple law to estimate the decay rate $F(\tau)$? This law would be the equivalent to the Omori law, which describes the decay rate of aftershock activity after tectonically driven earthquakes. We therefore compare the analytic solution for the postinjection seismicity rate (Appendix A, equation A-6) to this empirically determined law given by Utsu et al. (1995). It is defined by $\frac{dN}{dt} = \frac{C_1}{(C_2+t)^p}$, where N is the number of aftershocks following a main shock, C_1, C_2 and p are empirical constants and t is the time after the main shock. The exponent p of Omori's law exhibits a large variability from one aftershock sequence to another and typically is in the range from 0.3 to 2.0 (Helmstetter and Sornette, 2002). This variability has been attributed to variations in the state of stress, temperature, structural heterogenities, material parameters, etc., in different tectonic regimes. However, a single, dominant factor controlling this parameter has not yet been identified (Lindman et al., 2006).

The constant C_1 is dependent on the magnitude of the main shock and represents a measure for aftershock productivity. It is a point of controversy whether C_2 has a physical meaning, or if it is related to the incompleteness of the aftershock catalog at brief times after the main shock (Lindman et al., 2006). By comparing Omori's law to the postinjection seismicity rate $R_{0b}(\tau)$ we obtain the following decay law for fluid-induced seismicity after termination of reservoir stimulations

$$R_{0b}(\tau) \approx \frac{R_{0a}}{\tau^p} = \frac{q\xi}{C_{\max}}\frac{1}{\tau^p}. \qquad (7)$$

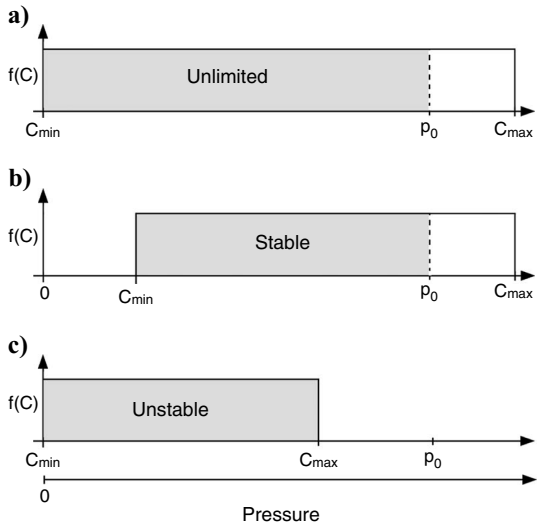

Figure 2. Schematic illustration of analyzed critical pore pressure distributions: The gray area indicates the pressure range in which event triggering is possible. The expression $f(C)$ is the probability density function. (a) Reference case, (b) stable case, (c) unstable case.

In Figure 3, a comparison between the analytic solution R_{0b} and our modification of Omori's law (equation 7) is shown. The decay rate of seismic activity during the early postinjection phase ($\tau \approx 1$) is best approximated by an exponent of $p = 2$. For longer times ($\tau \to \infty$) the decay rate is characterized by a smaller p-value of approximately one.

Stable preexisting fractures

We now analyze a model of fracture-strength distribution representing stable preexisting fractures (see Figure 2b). Critical pore pressures are distributed between $C_{\min} > 0$ and $C_{\max} \geq p_0$ in this case. Accordingly, stress changes induced by pore pressure perturbations smaller than $C_{\min}$ are insufficient to reactivate any preexisting fractures. If so, the upper limit of the seismically active volume is given by $r_{C_{\min}}$. A purely analytic solution cannot be obtained for this time-dependent limit. However, for a given set of parameters D, q, t_0 and $C_{\min}$ the limit $r_{C_{\min}}$ can be calculated numerically. After calculation of the pressure perturbation corresponding to equations A-1 and A-2 in Appendix A, $r_{C_{\min}}$ can be obtained at given times t. The seismicity rate during and after injection then can be calculated according to equations A-3 and A-4.

Figure 4 shows seismicity rates resulting from the stable case (see Figure 2b). The seismicity rate is decreasing already during injection, if $C_{\min} > 0$. The higher the value of $C_{\min}$, the stronger the decrease. This shows that the reactivation of stable preexisting fractures is most likely during the early part of the injection phase. The observation of decreasing seismicity during a fluid injection with constant strength consequently indicates the existence of fractures in a stable state.

Also the decay rate of seismicity after termination of injection is greater than in the reference case, if $C_{\min} > 0$. The higher the value of $C_{\min}$, the higher the decay rate. This results in shorter phases of postinjection seismicity. Accordingly, seismicity will be sustained for a long time after termination of reservoir stimulations only if fractures characterized by low strength (a low-critical pressure value) are preexistent in the reservoir rock. This is the case only if preexisting fractures in some locations are in a stress state close to failure.

In any case, the decay rate of seismicity after injection can be approximated well by the modified Omori law (equation 7), if $C_{\min} > 0$. This is shown in Figure 4. The p-values, resulting in the best fit

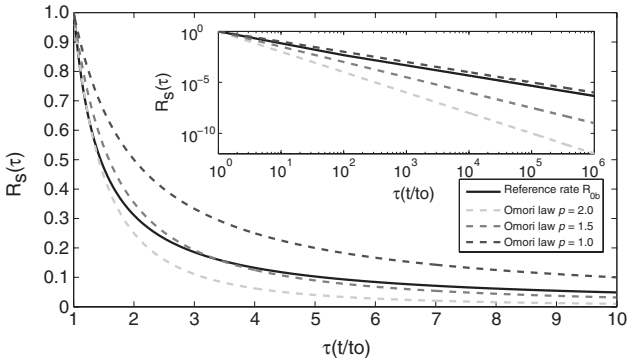

Figure 3. Comparison between the Omori law for postinjection seismicity (equation 7) and the analytic solution of the postinjection reference rate R_{0b} (equation A-6 of Appendix A). The inner plot shows the correlation in a logarithmic scale.

to the postinjection seismicity rates, always are larger than in the reference case. We determine these p-values by applying a least-square fit. Furthermore, we replace R_{0a} in the Omori law by the seismicity rate at the time t_0.

To quantify the influence of $C_{\min}$ on the decay rate, we determine p-values in dependence on $C_{\min}$. We do this for different sets of parameters D, q and t_0 and consider the time period $t_0 < t < 2t_0$, that is, $\tau \sim 1$ for the analysis. The result is shown in Figure 5a. In all cases the obtained p-values are linearly rising with $C_{\min}$. However, the slope is different for changing sets of parameters D, q and t_0. In Figure 5b, the x-axis is scaled to $x = \frac{C_{\min} D^{\frac{3}{2}} \sqrt{t_0}}{q}$. Now the dependency of the p-value on x is the same for all combinations of parameters. By applying a simple linear regression we obtain the following p-value scaling rule:

$$p \approx 2.0 + \frac{4\pi 85 C_{\min} D^{\frac{3}{2}} \sqrt{t_0}}{q} = p_{\text{ref}} + \frac{85 C_{\min} \sqrt{D t_0}}{a_0 p_0}. \quad (8)$$

In this formula $p_{\text{ref}} = 2$ represents the p-value corresponding to the decay rate in the reference case for $\tau \sim 1$, and a_0 is the radius of a spherical pressure source. In Appendix B it is shown that the scaling rule (equation 8) can be confirmed by a dimension analysis with application of the Π-theorem (Barenblatt, 1996).

Corresponding to equation 8, the decay rate of induced seismicity after termination of reservoir stimulations is controlled by the factor $C_{\min}\sqrt{D}$ and the parameters q and t_0 of the injection. Larger values of $C_{\min}$, D and t_0 result in a faster decay of seismicity during the postinjection phase, although a larger source strength q results in activity being sustained for a longer period. In addition to its physical relevance, equation 8 opens up a possibility to reconstruct parameters of our model. If the source parameters are known, which usually is the case for fluid injection experiments, the factor $C_{\min}\sqrt{D}$ can be estimated by analyzing only the characteristic p-value. We will perform this reconstruction for synthetic and real data sets in later sections.

Unstable preexisting fractures

We now analyze seismicity rates resulting from the unstable case, that is, $C_{\max} < p_0$ and $C_{\min} = 0$ (Figure 2c.) This setting corresponds to the existence of an unstable, preexisting fracture system in a reservoir rock. The seismically active volume is limited by $r_{C_{\max}}$ in this case. Figure 6 shows resulting seismicity rates normalized to $\frac{q\xi}{C_{\max}}$. All parameters of the calculation are given in the caption. We note that even though rates corresponding to low values of $C_{\max}$ are appearing below rates resulting from high values of $C_{\max}$, the absolute number of triggered events is inversely proportional to $C_{\max}$. For values of $C_{\max}$ below the source pressure p_0, the seismicity rate increases during the injection phase. This increase can be explained as a result of the absence of fractures in a stable state, which most likely are reactivated during the early phase of injection (see Figure 4).

Remarkably, the increase of seismic activity continues in the early postinjection phase, as long as $r_{C_{\max}} > r_{bf}$. However, the probability of triggering an event with magnitude larger than a given one is proportional to the seismicity rate (Shapiro et al., 2007; Shapiro and Dinske, 2009). Thus, if $C_{\max} < p_0$, the probability of triggering events with large magnitudes is especially high during the late period of the injection phase and the early period of the postinjection phase. This coincides with existing experience obtained by stimulation of enhanced geothermal systems (EGS) (Majer et al., 2007). The moment with the highest probability of triggering an event with significant magnitude hence corresponds to the time of maximum seismicity rate. This moment is marked with arrows in Figure 6. After this time the seismicity decays corresponding to the reference rate R_{0b}. Henceforward, the decay rate of seismicity is dependent on $C_{\max}$ only directly after termination of injection. Thus, for further analysis we neglect the influence of $C_{\max}$ on the p-value.

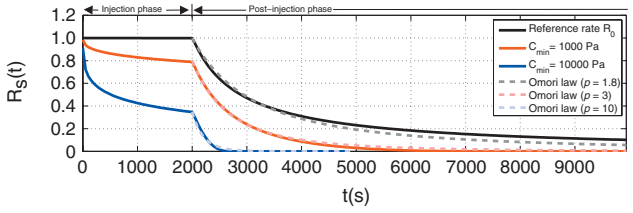

Figure 4. Seismicity rate in the stable case. The seismicity is normalized to $\frac{q\xi}{\Delta C}$. Parameters: $D = 1\ \frac{\text{m}^2}{\text{s}}$, $t_0 = 2000$ s, $p_0 = 1$ MPa, $a_0 = 4$ m, $C_{\max} = 1$ MPa. The dashed lines show the modified Omori law with $p = 1.8$, $p = 3.0$ and $p = 10.0$.

NUMERICAL MODELING

To validate the theory, we apply it to synthetic data sets. For the creation of these data sets, we perform FE modeling of pore pressure diffusion in 3D media in accordance with the methodology described in Rothert and Shapiro (2003).

Figure 7 shows postinjection seismicity resulting from six differ-

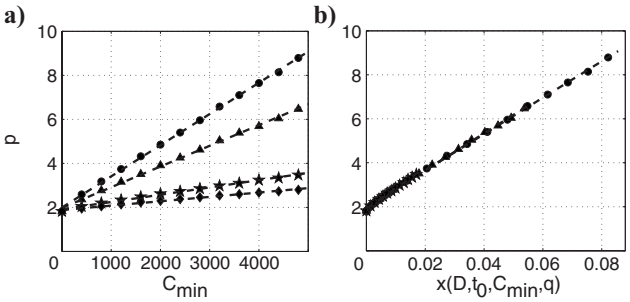

Figure 5. (a) p-value scaling. The markers show p-values in dependency on $C_{\min}$. Parameters: Circles: $t_0 = 2500$ s, $D = 1.2\ \frac{\text{m}^2}{\text{s}}$, $p_0 = 0.8$ MPa, $a_0 = 1$ m. Triangles: $t_0 = 2000$ s, $D = 1\ \frac{\text{m}^2}{\text{s}}$, $p_0 = 1$ MPa, $a_0 = 1$ m. Stars: $t_0 = 1000$ s, $D = 0.8\ \frac{\text{m}^2}{\text{s}}$, $p_0 = 2$ MPa, $a_0 = 1$ m. Diamonds: $t_0 = 3000$ s, $D = 0.5\ \frac{\text{m}^2}{\text{s}}$, $p_0 = 5$ MPa, $a_0 = 1$ m. (b) Same as (a), but the x-axis now is scaled to $x = C_{\min}\frac{\sqrt{Dt_0}}{4\pi p_0 a_0}$.

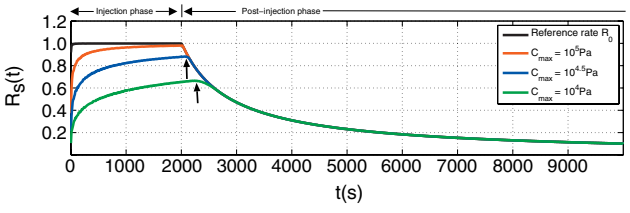

Figure 6. Seismicity rate in the unstable case. The seismicity is normalized to $\frac{q\xi}{C_{\max}}$. Parameters: $D = 1\ \frac{\text{m}^2}{\text{s}}$, $t_0 = 2000$ s, $p_0 = 1$ MPa, $a_0 = 4$ m, $C_{\min} = 0$ Pa. The arrows denote the time of maximum probability to induce an event with significant magnitude.

ent models. C_{min} varies from 0 Pa (Figure 7a) to 5000 Pa (7f). In all models, C_{max} equals the source pressure $p_0 = 1$ MPa. The seismicity is normalized to the value at the termination of the source pressure ($t = t_0 = 2000$ s). In addition to the modeled postinjection seismicity, the analytic solution (equation A-4 of Appendix A) is shown. For all calculated rates, the analytic solution coincides with the modeled seismicity. The dashed lines in Figure 7 represent the modified Omori law with p-value resulting in the best fit to the modeled seismicity. The best fit is obtained by applying a least-square fit. We see that postinjection seismicity can be approximated quite well with the modified Omori law. In the figure it becomes apparent that seismicity in the early postinjection phase is slightly underestimated, whereas later seismicity is slightly overestimated, especially for models with high values of C_{min}.

We now perform a reconstruction of the minimum criticality used in the models. This is done also to prove the accuracy of the determined p-values. We reconstruct the C_{min} values according to equation 8 using the parameters of the models. Figure 8 shows the reconstructed C_{min} values plotted against the C_{min} values used in the models. The figure shows that the reconstruction is working with good accuracy for synthetic data sets.

CASE STUDIES

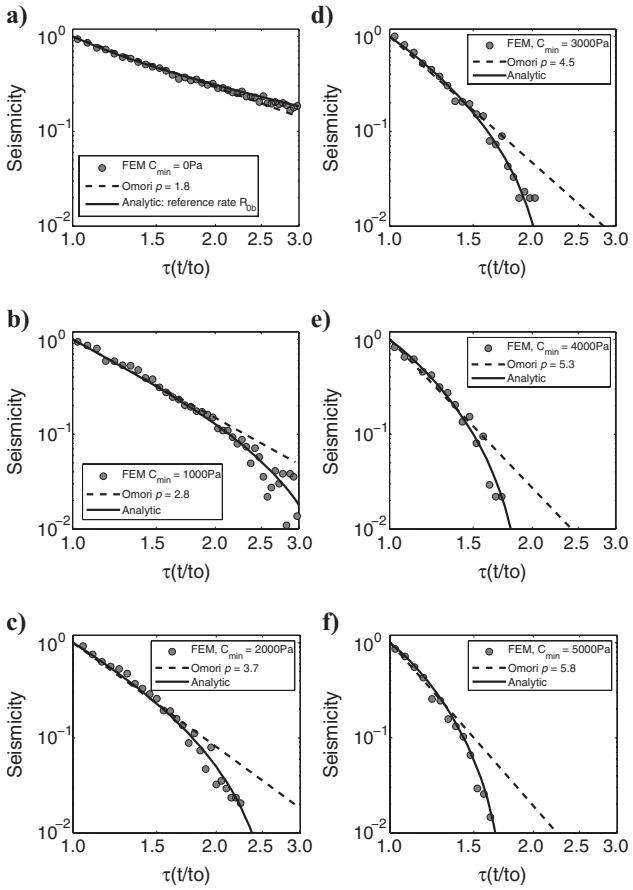

Figure 7. Postinjection seismicity: Comparison among finite-element modeling, analytic calculation and the modified Omori law. Parameters of the models: $D = 0.1$ $\frac{m^2}{s}$, $a_0 = 1$ m, $p_0 = 1$ MPa, $t_0 = 2000$ s; C_{min} varies from 0 Pa (a) to 5000 Pa (f).

Fenton Hill

We apply the developed theory to real data assembled during the Fenton Hill (New Mexico, USA) hot dry rock injection in 1983. During the injection experiment 11,366 events were recorded and located with accuracy better than 100 m (House, 1987). The overpressure at the open-hole section was approximately constant with magnitude $p_0 = 14$ MPa during the 62 hours of injection. Microseismic monitoring stopped 85 hours after injection start. This corresponds to a value of $\tau \approx 1.4$.

Figure 9 shows the spatio-temporal distribution of the induced events. In Figure 9a, events are shown in the r-t domain. Here the event locations are scaled corresponding to an effective isotropic medium (Shapiro et al., 2003). The signatures in the event distribution are visible as assumed in the developed theory (see Figure 1 for comparison). We assume a diffusivity of $D = 0.15$ $\frac{m^2}{s}$, which Shapiro et al. (2003) estimated for the Fenton Hill injection.

Figure 9b and c show the correlation between observed postinjection seismicity, the modified Omori law, and the analytic solution (equation A-4 of Appendix A) in a linear (Figure 9b) and a double logarithmic scale (Figure 9c). The figures show that the decay of seismicity can be well approximated by the modified Omori law. A p-value of $p = 7.5$ results in the best fit to the observed postinjection seismicity. We use this p-value to reconstruct C_{min} for the Fenton Hill injection. For this purpose, the open-hole section is approximated by a surface-equivalent sphere with radius $a_0 = 1$ m (Rothert and Shapiro, 2007). The substitution of the Fenton Hill injection parameters in equation 8 results in $C_{min} \approx 5000$ Pa.

We note that this reconstructed value does not necessarily represent the lowest pressure at which event triggering is possible. In fact, it represents the minimum criticality value of an equal distribution in pressures that best approximates the lower bound of the real criticality distribution. However, its order of magnitude is in agreement with the value of $C_{min} \approx 1000$ Pa reconstructed by Rothert and Shapiro (2007). We now use $C_{min} = 5000$ Pa to calculate seismicity rates according to equations A-4 and A-5 of Appendix A.

Figure 9d shows the seismicity during the entire Fenton Hill injection program. In addition, it presents seismicity rates calculated according to two different values of C_{max}. Even though the used values of C_{max} differ in two orders of magnitude, a deviation between the seismicity rates is significant only during the first 10 hours of injection. We conclude from this that there is no satisfactory resolution for C_{max} in the temporal distribution of the induced events.

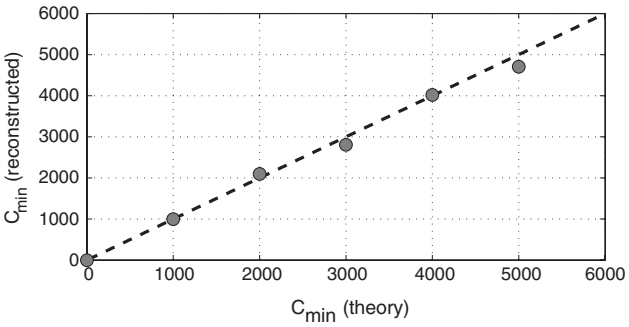

Figure 8. Reconstructed values of C_{min}: Analysis of the six FE models shown in Figure 7. The marker shows the reconstructed values of C_{min}.

Soultz 2000

In July 2000, a hydraulic stimulation was carried out at the European Hot Dry Rock (HDR) research site at Soultz, France, to establish a new geothermal reservoir at a depth of 4500 to 5000 m (Dyer, 2001). Over six days, 23,400 m^3 of brine were injected. The injection commenced at a rate of 31 $\frac{l}{s}$. The result was an overpressure of 12 MPa at the open-hole section. After one day of injection, the flow rate was increased to 40 $\frac{l}{s}$ and then 27 hours later to 50 $\frac{l}{s}$. The injection continued at 50 $\frac{l}{s}$ for approximately 90 hours until the well was shut in. The overpressure at the open-hole section at the time of the shut in was about 14 MPa. During the program, 31,511 potential seismic events were recorded, from which 13,986 seismic events were located (Dyer, 2001).

Figure 10 shows the spatio-temporal distribution of the induced events. The back front signature after injection is not as distinct as in the Fenton Hill data. We assume that this is a result of heterogeneity and strong anisotropy of this injection site. Also a modification of the registration system, which was performed approximately 19 hours after termination of injection (Dyer, 2001), might have perturbed the signature. However, the signature is sufficiently distinct to be identified. We show theoretical back front curves corresponding to the minimal and maximal principal components of the diffusivity tensor estimated by Delépine et al. (2004) for the anisotropic case. These curves represent the lower and upper boundaries of the back front signature. As for the Fenton Hill data, the decay of seismicity after end of injection can be well approximated by the modified Omori law. The best fit is obtained for an exponent of $p = 9.5$. The reconstruction of $C_{\min}$ under assumption of $a_0 = 1$ m results in $C_{\min} \approx 4500$ Pa. For the reconstruction we assumed a scalar diffusivity of $D = 0.15 \frac{m^2}{s}$. This value was estimated by Delépine et al. (2004) in the isotropic case.

DISCUSSION

Our simple theoretical model is developed based on various assumptions including homogeneity and isotropy of hydraulic transport properties in rocks. These assumptions are of course never completely fulfilled in nature. To clarify the influence of heterogeneities and anisotropy, further investigations are necessary. Nevertheless, the analysis of the case studies shows that our model can explain the main characteristics of the observed seismicity rates. However, there are some apparent deviations between theory and observations that we will discuss now.

Both case studies show an obvious disagreement between calculated and observed seismicity rates during the early injection phase. We attribute this to different short-term processes in direct vicinity of the open-hole section. Here nonlinearities in the fluid rock interaction, which can be caused by high-pressure perturbations, may have a considerable influence. The geometry of the pressure source (open-hole section) should have the biggest influence on the seismicity rate soon after start of injection. In addition, a delayed pressure buildup after the start of injection should influence the trend of the seismicity rate. This could compensate the calculated decrease of the seismicity rate during the early injection phase.

In contrast to the seismicity rate shortly after the start of injection, the observed decay rates of seismicity after the termination of injection can be explained quite accurately with our model. In both case studies, the decay rates show a linear trend in the double logarithmic scale. This demonstrates the validity of the Omori law. The correlation between observed decay rates and the Omori law is even better than the fit to the analytic solution of the seismicity rate. This may indicate a deviation from a uniform fracture-strength distribution in rocks. However, it is striking that postinjection seismicity at Soultz-sous-Forêts shows a change in the decay characteristic at $\tau \approx 1.14$ ($t \approx 161$ h) (see Figure 10). We note that this change may be induced by a modification of the monitoring system, which was performed precisely at this time (Dyer, 2001). Another possible explanation might be the reactivation of a second fracture system, which was reached by the pressure perturbation at long periods of times. This second fracture system should then be located at a longer distance from the injection point. Furthermore, it should be characterized by lower fracture strength than the fracture system close to the injection point. Both decay rates are characterized by a straight trend in the double logarithmic scale. Again this points out a decay of the Omori type.

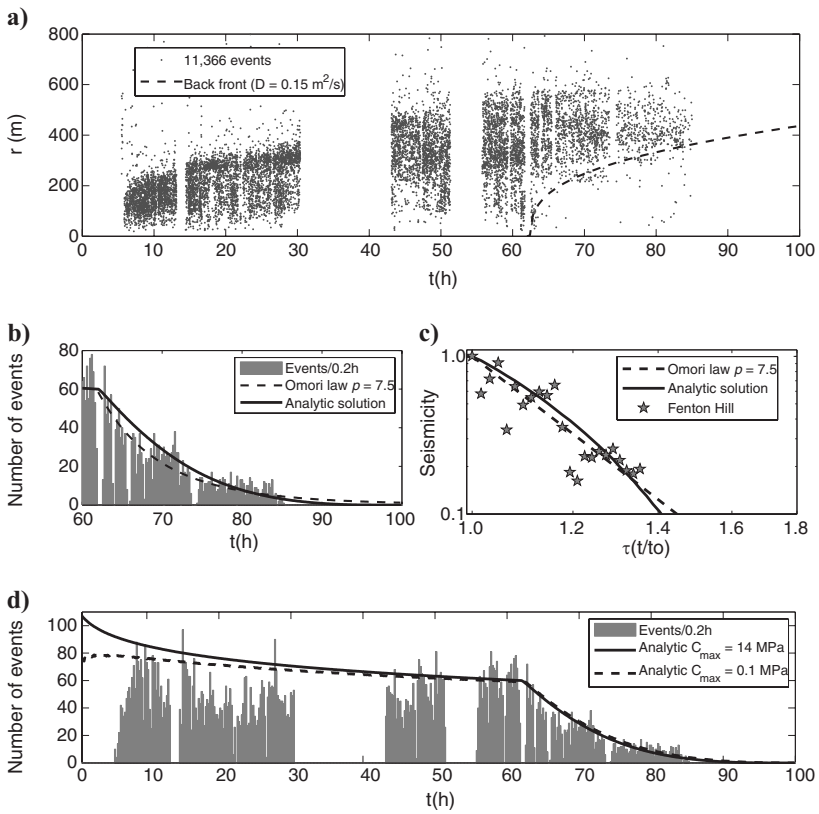

Figure 9. Fenton Hill 1983: Spatio-temporal distribution of induced events. (a) Event distribution in the *r-t* domain. Views (b) and (c), correlation between postinjection seismicity, modified Omori law (equation 7) and the analytic solution (equation A-4 of Appendix A) in (b) linear and (c) double logarithmic scale. (d) Registered and calculated seismicity rate during and after injection. The gaps in the seismicity are a result of problems with the registration system.

Our model is based on the assumption of uniformly distributed critical pressures. We have chosen this model to allow a well-defined separation of the influences caused by a modification of the fracture-strength distribution in rocks. Nevertheless, it is possible to calculate seismicity rates corresponding to nonuniform criticality distribution functions with the proposed method. This can be done by splitting a criticality range into small sections, calculating the corresponding rates and summing them up under consideration of a weighting function. Even if in nature critical pressures are distributed nonuniformly, our model is able to demonstrate the major scaling characteristics of the seismicity rate dependent on the fracture strength of preexisting fractures.

CONCLUSIONS

We have presented a model describing the seismicity rate of fluid injection-induced seismicity. The presented analysis is based on the assumption of linear pore pressure diffusion as the governing mechanism leading to the triggering of induced seismicity. We introduced a method to calculate the seismicity rate corresponding to uniformly distributed critical pressures.

We calculated the analytic solution for the postinjection seismicity rate corresponding to an unlimited range in critical pressures and compared it to the Omori law of aftershock occurrence. The comparison demonstrated a good correlation between postinjection seismicity and a modified Omori law with exponent p between $p = 2$ and $p = 1$. The analysis of real data examples has shown that the obtained scaling law fits the postinjection seismicity quite well, but the p-value has to be chosen larger than $p = 2$. To explain the occurrence of larger exponents p, we analyzed the way in which the fracture-strength distribution of preexisting fractures controls the seismicity rate. The analysis reveals that the decay rate of seismicity after reservoir stimulations is strongly dependent on the strength of preexisting fractures in the reservoir rock. If the strength of a fracture system is weak, that is, the fracture system is close to failure, the p-value is low. Thus, seismicity is decaying slowly after termination of injection. In the case of a highly unstable fracture system, the seismicity rate increases during the injection and early postinjection phase. This explains the occurrence of events with higher magnitudes during the later injection and early postinjection phase.

In the case of stable preexisting fractures, a fraction of seismicity already decays during the injection phase. The decay rate of seismicity after injection can be approximated by our modified Omori law with increased p-value ($p > 2$). This dependency of the p-value opens up a possibility to reconstruct strength parameters of preexisting fractures, which can be useful for the development of geomechanical models. We note that the reconstruction procedure is working without information about the locations of induced events.

We applied our model to synthetic and real data sets. The results obtained support the developed theory. Observed decay rates of seismicity after the Fenton Hill as well as the Soultz 2000 injection can be well approximated by our modification of Omori's law. For the Fenton Hill and Soultz 2000 injection sites, we reconstructed minimum criticality values of 5000 Pa and 4500 Pa, respectively. For the development of meaningful risk studies, it is of great importance to ensure accurate and consistent microseismic monitoring during and after reservoir stimulations.

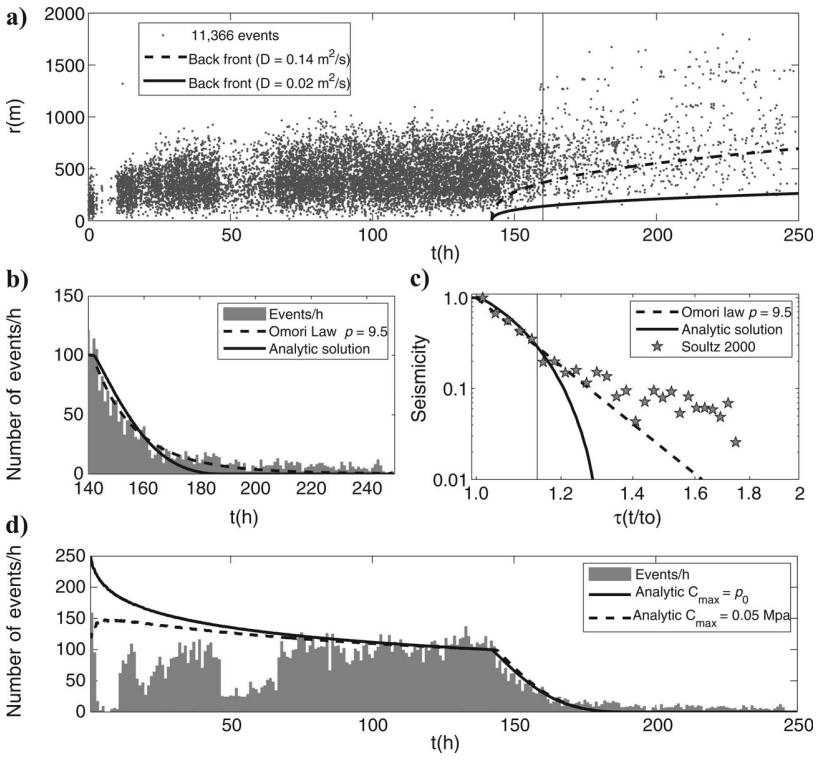

Figure 10. Soultz 2000: Spatio-temporal distribution of induced events. (a) Event distribution in the r-t domain. Views (b) and (c), correlation between postinjection seismicity, modified Omori law (equation 7), and the analytic solution (equation A-4 of Appendix A) in (b) linear and (c) double logarithmic scale. (d) Registered and calculated seismicity rate during and after injection. The gaps in the seismicity during injection are a result of problems with the registration system. The vertical lines in (a) and (c) indicate the time of a modification in the registration system.

ACKNOWLEDGMENTS

We thank the sponsors of the Physics and Application of Seismic Emission (PHASE) consortium project and the Federal Ministry for the Environment, Nature Conservation and Nuclear Safety as a sponsor of the project Konzepte zur Begrenzung der mikroseismischen Aktivität bei der energetischen Nutzung geothermischer Systeme im tiefen Untergrund (MAGS) for supporting the research presented in this paper.

APPENDIX A EQUATIONS

Solutions of the diffusion equation (equation 1):

$$p(r,t) = \frac{q}{4\pi rD}\, erfc\left(\frac{r}{\sqrt{4Dt}}\right), \quad \text{(A-1)}$$

for times $t < t_0$. And

$$p(r,t) = \frac{q}{4\pi rD}\left[erfc\left(\frac{r}{\sqrt{4Dt}}\right) - erfc\left(\frac{r}{\sqrt{4D(t-to)}}\right)\right], \tag{A-2}$$

for times $t > t_0$. Here $erfc(x)$ is the complementary Gaussian error function: $erfc(x) = 1 - erf(x)$.

Solution for the seismicity rate (equation 5) during injection ($t < t_0$):

$$R_s(t) = \frac{4\pi\xi}{\Delta C}\int_{r_{C_{\max}}}^{r_{C_{\min}}} r^2 \frac{\partial}{\partial t}p(r,t)dr = \frac{q\xi}{\Delta C}\left[erf\left(\frac{r}{\sqrt{4Dt}}\right) - \frac{r}{\sqrt{Dt\pi}}\, exp\left(-\frac{r^2}{4Dt},\right)\right]_{r=r_{C_{\max}}}^{r=r_{C_{\min}}}. \tag{A-3}$$

After injection ($t > t_0$):

$$R_s(t) = \frac{q\xi}{\Delta C}\left[erf\left(\frac{r}{\sqrt{4Dt}}\right) - \frac{r}{\sqrt{Dt\pi}}\, exp\left(-\frac{r^2}{4Dt}\right) - erf\left(\frac{r}{\sqrt{4D(t-t0)}}\right) + \frac{r}{\sqrt{D(t-t_0)\pi}} \times exp\left(-\frac{r^2}{4D(t-t_0)}\right)\right]_{r=max\{r_{C_{\max}},r_{bf}\}}^{r=r_{C_{\min}}}. \tag{A-4}$$

Reference rate R_0 after injection ($t > t_0$):

$$R_{0b}(t) = \frac{q\xi}{C_{\max}}\left[\frac{r_{bf}}{\sqrt{\pi Dt}}\left[\exp\left(\frac{-r_{bf}^2}{4Dt}\right) - \exp\left(\frac{-r_{bf}^2}{4D(t-to)}\right)\right] - erf\left(\frac{r_{bf}}{\sqrt{4Dt}}\right) + erf\left(\frac{r_{bf}}{\sqrt{4D(t-to)}}\right)\right]. \tag{A-5}$$

Substitution of r_{bf} and $\tau = \frac{t}{t_0}$:

$$R_{0b}(\tau) = R_{0a}\left[erf\left(\sqrt{\frac{3}{2}\tau \ln\left(\frac{\tau}{\tau-1}\right)}\right) - erf\left(\sqrt{(\tau-1)\frac{3}{2}\ln\left(\frac{\tau}{\tau-1}\right)}\right) + \sqrt{\frac{6}{\pi}}\left(\frac{\tau}{\tau-1}\right)^{-\frac{3\tau}{2}}\left(-\sqrt{\frac{\tau}{\tau-1}} + \left(\frac{\tau}{\tau-1}\right)^{\frac{3}{2}}\right)\sqrt{(\tau-1)\ln\left(\frac{\tau}{\tau-1}\right)}\right]. \tag{A-6}$$

APPENDIX B DIMENSION ANALYSIS

The radius $r_{C_{\min}}(t)$ depends on the quantities $D, C_{\min}, q, t, t_0$. Their dimensions are

$$[D] = \frac{L^2}{T}, \quad [C_{\min}] = P, \quad [q] = \frac{PL^3}{T}, \quad [t] = T, \quad [t_0] = T, \tag{B-1}$$

where T, L and P denote dimensions of time, length and pressure. Only two dimensionless combinations θ and τ can be constructed from these quantities

$$\theta = \frac{C_{\min}D^{\frac{3}{2}}\sqrt{t}}{q}, \quad \tau = \frac{t}{t_0}. \tag{B-2}$$

The quantity $\sqrt{Dt}$ has the dimension of length. The Π-theorem of the dimension analysis, see Barenblatt (1996), states that the radius $r_{C_{\min}}$ then must have the form

$$r_{C_{\min}} = \sqrt{Dt}F(\theta,\tau), \tag{B-3}$$

where $F(\theta,\tau)$ is a dimensionless function. Applying this result to equation A-4 of Appendix A, we obtain the following relation for the postinjection rate soon after end of injection ($t \approx t_0$, $\tau \approx 1$),

$$R_s(t) = \frac{q\xi}{\Delta C}F\left(\frac{C_{\min}D^{\frac{3}{2}}\sqrt{t_0}}{q}\right). \tag{B-4}$$

This result confirms the derived p-value scaling rule (equation 8).

REFERENCES

Barenblatt, G. I., 1996, Scaling, self-similarity, and intermediate asymptotics: Cambridge University Press.

Bosl, W. J., and A. Nur, 2002, Aftershocks and pore fluid diffusion following the 1992 Landers earthquake: Journal of Geophysical Research, **107**, 2366–2377, doi: 10.1029/2001JB000155.

Carslaw, H. S., and J. C. Jaeger, 1959, Conduction of heat in solids: Oxford University Press.

Delépine, N., N. Cuenot, E. Rothert, M. Parotidis, S. Rentsch, and S. A. Shapiro, 2004, Characterization of fluid transport properties of the Hot Dry Rock reservoir Soultz-2000 using induced microseismicity: Journal of Geophysics and Engineering, **1**, 77–83, doi: 10.1088/1742-2132/1/1/010.

Dieterich, J., 1994, A constitutive law for rate of earthquake production and its application to earthquake clustering: Journal of Geophysical Research, **99**, 2601–2618, doi: 10.1029/93JB02581.

Dyer, B. C., 2001, Soultz GPK2 stimulation June/July 2000, Seismic monitoring report, Semore Seismic Report.

Fehler, M. C., 1989, Stress control of seismicity patterns observed during hydraulic fracturing experiments at the Fenton Hill hot dry rock geothermal energy site, New Mexico: International Journal of Rock Mechanics and Mining Science & Geomechanics Abstracts, **26**, 211–219, doi: 10.1016/0148-9062(89)91971-2.

Gavrilenko, P., 2005, Hydromechanical coupling in response to earthquakes: on the possible consequences for aftershocks: Geophysical Journal International, **161**, 113–129, doi: 10.1111/j.1365-246X.2005.02538.x.

Helmstetter, A., and D. Sornette, 2002, Diffusion of epicenters of earthquake aftershocks, Omori's law, and generalized continuous-time random walk models: Physical Review E, **66**, 061104, doi: 10.1103/PhysRevE.66.061104.

House, L., 1987, Locating microearthquakes induced by hydraulic fracturing in crystalline rock: Geophysical Research Letters, **14**, 919–921, doi: 10.1029/GL014i009p00919.

Hudson, J. A., F. H. Cornet, and R. Christiansson, 2003, ISRM suggested methods for rock stress estimation-Part 1: Strategy for rock stress estimation: International Journal of Rock Mechanics and Mining Sciences, **40**, 991–998, doi: 10.1016/j. ijrmms.2003.07.011.

Hummel, N., and T. M. Müller, 2009, Microseismic signatures of non-linear pore-fluid pressure diffusion: Geophysical Journal International, **179**, 1558–1565, doi: 10.1111/j.1365-246X.2009.04373.x.

Lindman, M., B. Lund, R. Roberts, and K. Jonsdottir, 2006, Physics of the Omori law: Inferences from interevent time distributions and pore pressure diffusion modeling: Tectonophysics, **424**, 209–222, doi: 10.1016/j.tecto.2006.03.045.

Majer, E. L., R. Baria, M. Stark, S. Oates, J. Bommer, B. Smith, and H.

Asanuma, 2007, Induced seismicity associated with enhanced geothermal systems: Geothermics, **36**, 185–222, doi: 10.1016/j.geothermics.2007.03.003.
Nur, A., and J. R. Booker, 1972, Aftershocks caused by pore fluid flow?: Science, **175**, 885–887, doi: 10.1126/science.175.4024.885.
Omori, F., 1894, On the aftershocks of earthquakes: Journal of Colloid Science, **7**, 111–200.
Parotidis, M., and S. A. Shapiro, 2004, A statistical model for the seismicity rate of fluid-injection-induced earthquakes: Geophysical Research Letters, **31**, L17609, doi: 10.1029/2004GL020421.
Parotidis, M., S. A. Shapiro, and E. Rothert, 2004, Back front of seismicity induced after termination of borehole fluid injection: Geophysical Research Letters, **31**, L02612, doi: 10.1029/2003GL018987.
Rothert, E., and S. A. Shapiro, 2003, Microseismic monitoring of borehole fluid injections: Data modeling and inversion for hydraulic properties of rocks: Geophysics, **68**, 685–689, doi: 10.1190/1.1567239.
Rothert, E., and S. A. Shapiro, 2007, Statistics of fracture strength and fluid-induced microseismicity: Journal of Geophysical Research, **112**, B04309, doi: 10.1029/2005JB003959.
Scholz, C. H., 2002, The mechanics of earthquakes and faulting, second edition: Cambridge University Press.
Shapiro, S. A., and C. Dinske, 2009, Scaling of seismicity induced by nonlinear fluid-rock interaction: Journal of Geophysical Research, **114**, B09307, doi: 10.1029/2008JB006145.
Shapiro, S. A., C. Dinske, and J. Kummerow, 2007, Probability of a given-magnitude earthquake induced by a fluid injection: Geophysical Research Letters, **34**, L22314, doi: 10.1029/2007GL031615.
Shapiro, S. A., E. Huenges, and G. Borm, 1997, Estimating the crust permability from fluid-injection-induced seismic emission at the KTB site: Geophysical Journal International, **131**, F15–F18, doi: 10.1111/j.1365-246X.1997.tb01215.x.
Shapiro, S. A., R. Patzig, E. Rothert, and J. Rindschwentner, 2003, Triggering of seismicity by pore-pressure perturbations: Permeability-related signatures of the phenomenon: Pure and Applied Geophysics, **160**, 1051–1066, doi: 10.1007/PL00012560.
Utsu, T., Y. Ogata, and R. S. Matsu'ura, 1995, The centenary of Omori formula for decay law of aftershock activity: Journal of Physics of the Earth, **43**, 1–33.
Zoback, M. D., and H.-P. Harjes, 1997, Injection-induced earthquakes and crustal stress at 9 km depth at the KTB deep drilling site, Germany: Journal of Geophysical Research, **102**, 18477–18491, doi: 10.1029/96JB02814.

Chapter 4

Inter event times of fluid-induced earthquakes suggest their Poisson nature[1]

Key points:

- No signatures of aftershock triggering can be identified in the spatio-temporal distribution of fluid injection-induced earthquakes at EGS sites
- The Poisson process describes the distribution of fluid-induced earthquakes in time and injection volume domain
- Fluid-induced earthquakes are directly triggered by the stress perturbation caused by injection of pressurized fluids
- Stress changes caused by preceding events are only of second order importance for the seismogenesis of fluid injection-induced earthquakes

[1]This article has been published in Geophysical Research Letters: C. Langenbruch, C. Dinske and S.A. Shapiro (2011). Inter event times of fluid induced earthquakes suggest their Poisson nature. http://dx.doi.org/10.1029/2011GL049474. Published by John Wiley & Sons, Ltd on behalf of American Geophysical Union (AGU).

Inter event times of fluid induced earthquakes suggest their Poisson nature

C. Langenbruch,[1] C. Dinske,[1] and S. A. Shapiro[1]

Received 30 August 2011; revised 3 October 2011; accepted 3 October 2011; published 4 November 2011.

[1] We analyze the inter event time distribution of fluid-injection-induced earthquakes for six catalogs collected at geothermal injection sites at Soultz-sous-Forêts and Basel. We find that the distribution of waiting times during phases of constant seismicity rate coincides with the exponential distribution of the homogeneous Poisson process (HPP). We analyze the waiting times for the complete event catalogs and find that, as for naturally occurring earthquakes, injection induced earthquakes are distributed according to a non homogeneous Poisson process in time. Moreover, the process of event occurrence in the injection volume domain is a HPP. These results indicate that fluid-injection-induced earthquakes are directly triggered by the loading induced by the fluid injection. We also consider the spatial distance between events and perform a nearest neighbor analysis in the time-space-magnitude domain. Our analysis including a comparison to a synthetic catalog created according to the ETAS model reveals no signs of causal relationships between events. Therefore, coupling effects between events are very weak. The Poisson model seems to be a very good approximation of fluid induced seismicity. **Citation:** Langenbruch, C., C. Dinske, and S. A. Shapiro (2011), Inter event times of fluid induced earthquakes suggest their Poisson nature, *Geophys. Res. Lett.*, *38*, L21302, doi:10.1029/2011GL049474.

1. Introduction

[2] The analysis of waiting times between earthquakes [see, e.g., *Bak et al.*, 2002; *Corral*, 2006] has contributed to the development of statistical models of seismicity. These models are essential to effectively assess seismic hazards. However, the waiting time distribution of earthquakes induced by the injection of pressurized fluids into geothermal and hydrocarbon reservoirs has not yet been studied. It has been established to model the occurrence of naturally triggered earthquakes according to a non homogeneous Poisson process in time [see *Ogata*, 1998; *Shcherbakov et al.*, 2005]. The inhomogeneous nature of the process reflects changes of the seismicity rate [see *Toda et al.*, 1998] which are attributed to the occurrence of aftershock sequences. We analyze seismic sequences induced by borehole fluid injections into geothermal reservoirs at Soultz-sous-Forêts [see *Baria et al.*, 1999] and Basel [see *Häring et al.*, 2008] to test whether their waiting time distributions suggest the Poisson nature of fluid induced earthquakes. Further, we replace the time by the injected fluid volume and analyze the distribution of fluid volume injected between the occurrences of successive events. To deepen our analysis we include information about the spatial distance between events and perform a nearest neighbor analysis in the time-space-magnitude domain according to *Zaliapin et al.* [2008]. We start the analysis for simple cases of constant seismicity rate.

2. Stationary Induced Seismicity: A Homogeneous Poisson Process

[3] A sequence of independently occurring events is described by a Poisson process. In the most simple case of a Poisson process with constant intensity λ(expected number of events per unit time), the process is called a homogeneous Poisson process (HPP). The probability $P(n, \lambda, t)$ to have n events in the time interval $[0, t]$ is then given by:

$$P(n, \lambda, t) = \frac{(\lambda t)^n}{n!} e^{-\lambda t}, \tag{1}$$

with corresponding probability density function (PDF) of inter event times (IET) between successive events:

$$pdf(\Delta t) = \lambda e^{-\lambda \Delta t}. \tag{2}$$

Because this relation depends on the intensity λ, it is reasonable to analyze the distribution of normalized IET given by: $\Delta\tau = \Delta t\lambda$ [see also *Corral*, 2006]. This normalization results in an expected value $\langle \Delta\tau \rangle = 1$ and a $pdf(\Delta\tau) = e^{-\Delta\tau}$.

[4] Figure 1 shows the temporal distribution of induced seismicity and applied fluid flow rates during six injection experiments. From the earthquake catalogs we select phases of approximately constant event rate (see Figure 1) and calculate normalized inter event times between successive events according to $\Delta\tau_i = (t_i - t_{i-1})\,\hat{R}$. Here $\hat{R}$ is the mean seismicity rate of a stationary phase. Figure 2 (left) presents the number of normalized IET $\Delta\tau$ within logarithmically binned time intervals for the identified stationary phases, 400 events simulated according to a HPP and the distribution $e^{-\Delta\tau}$ of the HPP. In Figure 2 (right) the PDF of IET are shown, which are obtained after dividing the number of counts in a time interval by its length and normalizing the overall probability to one. Apart from negligible deviations that also occur for the simulated events, the distributions of $\Delta\tau$ coincide with the $pdf(\Delta\tau) = e^{-\Delta\tau}$ of the HPP. This implies that successively occurring events are not causally related to each other. Before we discuss possible sources and implications of this result in detail, we analyze the complete catalogs shown in Figure 1.

3. Complete Induced Seismic Sequences: A Non Homogeneous Poisson Process

[5] Usually, the occurrence of naturally triggered earthquakes is modeled according to a non homogeneous Poisson

[1]Fachrichtung Geophysik, Freie Universität Berlin, Berlin, Germany.

0094-8276/11/2011GL049474

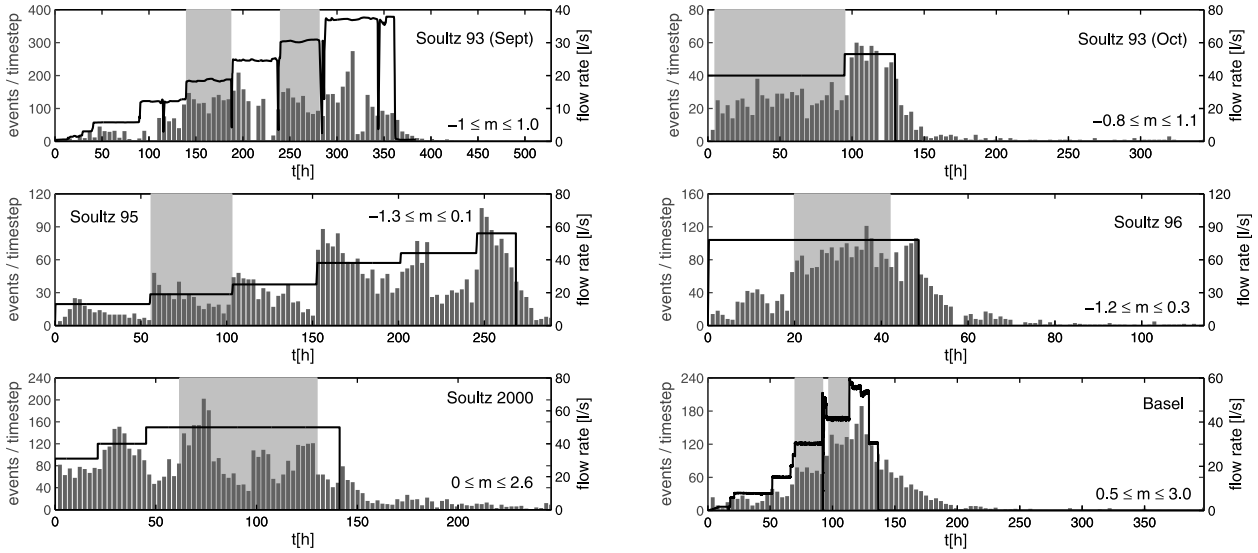

Figure 1. Rates of seismicity induced by borehole fluid injections (gray bars), flow rates (black lines) and selected stationary phases (gray areas). The minimum number of events in a stationary phase is 400. Except of the Soultz 93 (Sept) and the Basel case studies, flow rates are shown schematically. Time is given relative to the occurrence of the first event. Only events with magnitude larger than the magnitude of completeness are included in the catalogs. The magnitude ranges of events are shown in the lower right corners.

process (NHPP) in time. If the occurrence of fluid-injection-induced earthquakes can also be described in this way, the probability to induce n events by a fluid injection in the time interval $[0, t]$ can be calculated according to:

$$P(n, \lambda(t), t) = \frac{\left[\int_0^t \lambda(t')dt'\right]^n}{n!} \exp\left[-\int_0^t \lambda(t')dt'\right], \qquad (3)$$

where $\lambda(t)$ corresponds to the time dependent intensity of the process given by the seismicity rate. In Figure 3 we compare the IET distributions of the complete seismicity catalogs to IET distributions calculated for events simulated according to a NHPP with time dependent intensities corresponding to the seismicity rates shown in Figure 1. The probability density functions calculated from the simulated NHPP and the induced events coincide over the whole value range of Δt. Thus, the NHPP model can explain the distribution of fluid injection induced events in time.

4. Inter Event Volume

[6] The temporal distribution of fluid-injection-induced seismicity is given by a NHPP in all six case studies. We now analyze why the Poisson process is inhomogeneous, that is, why the intensity of the process is changing with time. We start with a comparison to naturally triggered seismicity.

[7] A frequently used statistical model for the process of earthquake occurrence is the Epidemic Type Aftershock Sequence (ETAS) model [see, e.g., *Ogata*, 1998]. According to the ETAS model the seismicity consists of independent background events and aftershocks. Background events are directly triggered by tectonic loading. They are distributed according to a HPP in time, because the tectonic loading rate is approximately constant. In contrast, aftershocks are caused by the occurrence of a background event. Each aftershock again has a certain probability to trigger its own aftershocks and so on. This leads to nested aftershock sequences that result in seismicity rate (intensity) changes and thus are the cause of inhomogeneities. Based on this idea we build a similar model for the case of fluid-injection-induced seismicity. To avoid misunderstandings we note that at all analyzed injection locations the background seismicity caused by tectonic loading is vanishing small. For example in Basel the background rate is $\lambda_b = 3.38 * 10^{-4}$ *ev/day*

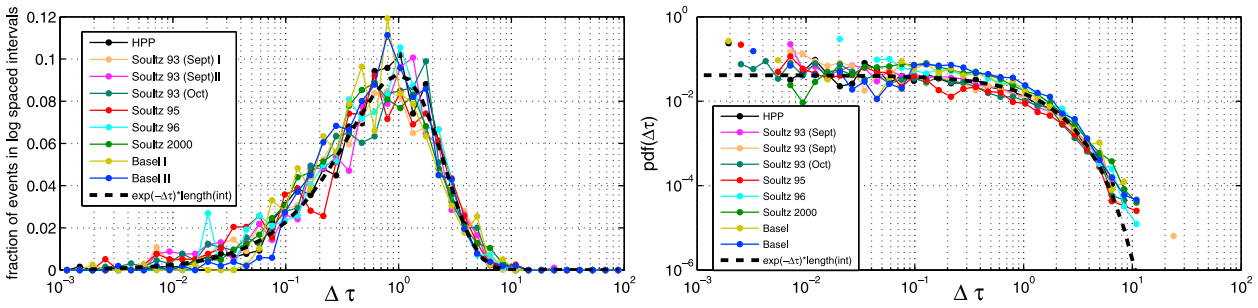

Figure 2. Inter event time analysis during stationary phases (see Figure 1). (left) Fraction of normalized IET falling in the log spaced intervals of $\Delta\tau$. (right) Probability density functions of $\Delta\tau$.

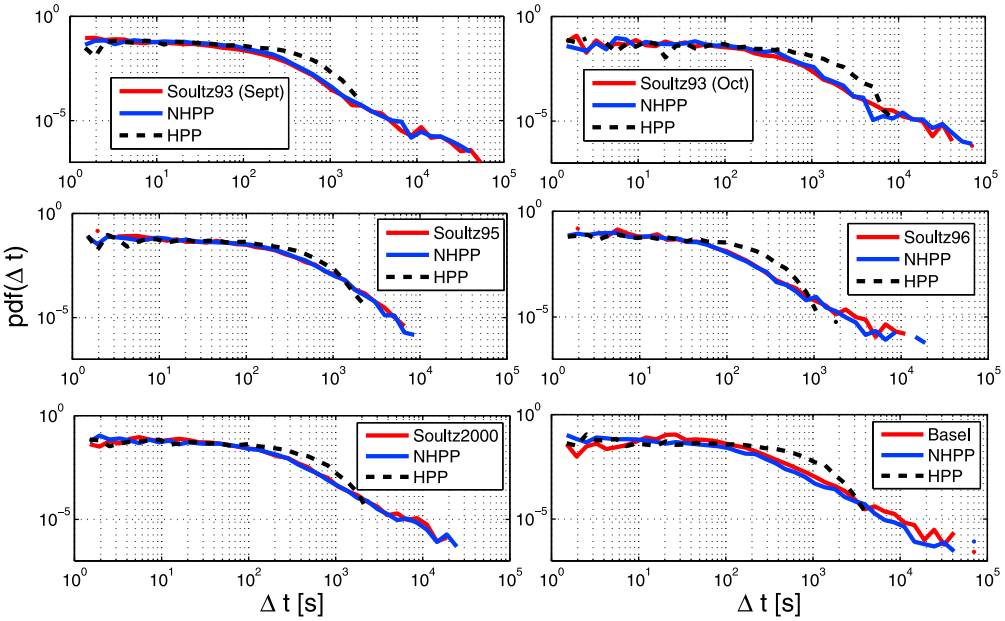

Figure 3. The $pdf(\Delta\tau)$ of the complete catalogs as shown in Figure 1 (red) and $pdf(\Delta\tau)$ of events simulated according to a NHPP (blue). The dashed black line corresponds to the PDF resulting from events simulated according to a HPP.

[*Bachmann et al.*, 2011]. It means that all events included in the catalogs are a consequence of the injection of fluids and not of tectonic loading. The analogue to the tectonic loading rate in the fluid-injection-induced case is given by the applied injection flow rate. The intensity of independent background events should hence be proportional to the flow rate. Indeed it has been shown by *Shapiro and Dinske* [2009] that the cumulative number of events induced by a fluid injection will be proportional to the cumulative fluid volume injected into the borehole, if the flow rate is a non decreasing function. We therefore consider the process of event occurrence in the injection-volume domain and analyze the inter event volume (IEV) ΔV, that is, the fluid volume injected between the occurrence of successive events. The cumulative number of events in the time domain is given by $N_{ev}(t) = C_1 Q_c(t)$, with $Q_c(t)$ the cumulative fluid volume injected until the time t and C_1 a constant characterized by the seismo-tectonic state at the injection region [see *Shapiro et al.*, 2010]. By transferring this expression to the volume domain we obtain $N_{ev}(Q_c) = \lambda_V Q_c$. If the process of event occurrence is a HPP in the volume domain, λ_V corresponds to the expected number of events per injected unit volume. The probability to induce n events by injection of a fluid volume Q_c is then given by:

$$P(n, \lambda_V, Q_c) = \frac{(\lambda_V Q_c)^n}{n!} e^{-\lambda_V Q_c}, \tag{4}$$

with corresponding PDF of normalized IEV $\Delta V_n = \Delta V \lambda_V$:

$$pdf(\Delta V_n) = e^{-\Delta V_n}. \tag{5}$$

Figure 4 shows the distribution of ΔV_n for the six case studies. All events induced during injection of fluid have been analyzed. Apart from negligible deviations all PDF coincide with the exponential PDF of the HPP (equation (5)). Successively occurring events are hence not causally related to each other or this relation is very weak. Thus, intensity (seismicity rate) changes are dominantly caused by flow rate (loading rate) changes and not by the occurrence of aftershocks. Figure S1 in the auxiliary material supports this finding. It shows that even the strongest events in the Basel catalog leave no signatures in the seismicity rate.[1]

[8] Note, that we do not consider events occurring after termination of fluid injections in our analysis of IEV to make the results as clear as possible. Because during an injection with non decreasing flow rates the complete fluid flow inside the reservoir contributes to the triggering process of seismic events, the number of induced events is proportional to the applied flow rate. If the injection of fluid is terminated, the fluid flow inside the reservoir that contributes to the triggering process is limited to the reservoir volume characterized by a non decreasing flow [see *Parotidis and Shapiro*, 2004]. This limitation results not in an immediate drop down of directly triggered events to zero but in a decrease of the intensity analogously to Omori's law [see *Langenbruch and Shapiro*, 2010]. The a priori assumption of a constant background rate in the time domain is hence not reasonable if flow rates are not constant or if events after injection termination are analyzed.

5. Nearest Neighbor Analysis

[9] The inter event volume analysis resulted in an exponential distribution implying that successively occurring events are not causally related to each other. However, there are two possible explanations for our finding. First, all events could be triggered by the loading caused by the injection of fluid. In this case, fluid-injection-induced seismicity consists only of independent background seismicity distributed according to a HPP in the injection-volume domain. The stress perturbation caused by the occurrence of

[1] Auxiliary materials are available in the HTML. doi:10.1029/2011GL049474.

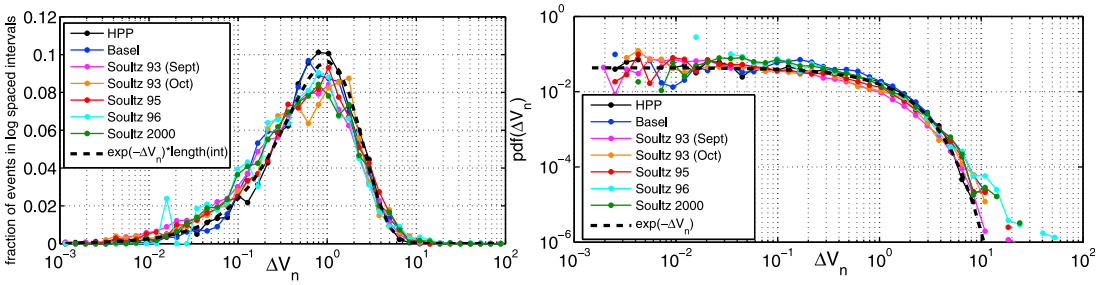

Figure 4. Inter event volume analysis. (left) Fraction of normalized IEV falling in the log spaced intervals of ΔV_n. (right) Probability density functions of ΔV_n.

a background event would then not be sufficient to trigger aftershocks. Alternatively, *Touati et al.* [2011] argue based on the ETAS model that, in case of a high background rate, aftershock sequences triggered by different background events may overlap in time. Because the background events are independent (HPP),events from different aftershock sequences, which may be successive in the complete catalog, are also independent.

[10] To investigate whether aftershock sequences are hidden in the catalogs we consider also the spatial distance between events and perform a nearest neighbor analysis in the time-space-magnitude domain. The time-space-magnitude distance between two events i and j is defined as [see *Zaliapin et al.*, 2008]:

$$n_{ij} = t_{ij} r_{ij}^{d} 10^{-b(m_i)}. \quad (6)$$

Here $t_{ij} = t_i - t_j$ is the inter event time, r_{ij} the inter event distance, d the fractal dimension of earthquake hypo-centers, m_i the magnitude of the event with index i and b the b-value of the Gutenberg-Richter relation. We replace t_{ij} in equation (6) by the fluid volume ΔV_{ij} injected between events i and j to achieve a homogeneous flow of events. Two events i and j are defined as nearest neighbors if their distance is given by: $\eta_j = \min_i n_{ij}$.

[11] In Figure 5 we examine the magnitude normalized volume and space components of the nearest neighbor distance η, namely $V = \Delta V_{ij}\ 10^{-bm_i/2}$ and $R = r_{ij}^{d}\ 10^{-bm_i/2}$. Examples are shown for (a) the Basel case study (b) randomly selected events of the Basel case study used as background events for (c) a ETAS simulation (see Appendix). *Zaliapin et al.* [2008] demonstrate that two distinct clusters appear if the event catalog contains two different classes of events. The first cluster around the line of $\log_{10}(V) + \log_{10}(R) =$

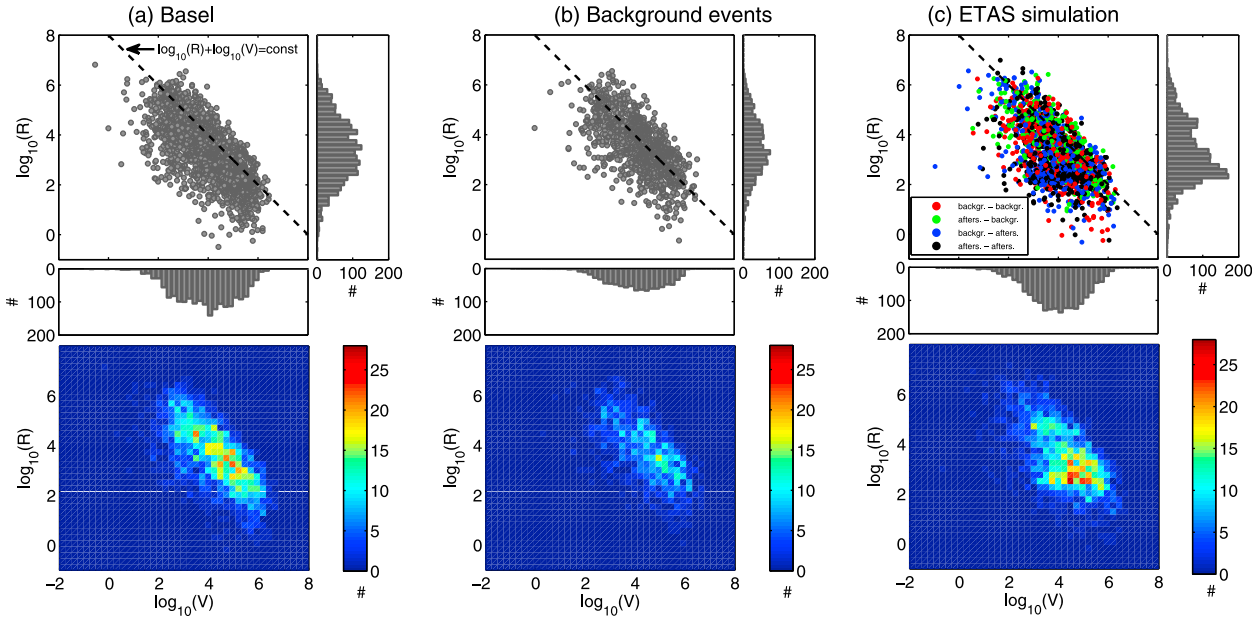

Figure 5. Space and volume components R and V of the nearest neighbor distances η for events of (a) the Basel case study, (b) randomly selected events of the Basel case study used as background events for (c) the ETAS model simulation according to parameters of the Basel case study (see Appendix). The lower panels show the density of points plotted in the panels above. In addition histograms of the space and volume components are shown. The color coding in Figure 5c indicates the type of events that build a nearest neighbor pair. A fractal dimension of hypocenters $d = 2.6$ is assumed.

const corresponds to stationary but possibly space-inhomogeneous Poisson seismicity, whereas a second cluster around $\log_{10}(R) \approx const$ corresponds mainly to aftershock clustering. We observe that the components in Figure 5a form a single cluster around the line of $\log_{10}(V) + \log_{10}(R) = const$, indicating Poisson seismicity. In case Figure 5b we observe no changes in the relative distribution of the volume and space components. The data set shown in Figure 5c the ETAS simulation contains a significant number of aftershocks. While the synthetically added aftershocks leave no signatures in the volume component a clustering at low values of the space component is visible. This shows that if a significant number of aftershocks would be present in the Basel data signatures should be identifiable in the space component of the nearest neighbor distance. However, Figure 5c also illustrates that due to the high occurrence rate of events in time/volume the cluster build by causally related event pairs (background-aftershock (blue) and aftershock-aftershock (black)) tend to some extend into the Poisson cluster (background-background (red) and aftershock-background (green)) making a clear classification of events as background events and aftershocks impossible. Nevertheless, as shown in Figure 5a no signs of aftershock triggering are identifiable from the nearest neighbor analysis for the induced seismicity in Basel. This analysis confirms that aftershock triggering is not significant for the Basel case study.

6. Conclusions

[12] We observe that the inter event time distribution of fluid-injection-induced earthquakes for six catalogs collected at geothermal injection sites at Soultz-sous-Forêts and Basel during phases of constant seismicity rate coincides with the exponential waiting time distribution of the HPP. This implies that successively occurring events are not causally related to each other. The waiting times for the complete event catalogs are distributed according to a NHPP in time. Our finding that the occurrence of events is given by a HPP in the volume domain strongly supports the idea that, in contrast to naturally triggered earthquakes, seismicity rate changes are primarily related to changes of the injection flow rate and not to the occurrence of aftershocks.

[13] The nearest neighbor analysis has revealed no signs of causal relationships between fluid-injection-induced events. The absence of aftershock signatures can be to some extend related to the high occurrence rate of earthquakes in space and time. However, the comparison to the ETAS model shows that, if a significant number of causally related events would be present, signatures should be identifiable by the nearest neighbor analysis. Therefore, coupling effects between events are weak. Our results demonstrate that the Poisson model can be applied to calculate occurrence probabilities of fluid-injection-induced earthquakes for seismic hazard assessment.

Appendix A

[14] We briefly explain the ETAS simulation method used to build the synthetic catalog analyzed in Figure 5c. First, we randomly select 50% of the Basel events occurring during injection of fluid. By randomly selecting the events we break a part of possibly existing causal relations. The selected events are used as background events in the ETAS simulation. We calculate the occurrence of aftershocks corresponding to the conditional intensity function $\lambda(t)$ of the ETAS model [see *Ogata*, 1998] given by:

$$\lambda(t) = \lambda_b(t) + A \sum_{i:t<t_i} \exp[\alpha(m_i - m_0)] \left(1 + \frac{t - t_i}{c}\right)^{-p}, \quad \text{(A1)}$$

where $\lambda_b(t)$ is the time dependent temporal intensity of background events randomly chosen from the Basel catalog, p, c and $A = K/c^p$ are the parameters of the Omori law, α is the productivity parameter and m_0 is the magnitude of completeness. The second part of equation (A1) describes the probability of aftershock occurrence based on the history of event occurrence. The magnitudes of aftershocks are independently chosen from the Gutenberg-Richter distribution derived from the Basel catalog. To determine the location of an aftershock we first calculate the source radius r_s of each event according to *Brune* [1970] and *Kanamori* [1977], as function of moment magnitude M_w and stress drop $\Delta\sigma$:

$$r_s = \sqrt[3]{\frac{7}{16} \frac{10^{1.5M_w + 9.1}}{\Delta\sigma}}. \quad \text{(A2)}$$

A probable aftershock is located on a spherical shell with radius r_s around the mother event. Each position on the shell has the same probability to be the location of an aftershock. For the simulation we apply the following parameters derived from the Basel injection: $\Delta\sigma = 2.3$ *MPa* [*Goertz-Allmann et al.*, 2011], $m_0 = 0.45$, $b = 1.5$ and classical parameters of the Omori law [see, e.g., *Touati et al.*, 2011]: $A = 10\frac{1}{day}$, $p = 1.2$, $c = 0.01$ *days*. We use a productivity parameter $\alpha = 1.3$ for simulation, because this choice results in an consistent number of events in the simulated and the real earthquake catalog.

[15] **Acknowledgments.** We thank the Federal Ministry for the Environment, Nature Conservation and Nuclear Safety as a sponsor of the project MAGS and the sponsors of the PHASE consortium project for supporting the research presented in this paper. Furthermore, we thank A. Jupe for provision of the Soultz data sets. The Basel data are kindly provided by M. Häring and are courtesy of Geothermal Explorers.

[16] The Editor thanks Mark Naylor and an anonymous reviewer for their assistance in evaluating this paper.

References

Bachmann, C. E., S. Wiemer, J. Woessner, and S. Hainzl (2011), Statistical analysis of the induced Basel 2006 earthquake sequence: Introducing a probability-based monitoring approach for Enhanced Geothermal Systems, *Geophys. J. Int.*, *186*, 793–807, doi:10.1111/j.1365-246X.2011.05068.x.

Bak, P., K. Christensen, L. Danon, and T. Scanlon (2002), Unified scaling law for earthquakes, *Phys. Rev. Lett.*, *88*, 178501, doi:10.1103/PhysRevLett.88.178501.

Baria, R., J. Baumgärtner, A. Gerard, R. Jung, and J. Garnish (1999), European HDR research programme at Soultz-sous-Forêts (France) 1987–1996, *Geothermics*, *28*, 655–669, doi:10.1016/S0375-6505(99)00036-X.

Brune, J. N. (1970), Tectonic stress and the spectra of seismic shear waves from earthquakes, *J. Geophys. Res.*, *75*, 4997–5009, doi:10.1029/JB075i026p04997.

Corral, A. (2006), Dependence of earthquake recurrence times and independence of magnitudes on seismicity history, *Tectonophysics*, *424*, 177–193, doi:10.1016/j.tecto.2006.03.035.

Goertz-Allmann, B. P., A. Goertz, and S. Wiemer (2011), Stress drop variations of induced earthquakes at the Basel geothermal site, *Geophys. Res. Lett.*, *38*, L09308, doi:10.1029/2011GL047498.

Häring, M. O., U. Schanz, F. Ladner, and B. C. Dyer (2008), Characterisation of the Basel 1 enhanced geothermal system, *Geothermics*, *37*, 469–495, doi:10.1016/j.geothermics.2008.06.002.

Kanamori, H. (1977), The energy release in great earthquakes, *J. Geophys. Res.*, *82*, 2981–2987.

Langenbruch, C., and S. A. Shapiro (2010), Decay rate of fluid-induced seismicity after termination of reservoir stimulations, *Geophysics*, *75*, MA53-MA62, doi:10.1190/1.3506005.

Ogata, Y. (1998), Space-time point-process models for earthquake occurrences, *Ann. Inst. Stat. Math.*, *50*, 379–402, doi:10.1023/A:1003403601725.

Parotidis, M., and S. A. Shapiro (2004), A statistical model for the seismicity rate of fluid-injection-induced earthquakes, *Geophys. Res. Lett.*, *31*, L17609, doi:10.1029/2004GL020421.

Shapiro, S. A., and C. Dinske (2009), Scaling of seismicity induced by nonlinear fluid-rock interaction, *J. Geophys. Res.*, *114*, B09307, doi:10.1029/2008JB006145.

Shapiro, S. A., C. Dinske, C. Langenbruch, and F. Wenzel (2010), Seismogenic index and magnitude probability of earthquakes induced during reservoir fluid stimulations, *Leading Edge*, *29*, 304–309, doi:10.1190/1.3353727.

Shcherbakov, R., G. Yacolev, D. L. Turcotte, and J. B. Rundle (2005), Model for distribution of aftershocks interoccurence times, *Phys. Rev. Lett.*, *95*, 218501, doi:10.1103/PhysRevLett.95.218501.

Toda, S., R. S. Stein, P. A. Reasenberg, J. H. Dieterich, and A. Yoshida (1998), Stress transferred by the 1995 m_w = 6.9 Kobe, Japan, shock: Effect on aftershocks and future earthquake probabilities, *J. Geophys. Res.*, *103*, 24,543–24,565, doi:10.1029/98JB00765.

Touati, S., M. Naylor, I. G. Main, and M. Christie (2011), Masking of earthquake triggering behavior by a high background rate and implications for epidemic-type aftershock sequence inversions, *J. Geophys. Res.*, *116*, B03304, doi:10.1029/2010JB007544.

Zaliapin, I., A. Gabrielov, V. Keilis-Borok, and H. Wong (2008), Clustering analysis of seismicity and aftershock identification, *Phys. Rev. Lett.*, *101*, 018501, doi:10.1103/PhysRevLett.101.018501.

C. Dinske, C. Langenbruch, and S. A. Shapiro, Fachrichtung Geophysik, Freie Universität Berlin, D-12249 Berlin, Germany.

Auxiliary material for Paper 2011GL049474

The Auxiliary material contains one Figure file. The Figure shows the influence of the strongest events of the Basel case study on the seismicity rate.

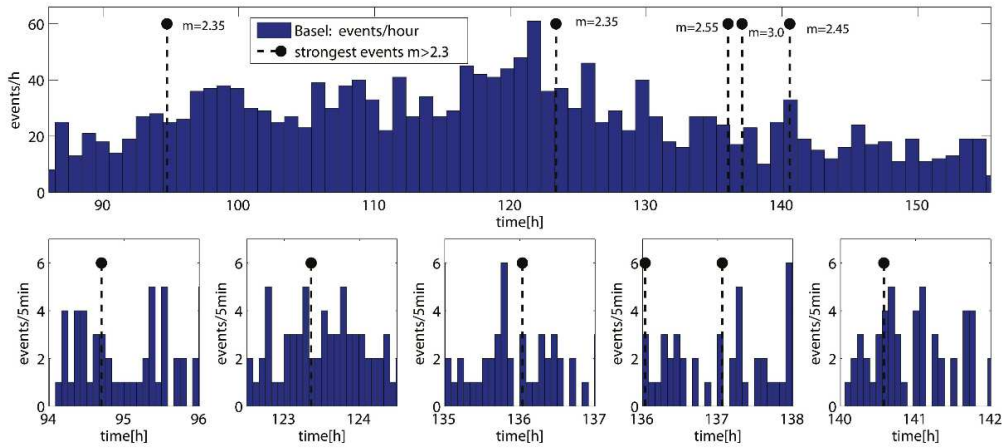

Figure S1: Seismicity rate around the strongest events of the Basel case study (For the complete catalog see Figure 1). The lower panels show a zoomed view around the occurrence times of the strongest events. No visible seismicity rate changes occur due to the occurrences of the events.

Chapter 5

Gutenberg-Richter relation originates from Coulomb stress fluctuations caused by elastic rock heterogeneity[1]

Key points:

- Elastic rock heterogeneity causes strong Coulomb stress fluctuations of power law type
- The Gutenberg-Richter law results from power law fluctuations of Coulomb stress
- Because of the universal fractal nature of elastic heterogeneity, the b-value is universal
- Deviations from the universal value of b=1 occur due to characteristic scales of seismogenic processes causing changes or limitations of fractal scaling

[1]This article has been published in Journal of Geophysical Research Solid Earth: C. Langenbruch and S.A. Shapiro (2014). Gutenberg-Richter relation originates from Coulomb stress fluctuations caused by elastic rock heterogeneity. http://dx.doi.org/10.1002/2013JB010282. Published by John Wiley & Sons, Ltd on behalf of American Geophysical Union (AGU).

AGU PUBLICATIONS

JGR

Journal of Geophysical Research: Solid Earth

RESEARCH ARTICLE

10.1002/2013JB010282

Key Points:
- Elastic heterogeneity causes strong Coulomb stress fluctuation of power law type
- Gutenberg-Richter relation results from power law fluctuations of Coulomb stress
- Universal fractal nature of elastic heterogeneity suggests a universal b value

Correspondence to:
C. Langenbruch,
Cornelius@geophysik.fu-berlin.de

Citation:
Langenbruch, C. and S. A. Shapiro (2014), Gutenberg-Richter relation originates from Coulomb stress fluctuations caused by elastic rock heterogeneity, *J. Geophys. Res. Solid Earth*, *119*, doi:10.1002/2013JB010282.

Received 12 APR 2013
Accepted 19 JAN 2014
Accepted article online 28 JAN 2014

Gutenberg-Richter relation originates from Coulomb stress fluctuations caused by elastic rock heterogeneity

C. Langenbruch[1] and S. A. Shapiro[1]

[1]Fachrichtung Geophysik, Freie Universität Berlin, Berlin, Germany

Abstract Based on measurements along boreholes, a characterization of the Earth's crust elastic heterogeneity is presented. We investigate its impact on Coulomb stress distribution and earthquake magnitude scaling. The analysis of elastic modulus distribution at various borehole locations in different regions reveals universal fractal nature of elastic heterogeneity. By applying a homogeneous far-field stress to a representative model of elastic rock heterogeneity, we show that it causes strong Coulomb stress fluctuations. In situ fluctuations of Coulomb stress are mainly controlled by in situ elastic moduli. Fluctuations caused by surrounding heterogeneities are only of minor importance. Hence, the fractal nature of elastic heterogeneity results in Coulomb stress fluctuations with power law size distribution. As a consequence, fault sizes and magnitudes of earthquakes scale according to the Gutenberg-Richter relation. Due to the universal fractal nature of elastic heterogeneity, the *b* value should be universal. Deviation from its universal value of $b \approx 1$ occurs due to characteristic scales of seismogenic processes, which cause limitations or changes of fractal scaling. Scale limitations are also the reason for observed stress dependency of the *b* value. Our analysis suggests that the Gutenberg-Richter relation originates from Coulomb stress fluctuations caused by elastic rock heterogeneity.

1. Introduction

Sonic well logs provide in situ measurements of physical properties and their fluctuations in the Earth's crust. The analysis of collected log data has contributed to the characterization of elastic rock heterogeneity, since it proved its fractal nature [see, e.g., *Leary*, 1997; *Dolan et al.*, 1998; *Goff and Holliger*, 1999]. Stress measurements along boreholes show that stress in the Earth's crust shows significant spatial heterogeneity [see, e.g., *Brudy et al.*, 1997; *Hickman and Zoback*, 2004; *Day-Lewis et al.*, 2010]. Consistently, a stress inversion study using earthquake mechanisms by *Rivera and Kanamori* [2002] suggests that stress unlikely is uniform in orientation or magnitude. Moreover, results of stress orientation analysis from borehole breakouts argue for a fractal nature of existing stress fluctuations [*Day-Lewis et al.*, 2010]. Even though it is evident that elastic heterogeneity of rocks naturally results in a fluctuating stress field, its impact on stress in rocks has not yet been characterized. Does elastic heterogeneity have a significant influence on stress at all? If so, does the fractal distribution of elastic moduli cause stress variations with power law size distribution? This would be of great importance, since it has been shown that fractal fluctuations result in power law scaling of earthquake magnitudes, expressed by the Gutenberg-Richter relation [*Gutenberg and Richter*, 1954; *Huang and Turcotte*, 1988]. In this paper, we analyze relations between elastic rock heterogeneity, stress fluctuations, and the Gutenberg-Richter *b* value of earthquakes. We start with a characterization of the Earth's crust elastic heterogeneity by analyzing sonic logs along the Continental Deep Drilling Site (KTB) main hole. Using derived parameters of elastic modulus distribution, we simulate an elastically heterogeneous 3-D random medium characterized by a power spectrum of fluctuations of power law type. The simulated medium is statistically equivalent to the log data and represents the rock surrounding the borehole.

We apply an externally homogeneous far-field stress and compute stress fluctuations inside the model. The externally applied stress field is determined from smoothed stress profiles along the KTB main hole [see *Ito and Zoback*, 2000]. In the next section, we interpret the occurring stress fluctuations in terms of fracture strength variations by determining the distribution of Coulomb failure stress (CFS) as a measure of fracture strength in rocks. In the final part, we analyze the scaling behavior of fracture strength distribution represented by the CFS. *Aki* [1981] describes the assemblage of faults by the concept of fractals and shows that the Gutenberg-Richter relation is equivalent to a fractal distribution of fracture sizes. The power law exponent of fault size distribution is equivalent to the *b* value of earthquakes, describing the ratio between

small- and large-magnitude earthquakes. Assuming that rupturing, once it is initiated (e.g., by an increase in stress or pore pressure), takes place inside isosets of Coulomb failure stress (CFS $\leq$ constant), we determine the scaling exponent of resulting fracture sizes and compare it to the *b* value. To characterize solely the influence of measurement-based elastic rock heterogeneity, we restrict the analysis to a static view and exclude assumptions about dynamic interaction of fractures; that is, we neglect stress fluctuations caused by possible seismic events on corresponding critically stressed isosets. Our modeling of the stress distribution in 3-D heterogeneous elastic structures is a minimum-assumption first-principle approach. It takes into account any type of interaction (i.e., multiple scattering) between elastic heterogeneities.

Laboratory studies [*Mogi*, 1962; *Scholz*, 1968; *Amitrano*, 2003], observations [*Schorlemmer et al.*, 2005], and modeling [*Huang and Turcotte*, 1988] suggest that the *b* value is not universal. Generally, a positive relation to the degree of rock heterogeneity complexity and an inverse relation to the level of differential stress is observed. The fractal dimension of elastic modulus distribution can be related to the degree of material heterogeneity complexity, because it describes the relation between large- and small-scale correlated structures. Therefore, we investigate if the range of theoretically possible fractal dimensions of elastic heterogeneity can explain observed *b* value variations.

Day-Lewis et al. [2010] find that the scaling behavior of physical property heterogeneity derived from well logs is universal. We investigate the scaling behavior of elastic heterogeneity at different drilling sites to analyze if the scaling of elastic rock heterogeneity and resulting CFS fluctuations in our model can be considered as universally valid. Thereafter, we discuss the importance of the finding that the fractal dimension of elastic heterogeneity measured from well logs at various drilling sites seems to be universal. Finally, we analyze relations between stress level and *b* value resulting from our model and argue that deviation of the *b* value from its universal value of $b \approx 1$ results from characteristic scales of seismogenic processes, which cause limitations or changes of fractal scaling.

The analysis presented in this paper will lead to the following main findings: Elastic rock heterogeneity is of fractal nature and causes strong Coulomb failure stress fluctuations with power law size distribution. The fractal scaling of the Coulomb stress fluctuations, in turn, explains the emergence of earthquake magnitude scaling according to the Gutenberg-Richter relation. Because the fractal dimension of elastic heterogeneity, determined from log data at various drilling sites in different regions, is more or less universal, the *b* value should be universal. Deviations of the *b* value from its universal value of $b \approx 1$ result only from characteristic scales of seismogenic processes, which cause limitations or changes of fractal scaling. Scale limitations are also the reason for observed stress dependency of the *b* value. These findings are unaffected by instrumental and measurement effects on the fractal dimension, because we can expect a statistically similar impact at different analyzed locations. Hence, the universality issue should remain mainly untouched.

We start the analysis by characterizing elastic rock heterogeneity of the Earth's crust based on sonic log measurements.

2. Characterization of Elastic Heterogeneity in the Earth's Crust

In this section, we characterize elastic heterogeneity of the Earth's crust by analyzing sonic log data collected along the Continental Deep Drilling site KTB-1 main hole located in southeastern Germany [see, e.g., *Pechnig et al.*, 1997]. We evaluate the depth section between 4450 m and 6017 m in the crystalline basement. This section is selected for the analysis, because fluid injected during an injection operation in the year 2000 stimulated the rock formation at this depth and induced numerous seismic events [see *Baisch et al.*, 2002]. The occurrence of seismic events indicates that the state of stress in this depth section is close to a critical one causing brittle failure of rocks.

Figures 1a and 1b show shear (μ) and bulk (K) moduli computed from 4 m averaged *P* and *S* wave travel time and density logs along the KTB-1 main hole. We averaged the raw data (sampled at 0.152 m) in 4 m intervals to eliminate inherent averaging of the logging process over the active length of the tool ($\approx$ 1 m) and to reduce high-frequency noise. The distributions of μ and K with depth are highly heterogeneous. Two narrow layers of paragneisses cut the metabasitic basement in depth sections 5210–5310 m and 5540–5640 m [*Pechnig et al.*, 1997]. The moduli in these depth sections are characterized by lower mean values, resulting

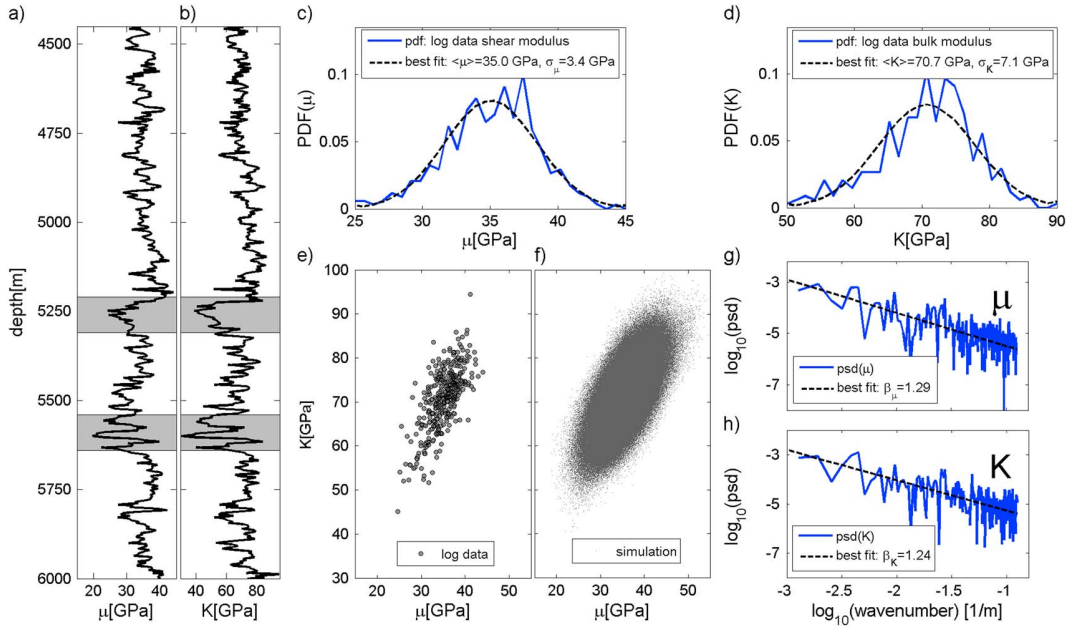

Figure 1. Characterization of elastic heterogeneity along the KTB main hole. (a, b) Shear and bulk moduli computed from 4 m averaged *P* and *S* wave travel time and density logs along the KTB-1 main hole. Grey shaded areas indicate gneiss layers [see *Pechnig et al.*, 1997], which we exclude from the analysis. (c, d) Probability density function (PDF) of μ and K obtained from Figures 1a and 1b. (e) Cross plot of μ and K values. (f) Cross plot of simulated random number pairs representing shear and bulk moduli. (g, h) Power spectral density function (PSDF) of μ and K log data.

in nonstationary statistics of the distribution. We exclude these layers from our analysis to ensure statistical stationarity of elastic parameter distribution.

We now determine the statistical parameters describing the distribution of shear and bulk moduli and create a random medium, which is statistically equivalent to the log data. This medium will represent the rock surrounding the borehole. Since we exclude the paragneiss layers from our analysis, the model will represent elastic heterogeneity occurring in one single type of rock. Figures 1c and 1d show the probability density functions (PDF) of shear and bulk moduli. We determine best fitting Gaussian distributions to obtain mean values ($< \mu >= 35.0$ GPa, $< K >= 70.7$ GPa) and standard deviations ($\sigma_\mu = 3.4$ GPa, $\sigma_K = 7.1$ GPa). Similarities between the distributions of μ and K with depth are visible in the logging data (see Figures 1a and 1b). This indicates a positive relation between both moduli. To analyze this relation in more detail, we present a cross plot of μ and K in Figure 1e. The moduli indeed show a positive relation, which we quantify by calculating Pearson's correlation coefficient Pc given by the covariance of μ and K divided by the product of their standard deviations. The moduli show a strong positive correlation quantified by $\mathrm{Pc}_{\mu,K} = 0.64$. We then apply the obtained mean values, standard deviations, and the correlation coefficient to simulate correlated random number pairs representing bulk and shear moduli. A cross plot of simulated moduli is presented in Figure 1f. Random assignment to a 3-D medium consisting of $100 \times 100 \times 100$ equally sized cells results in two related spatially uncorrelated media (see Figure 2a). These media represent the distribution of elastic moduli in space.

However, real rocks show spatial correlations of elastic properties. Data analysis from various drilling sites suggests unbounded fractal scaling of the Earth's crust heterogeneity. This is expressed in power law ($k^{-\beta}$) dependence of the log data's power spectra on the wave number k [*Leary*, 1997]. The scaling exponent β is given by

$$\beta = 2H + E, \tag{1}$$

where E is the Euclidean dimension and H is the Hurst exponent, which can be related to the fractal dimension D of the log data by [see, e.g., *Dolan et al.*, 1998]

$$D = (E + 1) - H. \tag{2}$$

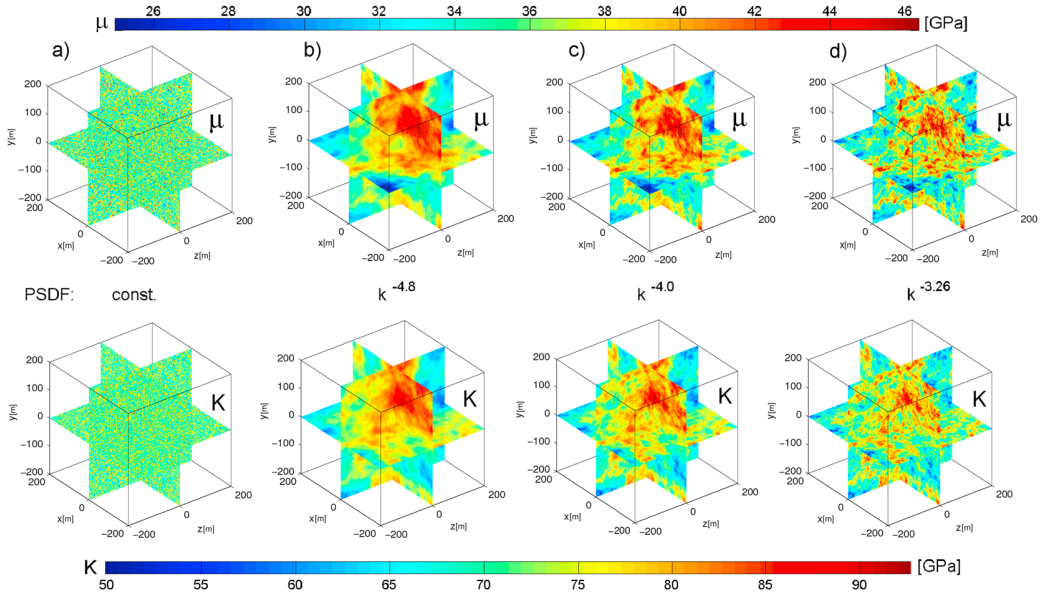

Figure 2. Random medium realizations. (a) Related spatially uncorrelated media representing shear (top) and bulk (bottom) moduli. The media result from a random assignment of simulated shear and bulk modulus pairs shown in Figure 1f. The spatial correlation according to a PSDF of power law type results in media with fractal dimension of (b) $D_{\mu,K} = 3.1$, (c) $D_{\mu,K} = 3.5$, and (d) $D_{\mu,K} = 3.87$. The media shown in Figure 2d represent the rock surrounding the KTB-1 borehole and are used for further modeling. The figure shows that the fractal dimension D is a measure for the degree of rock heterogeneity complexity.

In general, H can show values in the range $0 \leq H \leq 1$. Roughness of a fractal distribution is related to H, where higher values of H correspond to smoother distributions.

The power spectral densities of shear and bulk modulus logs at the KTB (see Figures 1g and 1h) possess power law dependence on the wave number in the complete range. Power law exponents β, which are determined by the slope of the power spectral density in the double logarithmic representation (Figures 1g and 1h), are given by $\beta_\mu = 1.29$ ($H_\mu = 0.145$) for shear modulus and $\beta_K = 1.24$ ($H_K = 0.12$) for bulk modulus. Because these values are obtained from 1-D sonic logs, the Euclidean dimension of a line ($E = 1$) is used for computation of the Hurst exponents according to equation (1). The low values of H are in agreement with observations of *Day-Lewis et al.* [2010]. They observe that a power law exponent of $\beta \approx 1$ is typical for physical property scaling derived from sonic well logs at various sites. The observed low values of H stand for a high degree of heterogeneity complexity of elastic properties.

We now use the determined Hurst exponents to spatially correlate the simulated distributions of μ and K shown in Figure 2a. Because the power law exponents of K and μ can be considered as equivalent, we apply fractal scaling according to a Hurst exponent $H = 0.13$ to both media. The value of $H = 0.13$ corresponds to the mean value of H_μ and H_K. Since we do not have any information about elastic property scaling in horizontal direction, we assume that Hurst exponents in vertical and horizontal direction are the same. Even though the Hurst exponent in sedimentary rocks may vary from vertical to horizontal direction, it should be approximately equal in the granite basement. Spatial correlation is obtained by filtering the media in the wave number domain. More precisely, the Fourier transforms of spatially uncorrelated shear and bulk modulus distributions are multiplied by the square root of the fractal power spectral density function $\mathrm{PSDF}(k) = k^{-\beta}$, in the wave number domain, where $k = \sqrt{k_x^2 + k_y^2 + k_z^2}$ is the wave number. Since we assign a distribution to a 3-D medium, the Euclidean dimension is given by $E = 3$. Considering the relation of $\beta = 2H + E$ and the computed Hurst exponent of $H = 0.13$, we apply a power law exponent of $\beta = 3.26$ to spatially correlate the media. By taking the inverse Fourier transform, we obtain the fractal random media in the spatial domain. Considering the relation $D = (E + 1) - H$, the resulting distributions of μ and K (see Figure 2d) are characterized by a fractal dimension of $D_{\mu,K} = 3.87$.

The simulated media (see Figure 2d) are representing the distribution of μ and K around the borehole, because they are statistically equivalent to the log data; that is, they show the same mean values, standard

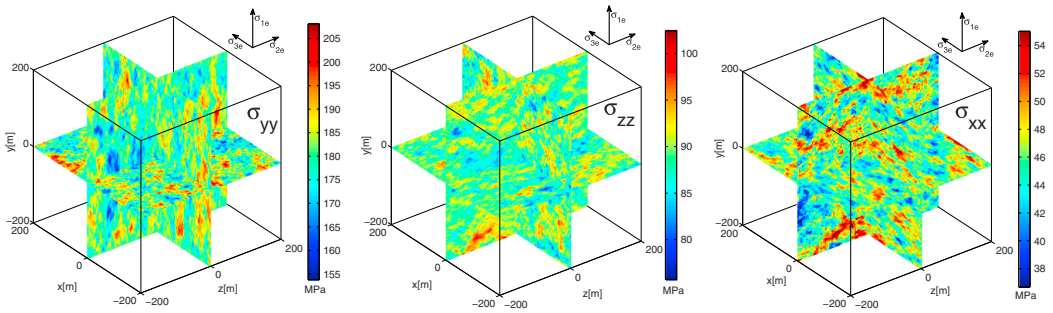

Figure 3. Stress modeling results: Normal stress component in $y(\sigma_{1e})$, $z(\sigma_{2e})$, and $x(\sigma_{3e})$ directions. The color bars are scaled to $\pm 20\%$ of the externally applied stresses. The directions of externally applied principal stresses are shown at the top of the figures. Due to elastic heterogeneity, stress strongly fluctuates inside the medium.

deviations, and correlation coefficient between K and μ. Moreover, the values along any 1-D profile in the simulated media possess a fractal dimension of 1.87 ($H = 0.13$), which is equivalent to the fractal dimension of the log data. In general, the fractal dimension of a distribution applied to a 3-D medium ($E = 3$) is in the range of $3 \leq D \leq 4$. This becomes clearer by considering that the fractal dimensions of a distribution applied to a line ($E = 1$), for instance, well log data, can possess fractal dimensions of $1 \leq D \leq 2$.

Again, we note that fields of elastic properties are heterogeneously distributed in the real three-dimensional space ($E = 3$) by their power spectra (i.e., their spatial correlation functions). These fields represent fractals in a space of the embedding dimension 4. The fourth dimension is given by the color in our figures. Corresponding fractals have fractal dimension between 3 and 4. The fractal dimension of the media simulated according to the well log data along the KTB main hole are characterized by a fractal dimension of $D_{\mu,K} = 3.87$. Figures 2b and 2c show fractal media characterized by lower fractal dimensions of $D_{\mu,K} = 3.1$ and $D_{\mu,K} = 3.5$, respectively. The figure illustrates that the fractal dimension describes the relation of small- to large-scale structures and can be related to the degree of rock heterogeneity complexity.

3. Stress Fluctuations in Elastically Heterogeneous Rocks

In this section, we analyze stress fluctuations resulting from elastic rock heterogeneity and establish relations between stress fluctuations and elastic properties. Therefore, the medium realization of elastic moduli (Figure 2d) is used as input to a finite element stress analysis model. We use the commercial software package ABAQUS. An externally homogeneous far-field stress is applied to determine the distribution of stress inside the elastically heterogeneous rock model. Compressive stresses are always defined positive in the following. We consider smoothed stress profiles reported by *Ito and Zoback* [2000]: $S_H = 0.045$ MPa/m, $S_V = 0.028$ MPa/m, and $S_h = 0.02$ MPa/m. The stress profiles are derived from hydraulic fracturing tests, breakouts, and drilling-induced fractures along the KTB main hole. A strike-slip stress regime is prevailing, and the differential stress is increasing with depth [*Brudy et al.*, 1997]. We calculate effective principal stresses, considering a hydrostatic pore pressure gradient of 0.0115 MPa/m, reported by *Huenges et al.* [1997] along the KTB main hole up to a depth of 9.1 km. The principal stress components of the externally applied stress field are defined at the corresponding boundary surfaces of the model medium as follows: $\sigma_{1e} = 180.9$ MPa $= \sigma_{yy}$, $\sigma_{2e} = 89.1$ MPa $= \sigma_{zz}$, and $\sigma_{3e} = 45.9$ MPa $= \sigma_{xx}$. These values correspond to maximum horizontal, vertical, and minimum horizontal effective principal stresses at a depth of 5.4 km. Again, we note that we consider this depth since a fluid injection in the year 2000 induced seismic events in this depth range. By evaluation of the ABAQUS model, we obtain the full stress tensor in each model cell. Figure 3 shows the resulting normal stress components in $y(\sigma_{1e})$, $z(\sigma_{2e})$, and $x(\sigma_{3e})$ directions. In the case of an elastically homogeneous medium the stress components would coincide with the externally applied stresses σ_{1e}, σ_{2e}, and σ_{3e} in all cells of the model. It means that the stress inside a homogeneous medium is independent of the elastic properties of the medium. However, as soon as the medium becomes elastically heterogeneous, stress fluctuations occur, which are controlled by the deviations of elastic properties from their mean values. We find that elastic heterogeneity has a significant influence on stress magnitudes, which vary by up to more than $\pm 20\%$ of the externally applied stresses. We note that the directions of

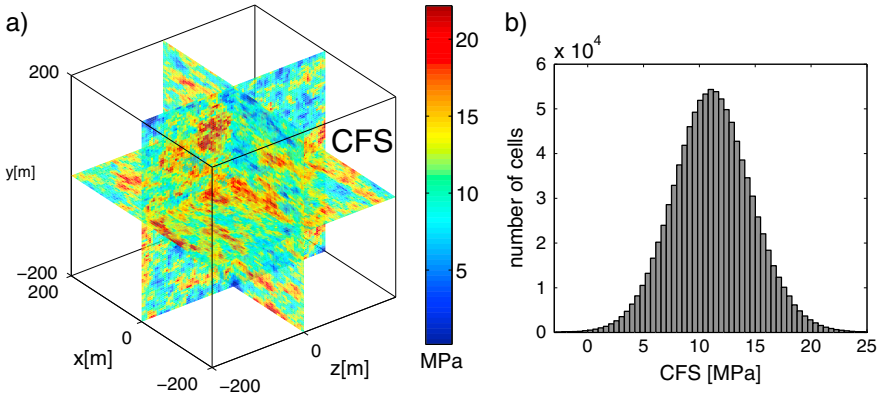

Figure 4. (a) Spatial distribution of Coulomb failure stress resulting from elastic heterogeneity derived from the KTB-1 main hole. (b) Histogram of CFS. Elastic heterogeneity of rocks causes Coulomb stress fluctuations of significant magnitude.

normal stresses shown in Figure 3 do not exactly correspond to principal stress directions. We find that due to elastic heterogeneity the orientation of principal stresses show small variations up to $\pm 6°$.

4. Fluctuations of Rock Strength

We now analyze the influence of elastic heterogeneity on fracture strength of rocks. The strength of fractures can be described by the Coulomb failure stress (CFS) associated with the Mohr Coulomb failure criterion according to the following [see, e.g., *Jaeger et al.*, 2007]:

$$\mathrm{CFS} = -\tau + \mu(\sigma_n - p_p) + S_0, \tag{3}$$

where τ and σ_n are shear and normal stress acting on the fault plane. S_0 is the cohesion, that is, the shear stress necessary to initiate failure in absence of normal stress, p_p is the pore pressure, and μ is the coefficient of internal friction. A fault is in a stable state if $\mathrm{CFS} > 0$. A fault is unstable if $\mathrm{CFS} \leq 0$, and failure occurs if $\mathrm{CFS} = 0$. We assume that the rock is able to fail in optimal orientation for failure in each model cell. It means that each cell can be considered as the location of a fracture optimally oriented for failure. Furthermore, we assume a friction coefficient of $\mu = 0.9$ and cohesionless fractures ($S_0 = 0$). To analyze solely the result of measurement-based elastic rock heterogeneity on fracture strength, we keep friction and cohesion constant in all model cells. Moreover, this is done because no direct measurements of heterogeneity of these parameters are available. Using the computed principal stresses in the individual model cells, we determine shear and normal stress acting on optimal oriented fractures and resulting CFS according to equation (3). We note that due to the rotations of principal stress components in the medium, the optimal orientation for failure in the coordinate system of externally applied stresses is not exactly the same in all model cells.

Figure 4 shows resulting spatial distribution and histogram of computed CFS. We find that elastic heterogeneity causes significant CFS variations. Some parts of the medium are in direct vicinity to failure, suggesting that already very small stress or pore pressure perturbations may cause brittle failure in rocks. This finding is confirmed by observed fluid-injection-induced seismicity [see *Baisch et al.*, 2002] and natural seismic activity in the vicinity of the KTB [see *Dahlheim et al.*, 1997]. Nevertheless, in the most stable parts of the model CFS perturbations of up to 20 MPa are needed to initiate failure. This range of fracture strength is in agreement with rock strength reconstructed from microseismicity in sedimentary and crystalline rocks [*Rothert and Shapiro*, 2007]. Figure 5 shows a cross plot of bulk and shear modulus pairs that where assigned to the model cells. The input is color coded according to the resulting CFS in the corresponding cells. The figure illustrates that in situ elastic moduli, stress, and fracture strength fluctuations are strongly related. It has been shown that an elastic heterogeneity causes stress fluctuations not only inside but also around itself [see, e.g., *Eshelby*, 1957, 1959]. Hence, stress fluctuations caused by elastic rock heterogeneity should only follow the same power law scaling as elastic rock heterogeneity if the stress in a given point is solely controlled by in situ elastic properties. Taking into account the distinct tendency of the color coding in

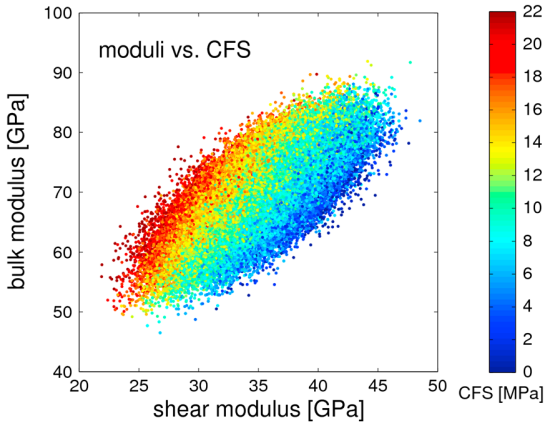

Figure 5. Cross plot of elastic input moduli of stress modeling. The markers are color coded according to the CFS in the corresponding cells. A clear relation between elastic input parameters and the Coulomb stress fluctuations is visible by the distinct trend of color coding. In situ Coulomb stress is mainly controlled by in situ elastic moduli. Stress changes caused by surrounding heterogeneities are existent and visible by the scatter in the tendency of color coding. However, this effect seems to be only of minor importance.

Figure 5, it becomes clear that in situ stress is mainly controlled by in situ elastic moduli, where the strength of CFS fluctuation is controlled by the deviation of elastic properties from their mean values. Stress changes caused by surrounding heterogeneities are existent and visible by the scatter in the tendency of color coding. However, this effect seems to be only of minor importance. In general, cells characterized by a low bulk modulus and a high shear modulus are in a stress state close to failure. The fracture strength represented by the CFS is systematically increasing with increasing bulk modulus and decreasing shear modulus. Failure will hence most likely occur in parts of a rock characterized by low bulk modulus and high shear modulus, while parts of high bulk modulus and low shear modulus will act as barriers for fracture propagation. The direct relation between in situ elastic properties and CFS suggests that elastic heterogeneity causes stress fluctuations of power law type. We analyze scaling behavior of CFS and its implications for earthquake magnitudes scaling in the next section.

5. Earthquake Magnitude Scaling

Considering the fact that zones of failure in rocks are not continuous planes but exhibit self-similar fragmentation at all scales, *Aki* [1981] describes the assemblage of faults using the concept of fractals. Assuming that $M_0 \propto A^{\frac{3}{2}}$ and $\log(M_0) \propto \frac{3}{2}M$ [see *Kanamori and Anderson*, 1975], where M_0 is the seismic moment, A is the fault area and M is the magnitude, the Gutenberg-Richter relation [see *Gutenberg and Richter*, 1954]

$$\log(N_M) = a - bM \tag{4}$$

can be expressed in the following form [see *Aki*, 1981]:

$$\log(N_M) = a - b\ \log(A). \tag{5}$$

The constants a and b characterize earthquake productivity and the ratio between small- and large-magnitude earthquakes, respectively. The Gutenberg-Richter relation in the form of equation (5) suggests that the power law exponent of fault size distribution is equivalent to the b value of earthquakes. We now analyze if fracture sizes resulting from our model of elastic heterogeneity possess power law scaling and a scaling exponent similar to the b value of earthquake.

Failure will occur in all critically stressed cells characterized by CFS $\leq$ 0. Causes of a CFS decrease are, for instance, tectonic loading and an increase in pore pressure resulting from a fluid injection or ascending crustal fluids. In the most simple case of a constant CFS decrease ΔCFS in the complete medium, the isoset CFS$(x, y, z) \leq \Delta$CFS defines the number size distribution of faults and accordingly magnitude scaling. To analyze solely the result of measurement-based elastic rock heterogeneity, we do not introduce assumptions about dynamic interaction of fractures during the failure process and assume that all faults are formed simultaneously; that is, we neglect stress fluctuations caused by possible seismic events on corresponding critically stressed isosets. Our analysis is a minimum-assumption first-principle approach. Each single closed cluster of interconnected critically stressed cells represents one fault. In the previous section we have shown that the CFS is strongly related to the fractal distribution of elastic properties. Therefore, the fluctuations of CFS should also possess fractal scaling. Consequently, scaling of fault sizes is explicitly defined by the fractal dimension D_f of the isoset: CFS$(x, y, z) \leq \Delta$CFS. Again, we note that fields of elastic properties, distributed heterogeneously in the real three-dimensional space ($E = 3$), are embedded in dimension 4. The fourth dimension is given by the color in our figures. Corresponding fractals have fractal dimension between 3

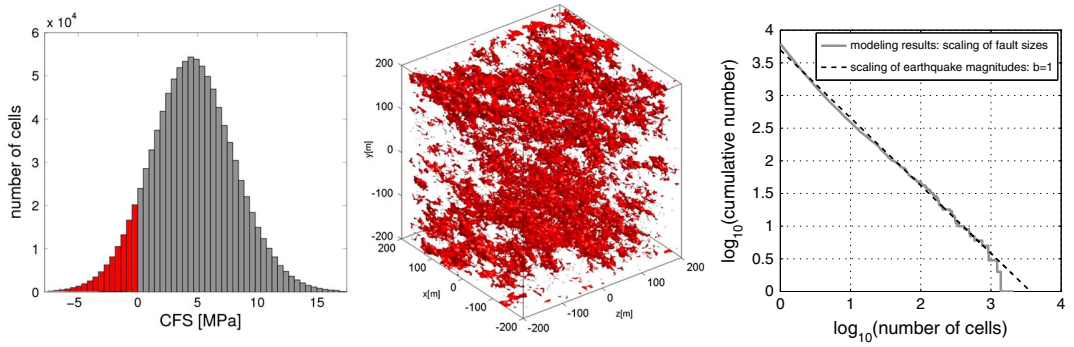

Figure 6. Fault size and magnitude scaling: Statistics of critically stressed clusters after a uniform CFS decrease of 5 MPa in the complete model medium. (left) Histogram of CFS. (middle) Fracture assemblage resulting from all cells characterized by CFS $\leq$ 0. (right) Cumulative size distribution of critically stressed clusters. As discussed above the logarithm of the number of cells (x axis) represents earthquake magnitudes. Elastic heterogeneity results in magnitudes scaling according to the Gutenberg-Richter relation with b value of $b \approx 1$.

and 4. If the distribution of CFS resulting from fields of elastic properties shows fractal scaling, the range of possible fractal dimensions of CFS distribution (D_{CFS}) is given by $3 \leq D_{\mathrm{CFS}} \leq 4$. Fractal dimensions of isosets $\mathrm{CFS}(x,y,z) \leq \Delta\mathrm{CFS}$ are embedded in the real three-dimensional space. They have fractal dimensions between 2 and 3. This is in agreement with *Isishenko and Kalda* [1991] who show that an isoset of a fractal distribution again is a fractal with fractal dimension of 1 unity less than the fractal distribution itself. The basic definition of a fractal distribution is given by

$$N = \frac{c}{r^D}, \tag{6}$$

where N is the number of objects with a linear dimension equal to or greater than r, D is the fractal dimension of the distribution, and c is a constant of proportionality [see, e.g., *Huang and Turcotte*, 1988]. Thus, the number of clusters N_j characterized by a volume equal to or larger than a given volume V_j, that is, the number of clusters consisting of j or more interconnected critically stressed cells, is given by

$$\begin{aligned} N_j &= c\, V_j^{\frac{-D_i}{3}} \\ \log(N_j) &= c - \frac{D_i}{3}\log(V_j), \end{aligned} \tag{7}$$

where $D_i = D_{\mathrm{CFS}} - 1$ is the fractal dimension of the isoset $\mathrm{CFS}(x,y,z) \leq \Delta\mathrm{CFS}$, and D_{CFS} is the fractal dimension of the CFS distribution. The constant c is given by the number of all clusters and is related to the a value of the Gutenberg-Richter relation. Since the limits of the fractal dimension of the CFS distribution are given by $3 \leq D_{\mathrm{CFS}} \leq 4$, D_i is in the range of $2 \leq D_i \leq 3$. If we consider that failure takes place in all cells of a cluster, the fault area is proportional to the number of cells. This assumption presumes very complex fracture surfaces. Correspondingly, magnitudes will be proportional to the logarithm of the number of cells. Comparison of equations (5) and (7) results in a b value given by

$$b = \frac{D_i}{3} = \frac{D_{\mathrm{CFS}} - 1}{3}. \tag{8}$$

Accordingly, the b value will be in the range of $\frac{2}{3} \leq b \leq 1$, since the limits of the fractal dimension of CFS are given by $3 \leq D_{\mathrm{CFS}} \leq 4$. If the CFS distribution is characterized by a fractal dimension equivalent to the fractal dimension of elastic modulus distribution ($D_{\mu,K} = 3.87$), fault sizes should scale with a b value of $b = \frac{D_{\mu,K}-1}{3} = 0.96$.

Figure 6 presents the CFS histogram, fracture assemblage, and cumulative size distribution of critically stressed clusters resulting from a uniform CFS decrease of $|\Delta\mathrm{CFS}| = 5$ MPa in the complete model medium. The size distribution is derived by implementation of a flood fill algorithm. A decrease of 5 MPa is applied to assure a statistically significant number of failing cells. All cells characterized by CFS $\leq$ 0 contribute to the fracture assemblage shown in Figure 6 (middle). As discussed above, the logarithm of the number of cells in the individual clusters of critically stressed cells (x axis of Figure 6, right) represents earthquake magnitudes. Resulting fault sizes exhibit power law scaling. Furthermore, the power law exponent of fault size scaling is remarkably similar to the b value of earthquakes, which is usually given by $b \approx 1$. A b value of $b \approx 1$

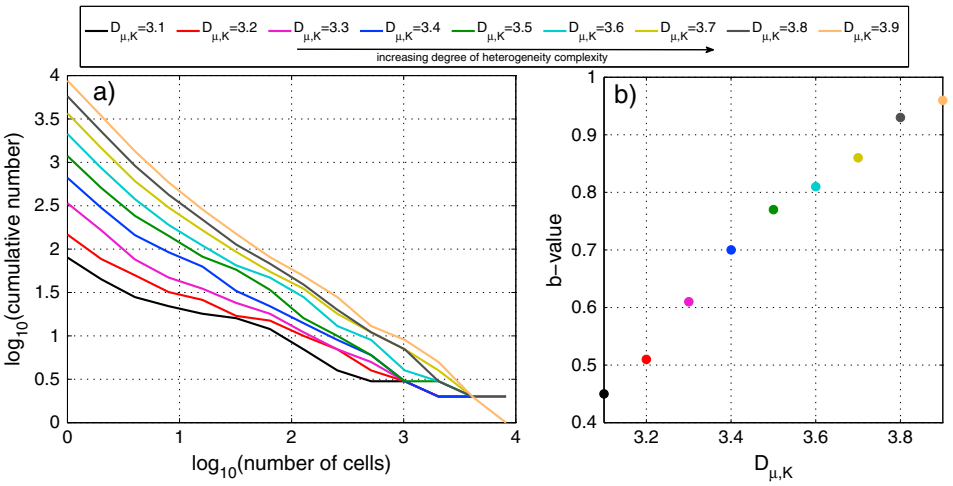

Figure 7. Influence of the fractal dimension of elastic parameter distribution ($D_{\mu,K}$) on fault size scaling. (a) Cumulative number size distributions resulting from stress modeling with input fractal dimension $D_{\mu,K}$ ranging from 3.1 to 3.9. The figure shows fault sizes computed for CFS decrease of $\Delta\mathrm{CFS} = 5$ MPa. (b) Relation between input fractal dimension $D_{\mu,K}$ and resulting b value. A positive relation between the degree of heterogeneity complexity, expressed by the fractal dimension, and the b value is visible.

is also observed for magnitude scaling of microseismicity induced by a fluid injection operation at the KTB [see *Dinske and Shapiro*, 2012].

Our results prove that fractal fluctuations of elastic moduli in the Earth's crust cause significant Coulomb stress fluctuations with power law size distribution. Earthquake magnitudes, determined by the resulting fault size distribution, scale according to a power law with exponent close to 1. The Gutenberg-Richter relation of earthquake magnitude scaling originates from Coulomb stress fluctuations caused by elastic rock heterogeneity. The assumption of a fault area A proportional to the number of cells presumes very complex fracture surfaces. Resulting b values can be interpreted as a lower limit. The upper bound of b values should be given for even fracture surfaces given by $V_j^{\frac{2}{3}} = A_j$, where A_j corresponds to the characteristic area of a critically stressed cluster. In this case the number N_j of characteristic areas equal to or larger than a given area A_j is given by $N_j \propto A_j^{\frac{-D_j}{2}}$. Correspondingly, the b value is given by $b = \frac{D_j}{2}$ and according to the limits of the fractal dimension in the range of $1 \leq b \leq 1.5$. The b value resulting from our model of elastic rock heterogeneity ($D_{\mu,K} = 3.87$) would be given by $b = 1.435$ in this case. However, we will assume complex fracture surfaces proportional to the number of cells of critically stressed cluster in the following and keep in mind that the upper bound of b values is given by $b = 1.5$, which is still in the range of observed values. Moreover, proportionality between the number of cells of a cluster and earthquake magnitude is expected, because the energy stored in a cluster is proportional to its number of cells.

6. Variability of *b* Value

Laboratory studies [*Mogi*, 1962; *Scholz*, 1968; *Amitrano*, 2003], observations [*Schorlemmer et al.*, 2005], and modeling [*Huang and Turcotte*, 1988] suggest that the b value is not universal. One observation of laboratory experiments is a positive relation between the degree of specimen heterogeneity and the b value. Figure 2 illustrates that the fractal dimension of elastic modulus distribution $D_{\mu,K}$ is related to the degree of rock heterogeneity complexity. $D_{\mu,K}$ is directly linked to the power law exponent of the PSDF and describes the ratio between small- and large-scale structures. Similarly, the b value describes the ratio between small- and large-magnitude earthquakes. We now determine if the degree of elastic heterogeneity complexity ($D_{\mu,K}$) can explain observed b value variations. Therefore, we apply PSDF with different power law exponents to the media shown in Figure 2a to simulate fractal media characterized by fractal dimensions $D_{\mu,K}$ in the range from 3.1 to 3.9. Stress modeling is performed as described in the previous sections. The cumulative number size distribution of critically stressed clusters is determined, and a least square fit is applied to determine the b value. Figure 7 shows in which way the b value depends on the fractal dimension $D_{\mu,K}$ of elastic property scaling. The obvious positive relation of b value and fractal

Table 1. Power Law Exponents of Elastic Heterogeneity Derived From Sonic Logs[a]

Location	β_K	β_μ
KTB-1	1.24	1.29
Basel-1	0.83	1.06
SAFOD Main Hole	1.10	1.21
Cotton Valley 21-10	1.02	1.15

[a]The table summarizes power law exponents of elastic modulus distribution, which we computed from sonic log data collected at Basel (Switzerland) [see, e.g., *Häring et al.*, 2008], Carthage Cotton Valley (U.S.) [see, e.g., *Rutledge and Phillips*, 2003], San Andreas Fault Observatory at Depth (U.S.) [see, e.g., *Hickman et al.*, 2007], and KTB (Germany). The exponents are calculated from the power spectral density of elastic modulus distribution (see Figures 1g and 1h for KTB example). It becomes clear that fractal scaling of elastic heterogeneity is of universal nature.

dimension $D_{\mu,K}$ confirms the observed increase in b value with specimen heterogeneity in the laboratory. One might think about the possibility that observed b value variations of earthquakes from one region to another are caused by variations of the fractal dimension of elastic modulus distribution. In this case it should be possible to estimate b values by analysis of log data. Table 1 summarizes power law exponents of elastic modulus distribution, which we computed from sonic log data collected at Basel (Switzerland) [see, e.g., *Häring et al.*, 2008], Carthage Cotton Valley (U.S.) [see, e.g., *Rutledge and Phillips*, 2003], San Andreas Fault Observatory at Depth (U.S.) [see, e.g., *Hickman et al.*, 2007], and KTB (Germany). All exponents have similar values very close to 1. Although the type and composition of rocks vary from one drilling site to another, scaling of elastic rock heterogeneity is more or less universal. This finding coincides with observations of *Day-Lewis et al.* [2010, and references therein]. They observe that a power law exponent of $\beta \approx 1$ is typical for physical property scaling derived from sonic well logs at various sites. Therefore, observed regional variations of the b value cannot be solely explained by regional variations of elastic heterogeneity and a b value estimation using sonic logs is not feasible. However, the universal nature of elastic heterogeneity shows that the scaling of our model medium (Figure 2d) can be considered as universally valid. The universal fractal nature of elastic heterogeneity should hence result in a universal b value close to $b = 1$. Although there are regional fluctuations of the b value, the b value for worldwide earthquake catalogs is given by $b = 1$.

A second observation [*Scholz*, 1968] is a b value decrease with increasing differential stress applied in the laboratory. *Schorlemmer et al.* [2005] connect the degree of differential stress to different tectonic stress regimes and find an inverse relation between differential stress level and b value. Thus, high differential stress should result in a low b value, and vice versa. We now analyze the influence of the stress level on the b value by varying the amount of CFS perturbation ΔCFS. The analysis performed in the following is always related to elastic property scaling derived from the KTB-1 well logs ($D_{\mu,K} = 3.85$). Figure 8 shows cumulative size distribution of critically stressed clusters and b values resulting from CFS perturbations in the range from −1.5 to −13.5 MPa. Higher decreases in CFS represent higher level of differential stress, since an increase in differential stress generally results in a decrease in CFS; that is, it brings fractures closer to failure. The b values presented in Figure 8b indeed show an inverse relation to differential stress level until a critical point is reached. After this point the b value is strongly increasing with $|\Delta CFS|$. Moreover, we observe that the total number of critically stressed clusters is increasing with $|\Delta CFS|$ until the critical point is reached (see Figure 8). Afterward, the total number decreases if $|\Delta CFS|$ is further increased.

The changing dependence of the b value on $|\Delta CFS|$ in our model clearly represents a break of fractal (power law) scaling of fault sizes. However, for formally defined fractals stress cannot have any influence on the power law exponent (b value), precisely because variability of the exponent stands for a break in scale invariance. *Isichenko* [1992] notes that no physical object in real space qualifies for the formal definition of a fractal, because each physical model has certain limits of applicability expressed in characteristic length scales involved. The formal definition of fractals, that is, unlimited power law scaling, applies only to systems of infinite size.

Finite model and cell size introduce characteristic scales to our model, which cause limitations or changes of fractal scaling. Clusters touching the boundaries of the model are counted as smaller than real because they actually may continue outside the model. This finite size effect biases the size distribution of clusters at all scales. The decrease in the b value with $|\Delta CFS|$ until the critical point is reached occurs due to this finite size effect. We discuss this point in more detail in the last paragraph of this section.

We find that the critical point, after which the b value dependence on stress changes (see Figure 8), is given by the percolation threshold, that is, the point where for the first time one single cluster of interconnected

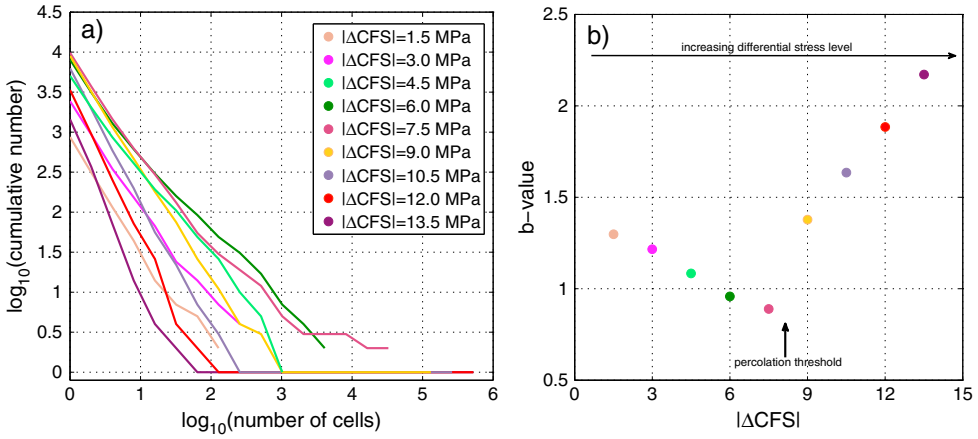

Figure 8. Influence of the CFS perturbation on scaling of critically stressed clusters. (a) Cumulative size distributions of critically stressed clusters resulting from CFS decrease $|\Delta CFS|$ in the range from 1.5 MPa to 13.5 MPa. Higher decrease in CFS corresponds to a higher differential stress level. (b) b values computed for the size distribution of critically stressed clusters shown in Figure 8a.

critically stressed cells connects the boundaries of the model medium. After the percolation threshold is exceeded, the b value increases, since more and more large clusters merge into the percolation cluster, while small clusters still can develop. For the same reason the total number of critically stressed clusters decreases after percolation. We note that we determine the b value in the range starting from a cumulative number of two clusters because of the bad statistic of a single large cluster. This also means that the percolation cluster is excluded from the determination of the b value, because it can be considered as an outlier of the number size distribution (see Figure 8a).

The structure of our model corresponds to 3-D simple cubic site percolation. In the case of spatially uncorrelated fields (e.g., Figure 2a) the critical site occupancy probability leading to the occurrence of a percolating cluster is given by $p_c = 0.53 - 0.59$ for 2-D and $p_c = 0.3116077$ for 3-D [see, e.g., *Lorenz and Ziff*, 1998]. It means that as soon as 31.16% of cells are critically stressed (CFS $\leq$ 0) a percolation cluster will occur for 3-D spatially uncorrelated random fields. Due to the spatial power law correlation of elastic moduli and corresponding CFS, we find a much lower threshold of $p_c = 0.11$. The percolation threshold introduces a characteristic-length scale into the model, which limits the range of self-similar (power law) behavior of fault size scaling and explains the increase in the b value after percolation.

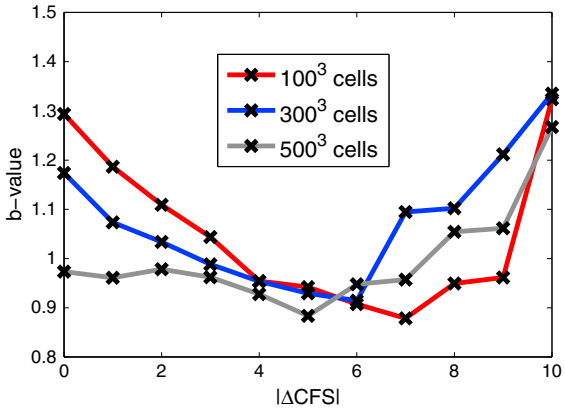

Figure 9. Influence of scale limitations on the relation between stress and b value. Fractal CFS distributions of different sizes (100^3 (red), 300^3 (blue), and 500^3 (grey) cells) are analyzed. The distributions are simulated based on mean value (< CFS >= 11.18 MPa) and standard deviation ($\sigma_{CFS} = 3.59$ MPa). Fractal dimension is set to $D = 3.87$. b values are computed in dependence on CFS decrease $|\Delta CFS|$. Our analysis suggests that the dependency of the b value on stress is caused by scale limitations.

Huang and Turcotte [1988] analyze 2-D fractal fields representing the difference between stress and strength. They find an inverse relation between stress level and b value in a larger range. Here it is important to note that the percolation threshold in 2-D is larger than the percolation threshold in 3-D. It also seems that *Huang and Turcotte* [1988] fit the cumulative size distributions in the complete range, whereas we determine the b value in the range starting from a cumulative number of two clusters.

To further analyze the influence of scale limitations on the relation between stress and b value, we analyze fractal distributions of a different size. Different realizations of fractal CFS distributions are simulated based on mean value ($<$ CFS $>=$ 11.18 MPa) and standard deviation ($\sigma_{CFS} = 3.59$ MPa). These values are obtained from the determined CFS distribution at the KTB, presented in Figure 4b. In agreement with the fractal dimension of elastic heterogeneity, the fractal dimension of the CFS distributions is set to $D = 3.87$. In Figure 9, b values resulting from fractal simulations of size 100^3, 300^3, and 500^3 cells are shown. The b values are computed in dependence on CFS decrease $|\Delta CFS|$. It becomes clear that the inverse relation between stress level and b value, which occurs until percolation is reached, has a less distinct tendency for model of larger size. For models of infinite size this finite size effect should vanish completely. The b values computed for the largest simulated CFS distribution of 500^3 cells are very close to the theoretically predicted value of $b = 0.96$ (see section 5). However, still a minor decrease is visible until percolation is reached. Interestingly, in the vicinity of percolation a power law scaling of cluster sizes must appear. This should be even the case for a medium without initial power spectrum of power law type, that is, without initial fractal scaling. In our case this means that the presence of percolation should change our model-based initial scaling, caused by fractal nature of elastic heterogeneity, to the percolation-caused scaling. In summary, our analysis suggests that the observed stress dependency of the b value occurs due to characteristic scales of seismogenic processes, which cause limitations or changes of fractal scaling. This finding suggests that a stress inversion using b values is ambiguous.

7. Discussion

Based on measurements along boreholes, we characterized elastic rock heterogeneity in the Earth's crust. Our results reveal universal fractal scaling of elastic heterogeneity. It does not make any difference in our model, whether the fractal nature of elastic heterogeneity is an inherent characteristic of rocks from its formation on or if it is a result of dynamic interaction during deformation, as proposed, for instance, by continuous damage models [see, e.g., *Amitrano*, 1999; *Girard et al.*, 2012]. Because elastic heterogeneity exists in the present-day stress field, it naturally causes fluctuations of stress. Our analysis of a measurement-based model of elastic rock heterogeneity suggests that stress fluctuations caused by elastic rock heterogeneity are of significant magnitude. Moreover, we find that in situ stress is primarily controlled by in situ elastic properties. The impact of surrounding heterogeneity is existent but seems to be only of minor importance. This gives an explanation for the observed fractal nature of stress fluctuations in the Earth's crust.

To analyze solely the result of measurement-based elastic heterogeneity on stress and fracture strength distribution, we keep other parameters of rock strength, like friction coefficient and cohesion, homogeneous in our model. Moreover, this is done because no direct measurements of heterogeneity of these parameters are available. For the same reason we do not introduce assumptions about dynamic interaction of fractures during the failure process and assume that all faults are formed simultaneously; that is, we neglect stress fluctuations caused by possible seismic events on corresponding critically stressed isosets. Our modeling of the stress distribution in 3-D heterogeneous elastic structures is a minimum-assumption first-principle approach. The result of our analysis represents the impact of measurement-based elastic rock heterogeneity and is not a result of assumptions made about heterogeneity of other parameters or dynamic interactions. Even if assumptions about dynamic interaction during the failure process or heterogeneity of other parameters are introduced to the model, the influence of elastic rock heterogeneity remains as characterized by our static analysis.

Because of the universal fractal nature of elastic heterogeneity and related CFS fluctuations, the b value should be universal and close to $b = 1$. It changes only due to the presence of characteristic scales of seismogenic processes. Also, the observed dependence of the b value on stress [see, e.g., *Schorlemmer et al.*, 2005; *Scholz*, 1968] can be explained by characteristic scales. Even if assumptions about dynamic interaction of fractures is introduced to our model, universality of the b value, resulting from the universal fractal nature of elastic heterogeneity, remains valid, because interaction should occur based on the same physical laws at all analyzed locations.

One example of a naturally existing characteristic scale is provided by the observation of a break of power law scaling, from small to large earthquakes, at the point where the dimension of the event equals the down dip width of the seismogenic layer [*Pacheco et al.*, 1992]. On a smaller scale, layering of rocks, that is, changes of rock type and composition, represents characteristic scales. In the same sense, the paragneiss

layer, which we excluded from the analysis along the KTB-1 main hole, would cause limitation of fractal scaling if included in the model building procedure. Moreover, naturally occurring CFS perturbations always are limited to finite rock volumes and may show complex geometries. This suggests that finite size effects, which have been considered to be statistical biases of numerical models, also exist in nature. For instance, *Shapiro et al.* [2011] analyze catalogs of fluid-injection-induced earthquakes [see *Langenbruch et al.*, 2010, 2011] at geothermal and hydrocarbon reservoirs. They show that finiteness and geometry of the stress and pore pressure perturbed zone, resulting from a fluid injection, cause strong deviations from a strict power law distribution of earthquake magnitudes. Both *a* and *b* values deviate from values resulting from a strict power law distribution of fault sizes. Temporal changes of characteristic length scales, like the size of the perturbed rock volume during a fluid injection, may explain *b* value variability in time. The most important length scale in laboratory experiments obviously is given by the finite size of a sample.

Other models have been proposed to explain the origin of the Gutenberg-Richter relation and variations of the *b* value. According to the critical point theory, the disappearance of characteristic length scales at or near the critical point originates in power law scaling [see, e.g., *Main*, 1996]. The critical point theory has, for instance, been applied to seismic precursory patterns before a cliff collapse [*Amitrano et al.*, 2005] and progressive damage models [*Girard et al.*, 2012]. It has been shown that the power law exponent of damage avalanche size in progressive damage models depends on the value of internal friction [see *Amitrano*, 1999]. This dependence occurs, because the distance to the critical point is controlled by the friction angle. In our model the value of friction changes the broadness of CFS distribution. In general, the distribution of CFS gets broader for smaller and narrower for larger values of friction. However, the coefficient of friction has no effect on CFS scaling and hence no influence on the *b* value.

Systems that naturally evolve into a critical state are known as self-organized critical systems. *Bak and Tang* [1989] argue that the Gutenberg-Richter power law distribution for energy released at earthquakes can be understood as a consequence of the Earth's crust being in a self-organized critical state.

While power law scaling in the above mentioned models result from assumptions about dynamic interaction, power law scaling in our model is the result of measured elastic rock heterogeneity. Power law scaling is hence an inherent characteristic of our model and does not only emerge at or near the critical point. Our analysis shows that before any assumptions about dynamic interaction are introduced, it is important to characterize the influence of measured in situ elastic rock heterogeneity based on well-established laws of physics. By analyzing solely the impact of the background rock heterogeneity characterized by real in situ measurements along boreholes, we show that even if dynamic interaction is neglected, faults and earthquake magnitudes scale according to the Gutenberg-Richter relation with a *b* value close to 1.

Moreover, we again point out the importance of 3-D models to simulate failure processes in rocks. Critical points, like, for instance, the percolation threshold or the point of macroscopic sample failure, will differ significantly in 2-D and 3-D models.

8. Conclusions

Elastic heterogeneity of the Earth's crust is of universal fractal nature and significantly impacts Coulomb stress distribution in rocks. In situ stress is mainly controlled by in situ elastic moduli. Stress fluctuations caused by surrounding heterogeneities are existent but seem to be only of minor importance. The fractal nature of elastic heterogeneity results in significant Coulomb stress fluctuations with power law size distribution. As a consequence, fault sizes and magnitudes of earthquakes exhibit power law scaling according to the Gutenberg-Richter relation. Consistent with observations in the laboratory, we find that in theory the *b* value is increasing with the degree of heterogeneity complexity, expressed in the fractal dimension of elastic modulus distribution. The theoretical limits of the *b* value, given by the lower and upper limits of the fractal dimension of elastic heterogeneity, are in the range of $b = \frac{2}{3}$ to $b = 1.0$ for complex fracture surfaces and 1.0 to 1.5 for even fractures. However, because the fractal dimension of elastic heterogeneity measured from borehole logs at various sites is universal, the *b* value should be universal. Deviations of the *b* value from its universal value of $b \approx 1$ result from characteristic scales of seismogenic processes, which cause limitations or changes of fractal scaling. Scale limitations are also the reason for observed stress dependency of the *b* value. These findings are unaffected by instrumental and measurement effects on the fractal dimension of elastic heterogeneity, because we can expect a statistically similar impact at different analyzed locations. Hence, the universality issue should remain mainly untouched. Because in all physical models

and ongoing seismogenic processes in nature characteristic scales are involved, which cause limitations or changes of fractal scaling, the *b* value deviates from its universal value. Since characteristic length scales, for instance, the finite size and geometry of the stress-perturbed volume or changes in rock composition, are site-dependent and, like the stress-perturbed rock volume, also time-dependent quantities, *b* values determined for different regions or at different times are diverse. In the same sense, the inverse relation between stress and *b* value, revealed by laboratory studies and observations, occurs due to existing scale limitations. In summary, our analysis shows that the universal fractal nature of elastic rock heterogeneity can be considered as the origin of the Gutenberg-Richter relation of earthquake magnitude scaling.

Acknowledgments

We thank the sponsors of the Physics and Application of Seismic Emission (PHASE) consortium project and the Federal Ministry for the Environment, Nature Conservation and Nuclear Safety as sponsor of the project MeProRisk II for supporting the research presented in this paper. Logging data were obtained under grants RG8604, RG8803, and RG 9001 of the Federal Ministry of Research and Technology and provided by the KTB Project Management, Geological Survey of Lower Saxony, Germany. We acknowledge two anonymous reviewers and the Associate Editor for helpful and constructive comments.

References

Aki, K. (1981), A probabilistic synthesis of precursory phenomena, in *Earthquake Prediction: An International Review*, edited by D. W. Simpson and P. G. Richards, pp. 566–574, Maurice Ewing Series 4, AGU, Washington, D. C., doi:10.1029/ME004p0566.

Amitrano, D. (2003), Brittle-ductile transition and associated seismicity: Experimental and numerical studies and relationship with the *b* value, *J. Geophys. Res.*, *108*(B1), 2044, doi:10.1029/2001JB000680.

Amitrano, D., J.-R. Grasso, and D. Hantz (1999), From diffuse to localised damage through elastic interaction, *Geophys. Res. Lett.*, *26*, 2109–2112, doi:10.1029/1999GL900388.

Amitrano, D., J.-R. Grasso, and G. Senfaute (2005), Seismic precursory patterns before a cliff collapse and critical point phenomena, *Geophys. Res. Lett.*, *32*, L08314, doi:10.1029/2004GL022270.

Baisch, S., M. Bohnhoff, L. Ceranna, Y. Tu, and H.-P. Harjes (2002), Probing the crust to 9-km depth: Fluid-injection experiments and induced seismicity at the KTB superdeep drilling hole, Germany, *Bull. Seismol. Soc. Am.*, *92*, 2369–2380, doi:10.1785/0120010236.

Bak, P., and C. Tang (1989), Earthquakes as a self-organized critical phenomenon, *J. Geophys. Res.*, *94*, 15,635–15,637, doi:10.1029/JB094iB11p15635.

Brudy, M., M. Zoback, K. Fuchs, F. Rummel, and J. Baumgärtner (1997), Estimation of the complete stress tensor to 8 km depth in the KTB scientific drill holes: Implications for crustal strength, *J. Geophys. Res.*, *102*(B8), 18,453–18,475, doi:10.1029/96JB02942.

Dahlheim, H., H. Gebrande, E. Schmedes, and H. Soffel (1997), Seismicity and stress field in the vicinity of the KTB location, *J. Geophys. Res.*, *102*(B8), 18,493–18,506, doi:10.1029/96JB02812.

Day-Lewis, A., M. Zoback, and S. Hickman (2010), Scale-invariant stress orientations and seismicity rates near the San Andreas Fault, *Geophys. Res. Lett.*, *37*, L24304, doi:10.1029/2010GL045025.

Dinske, C., and S. Shapiro (2012), Seismotectonic state of reservoirs inferred from magnitude distributions of fluid-induced seismicity, *J. Seismolog.*, *17*, 13–25, doi:10.1007/s10950-012-9292-9.

Dolan, S., C. Bean, and B. Riollet (1998), The broad-band fractal nature of heterogeneity in the upper crust from petrophysical logs, *Geophys. J. Int.*, *132*, 489–507, doi:10.1046/j.1365-246X.1998.00410.x.

Eshelby, J. (1957), The determination of the elastic field of an ellipsoidal inclusion, and related problems, *Proc. R. Soc. London A*, *241*(1226), 376–396.

Eshelby, J. (1959), The elastic field outside an ellipsoidal inclusion, *Proc. R. Soc. London A*, *252*, 561–569.

Girard, L., J. Weiss, and D. Amitrano (2012), Damage-cluster distributions and size effect on strength in compressive failure, *Phys. Rev. Lett.*, *108*, 225502, doi:10.1029/1999GL900388.

Goff, J., and K. Holliger (1999), Nature and origin of upper crustal seismic velocity fluctuations and associated scaling properties: Combined stochastic analyses of KTB velocity and lithology form, chance, and dimensions, *J. Geophys. Res.*, *104*, 13,169–13,182, doi:10.1029/1999JB900129.

Gutenberg, B., and C. F. Richter (1954), *Seismicity of Earth and Associated Phenomenon,* 2nd ed., Princeton Univ. Press, Princeton, N. J.

Häring, M. O., U. Schanz, F. Ladner, and B. C. Dyer (2008), Characterisation of the Basel-1 enhanced geothermal system, *Geothermics*, *37*, 469–495, doi:10.1016/j.geothermics.2008.06.002.

Hickman, S., and M. Zoback (2004), Stress orientations and magnitudes in the SAFOD pilot hole, *Geophys. Res. Lett.*, *31*, L15S12, doi:10.1029/2004GL020043.

Hickman, S., M. Zoback, W. Ellsworth, N. Boness, P. Malin, S. Roecker, and C. Thurber (2007), Structure and properties of the San Andreas Fault in central California: Recent results from the SAFOD experiment, *Sci. Drill.*, *1*, 29–32, doi:10.2204/iodp.sd.s01.39.2007.

Huang, J., and D. Turcotte (1988), Fractal distributions of stress and strength and variations of *b* value, *Earth Planet. Sci. Lett.*, *91*, 223–230, doi:10.1016/0012-821X(88)90164-1.

Huenges, E., J. Erzinger, J. Kück, B. Engeser, and W. Kessels (1997), The permeable crust: Geohydraulic properties down to 9101 m depth, *J. Geophys. Res.*, *102*, 18,255–18,265, doi:10.1029/96JB03442.

Isichenko, M. (1992), Percolation, statistical topography, and transport in random media, *Rev. Mod. Phys.*, *64*, 961–1043, doi:10.1103/RevModPhys.64.961.

Isichenko, M. B., and J. Kalda (1991), Statistical topography. I. Fractal dimension of coastlines and number-area rule for islands, *J. Nonlinear Sci.*, *1*, 255–277, doi:10.1007/BF01238814.

Ito, T., and M. Zoback (2000), Fracture permeability and in situ stress to 7 km depth in the KTB scientific drillhole, *Geophys. Res. Lett.*, *27*, 1045–1048, doi:10.1029/1999GL011068.

Jaeger, J., N. Cook, and R. Zimmerman (2007), *Fundamentals of Rock Mechanics,* 4th ed., Blackwell Publishing, Malden, Mass.

Kanamori, H., and D. Anderson (1975), Theoretical basis of some empirical relations in seismology, *Bull. Seismol. Soc. Am.*, *65*, 1073–1095.

Langenbruch, C., C. Dinske, and S. Shapiro (2011), Inter event times of fluid induced earthquakes suggest their Poisson nature, *Geophys. Res. Lett.*, *38*, L21302, doi:10.1029/2011GL049474.

Langenbruch, C., and S. Shapiro (2010), Decay rate of fluid-induced seismicity after termination of reservoir stimulations, *Geophysics*, *75*(6), MA53–MA62, doi:10.1190/1.3506005.

Leary, P. C. (1997), Rock as a critical-point system and the inherent implausibility of reliable earthquake prediction, *Geophys. J. Int.*, *131*, 451–466, doi:10.1111/j.1365-246X.1997.tb06589.x.

Lorenz, D., and R. Ziff (1998), Universality of the excess number of clusters and the crossing probability function in three-dimensional percolation, *J. Phys. A: Math. Gen.*, *31*, 8147–8157, doi:10.1088/0305-4470/31/40/009.

Main, I. (1996), Statistical physics, seismogenesis, and seismic hazard, *Rev. Geophys.*, *34*, 433–462, doi:10.1029/96RG02808.

Mogi, K. (1962), Magnitude-frequency relation for elastic shocks accompanying fractures of various materials and some related problems in earthquakes (2nd paper), *Bull. Earthquake Res. Inst.*, *40*, 831–853.

Pacheco, J., C. Scholz, and L. Sykes (1992), Changes in frequency–size relationship from small to large earthquakes, *Nature*, *355*, 71–73, doi:10.1038/355071a0.

Pechnig, R., S. Haverkamp, J. Wohlenberg, G. Zimmermann, and H. Burkhardt (1997), Integrated log interpretation in the German Continental Deep Drilling Program: Lithology, porosity, and fracture zones, *J. Geophys. Res.*, *102*, 18,363–18,390, doi:10.1029/96JB03802.

Rivera, L., and H. Kanamori (2002), Spatial heterogeneity of tectonic stress and friction in the crust, *Geophys. Res. Lett.*, *29*(6), 12-1–12-4, doi:10.1029/2001GL013803.

Rothert, E., and S. A. Shapiro (2007), Statistics of fracture strength and fluid-induced microseismicity, *J. Geophys. Res.*, *112*, B04309, doi:10.1029/2005JB003959.

Rutledge, J., and W. Phillips (2003), Hydraulic stimulation of natural fractures as revealed by induced microearthquakes, Carthage Cotton Valley gas field, east Texas, *Geophysics*, *68*(2), 441–452, doi:10.1190/1.1567214.

Scholz, C. (1968), The frequency-magnitude relation of microfracturing in rock and its relation to earthquakes, *Bull. Seismol. Soc. Am.*, *58*, 399–415.

Schorlemmer, D., S. Wiemer, and M. Wyss (2005), Variations in earthquake-size distribution across different stress regimes, *Nature*, *437*, 539–542, doi:10.1038/nature04094.

Shapiro, S., O. Krueger, C. Dinske, and C. Langenbruch (2011), Magnitudes of induced earthquakes and geometric scales of fluid-stimulated rock volumes, *Geophysics*, *76*, WC55–WC63, doi:10.1190/geo2010-0349.1.

Chapter 6

Conclusions and outlook

Ongoing seismogenic processes in the brittle Earth's crust are substantially driven by different aspects of stress. In this thesis, I presented a comprehensive analysis of the role of stress fluctuations in seismogenic processes. This includes an estimation of critical stress changes capable of triggering brittle failure and associated seismicity in rocks of the Earth's crust. In addition, the stress perturbation caused by the injection of pressurized fluids was quantified and the significance of stress changes generated by the occurrence of fluid-induced earthquakes was evaluated. Moreover, I investigated the impact of elastic rock heterogeneity on the distribution of stress in the Earth's crust. I related my results to the scale invariance of earthquakes. Finally, the observed stress dependency of the two fundamental power laws of statistical seismology was analyzed. Even though the main research target of this thesis is small-scale seismicity induced by the injection of pressurized fluids, the performed analysis provides insights into seismogenic processes in general because the observed scale invariance of the physics of earthquakes suggests a transferability of results obtained at different scales. My findings show that characterizing the role of stress fluctuations in seismogenic processes is crucial to understand the physics of earthquakes.

The performed analysis of the impact of elastic rock heterogeneity on the distribution of stress in the Earth's crust provided fundamental insights into the nature of seismogenic processes. My results suggest that the observed scale invariance of earthquakes results from scale-invariant fluctuations of stress in rocks. These fluctuations occur naturally because of the universal fractal nature of elastic rock heterogeneity in the Earth's crust. Scientific evidence for the fractal nature of elastic rock heterogeneity is given by measurements along boreholes. As a result, fault sizes and corresponding magnitudes of earthquakes scale according to a universal power law. This explains the emergence of the Gutenberg-Richter relation which implies the scale invariance of the frequency

magnitude scaling of earthquakes. The proposed physical origin of the scale invariance is different to existing models, which are usually based on the disappearance of characteristic scales at critical points. The obtained results are not only important for the frequency magnitude scaling of earthquakes in particular, but also for the observed scale invariance of earthquakes in general.

The analysis of fluid injection-induced earthquakes presented in this thesis shows that substantial progress can be made in the understanding of the role of different aspects of stress analyzing seismicity caused by the injection of pressurized fluids through boreholes. The investigation of fluid-induced earthquakes is in particular informative because the basic conditions during earthquake nucleation and rupturing at fluid injection sites are better accessible than for earthquakes on tectonic scale.

Based on the assumption that pore pressure diffusion is the governing process triggering fluid-induced earthquakes, the perturbation of stress, caused by the injection of pressurized fluids, has been quantified. In combination with the consideration of a close to critical state of stress in the Earth's crust, a physically based statistical model describing the seismicity rate of fluid-induced earthquakes during and after an injection of fluids was presented. My analysis of stress fluctuations caused by elastic rock heterogeneity verified the range of critical stress changes used in this model. Moreover, the heterogeneous nature of the criticality of stress in rocks, observed in previous studies, can be physically explained by the influence of elastic rock heterogeneity. I demonstrated that stress changes in the range of 10^3 to 10^7 Pa are capable of triggering brittle failure and associated seismicity in rocks of the Earth's crust. This result validates the concept of a critically stressed brittle crust and suggests that already stress changes just above perturbations caused by tidal forces are sufficient to trigger rupturing in the most critically stressed parts of rocks.

Most studies dealing with seismicity induced by the injection of pressurized fluids assume that all seismic events are directly triggered by the relaxation of stress and pore pressure perturbation initially created at the injection source. This hypothesis, which is consistent with the observation of a proportionality between the cumulative number of events and the cumulative injected fluid volume, is a basic assumption of works considering pore pressure diffusion as the governing mechanism of seismicity triggering. However, the occurrence of each event alters the state of stress in the rock volume surrounding its fault plane. This change could, if sufficiently large, result in a triggering of aftershocks as observed after tectonically driven earthquakes.

I verified the assumption of direct triggering of seismic events through the stress perturbation caused by injection of fluids. This was demonstrated by analyzing the waiting times between subsequent fluid-induced earthquakes at EGS sites. My results show that, even after the strongest seismic events, no signatures of aftershock triggering can be identified. Thus, stress changes resulting from the occurrence of preceding fluid-induced seismic events are insignificant compared to the stress changes caused directly by the injection of fluids. This is an important difference to naturally triggered earthquakes, for which aftershock triggering is an important factor. My results suggest that no coupling between events has to be included in statistical models describing the occurrence of fluid injection-induced earthquakes. The Poisson process statistically describes the occurrence of fluid-induced earthquakes. This finding is important for the development of models assessing the seismic risk associated with the injection of pressurize fluids. For instance, the Poisson model can be used to compute the probability of exceeding a given magnitude by injecting a certain amount of fluid. Thus, my results can help to inhibit the occurrence of larger magnitude events by a reasonable planning of fluid injections. Only if the seismic risk can be assessed and mitigated, the geothermal potential of the subsurface can be used efficiently and risk-free for sustainable power generation.

Temporal signatures of aftershock triggering are given by Omori's law, describing the temporal decay of aftershocks succeeding tectonic main shocks. In this work, I analyzed the decay rate of fluid injection-induced seismicity after the termination of the hydraulic reservoir stimulation. The investigation of seismicity occurring after the termination is of particular importance because the physical processes leading to the triggering of post-injection events have not been fully understood yet. Moreover, it has been observed that the strongest seismic events tend to occur shortly before and after the termination. I find that the decay rate of fluid-induced seismicity after the termination of the reservoir stimulation can be approximated by a modification of Omori's law. This signature in the temporal distribution of fluid-induced seismicity, however, is not a indicator of aftershock triggering, but of the underlying physical process triggering the seismic events. This process is given by the relaxation of pore pressure in the fluid-saturated pore and fracture space of rocks.

The decay characteristic of post-injection seismicity can be quantified by the p-value of the modified Omori law. I find that the p-value depends on the criticality of stress in rocks. Under the assumption that destabilizing stress changes of all magnitudes are capable of triggering seismicity, the p-value of the modified Omori law shows similar values as in the case of aftershocks sequences succeeding tectonic main shocks ($p \approx 1 - 2$). However, if the stress state in a

reservoir rock is less critical meaning that the pre-existing fracture system is more stable, the seismicity after injection is decaying faster. In the case of a highly unstable fracture system, the seismicity rate increases during the injection and the early post-injection phase. This can be an explanation for the occurrence of events with higher magnitudes during the later injection and early post-injection phase. The obtained findings physically justify the observation that seismicity induced by injections, aiming to create enhanced geothermal systems for power generation, is often sustained for a long period of time whereas seismicity at hydrocarbon reservoirs is decaying very fast after the termination of hydraulic fracturing treatments. Geothermal reservoirs are mostly located in tectonically active regions. Correspondingly, the state of stress in rocks at this region should be close to critical. In contrast, hydrocarbon reservoirs are mainly located in tectonically inactive regions where the state of stress should be less critical.

I pointed out that, in general, the dependence of the seismicity rate on the criticality of stress in rocks occurs because the seismically active volume is limited to a characteristic size. The seismically active volume is given by the rock volume which is sufficiently stress-perturbed by the injection of fluid to contain seismic events. The characteristic size of the seismically active volume is mainly determined through the hydraulic diffusivity of the rock and the lower limit of critical stress changes. Both quantities control the spatio-temporal development of the maximum triggering distance of seismic events from the injection source. Thus, the decay rate of seismicity, and thereby the p-value, depends on the minimum of critical stress changes in rocks. This opens up the possibility to estimate this value by analysis of the p-value. A reconstruction of the minimum critical effective stress changes at two different EGS sites resulted in a value of approximately 5000 Pa. This finding is one more indication that already stress changes just above tidal perturbations are sufficient to trigger rupturing in the most critically stressed parts of rocks. It supports the concept of a critically stressed Earth's crust.

Through the analysis of measurements along boreholes at various drilling sites located in different regions, I have shown that elastic rock heterogeneity is of universal fractal nature. This is expressed in a universal fractal dimension, describing the scaling of heterogeneity. Consequently, scale invariant stress fluctuations occur naturally in the Earth's crust. As a result, rupture planes and corresponding magnitudes of earthquakes scale according to a universal power law. This explains the emergence of the Gutenberg-Richter relation and suggests the universality of the b-value. My findings suggest that deviations of the b-value from its universal value of $b = 1$ result from characteristic scales of seismogenic processes. Each characteristic scale involved in a process results

in a change or a limitation of fractal scaling. Because in all physical models and ongoing seismogenic processes in nature characteristic scales are involved the b-value deviates from its universal value. Since characteristic scales - for instance, the finite size and geometry of the stress-perturbed volume or changes in rock composition - are site and in some cases also time-dependent quantities, b-values determined for different regions or at different times are diverse. In the same sense, the inverse relation between differential stress levels and the b-value, revealed by laboratory studies and scientific observations, occurs due to existing scale limitations. My analysis shows that elastic rock heterogeneity of universal fractal nature can be considered as the origin of the Gutenberg-Richter relation of earthquake magnitude scaling characterized by a universal b-value of $b = 1$. These results are not only relevant for frequency magnitude scaling of earthquakes in particular, but also for observed scale invariance of earthquakes in general.

Outlook

The investigations performed in this thesis raised some open questions. Because their analysis would go beyond the scope of this work they should be addressed in future research. The following questions are relevant topics for further research.

In chapter 3 I observed a change of the p-value during the decay of seismicity after the reservoir stimulation of the geothermal reservoir at Soultz-sous-Forêts in the year 2000. Some explanations have been discussed in chapter 3. However, the variation of the scaling exponent of Omori's law could be related to a change of the governing physical process leading to the triggering of the seismic events. Figure 6.1 shows the decay characteristic of seismicity after termination of the hydraulic stimulation of geothermal reservoirs at Basel (2006) and Soultz-sous-Forêts (1993). The Basel catalog is especially interesting because seismicity is registered for a long time after termination of the reservoir stimulation. In addition, the decay of seismicity at Soultz-sous-Forêts in the year 2000 is shown again. A change of the p-value is observable for all analyzed catalogs of post-injection seismicity. Interestingly, the p-value for longer times after the termination of stimulation shows similar values as in the case of tectonic aftershock sequences ($p \approx 1 - 2$). The faster decay of seismic activity close after injection termination should be governed by the relaxation of pore pressure in the fluid saturated pore and fracture spaces of rocks as demonstrated in chapter 3. The change of the p-value at later times, however, indicates that another triggering mechanism could become dominant at larger time scale. Which parameters control the point of variation of the p-value? Can characteristic

scales be identified which cause the deviation from a time scale invariant decay of seismicity? Are the seismic events in the scaling range of $p \approx 1-2$ aftershocks triggered by indirect stress changes generated by the occurrence of previous fluid-induced earthquakes? Other possible explanations could be the influence of anisotropy or non-linearity in the process of pore pressure diffusion or thermal effects. The influence of these mechanisms on the seismicity rate of fluid injection induced earthquakes should be investigated in future studies.

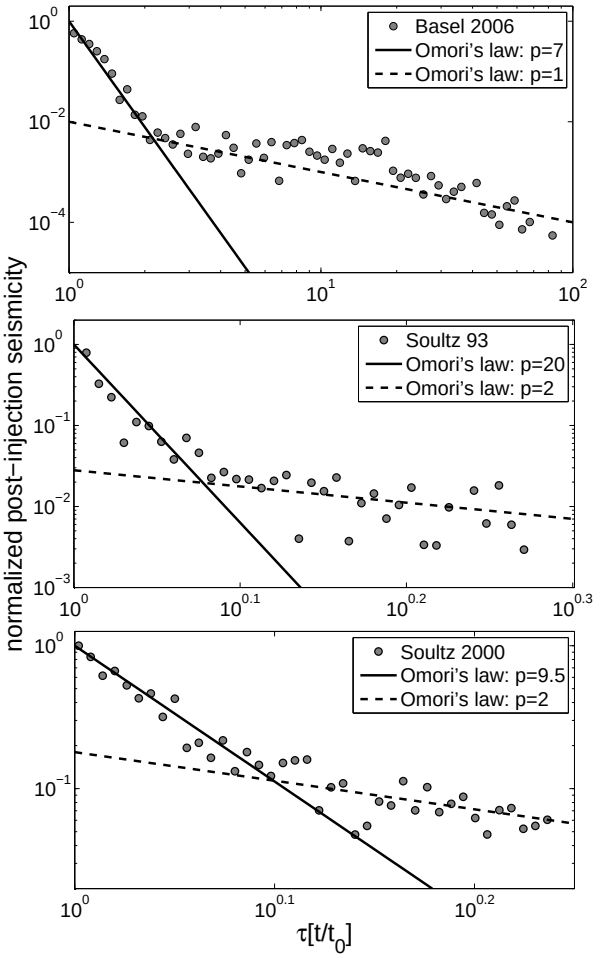

Figure 6.1: Decay rate of seismic activity after termination of the reservoir stimulation at Basel 2006 (top), Soultz-sous-Forêts 1993 (middle) and Soultz-sous-Forêts 2000 (bottom). The seismicity is normalized to the seismic activity at injection stop. The x-axis gives the time after injection start normalized by the time of injection stop. The modification of Omori's law (Eq. 3.8) describing the decay of seismic activity is shown. A change of the p-value is obvious in all three analyzed cases. While the p-value close after injection termination is high, the p-value for later times shows similar values as in the case of tectonic aftershock sequences ($p \approx 1-2$).

A further point of possible future research is the analysis of inter event times of fluid-induced earthquakes at hydrothermal systems. Fluid injections at hydrothermal systems are characterized by a injection (well head) pressure close to zero because the geological sedimentary formation at these locations contain sufficient natural pathways for fluids. Therefore, hydrothermal systems do not have to be hydraulically stimulated to allow for a sufficient circulation of fluids. Nevertheless, fluid injection-induced seismicity occurs also at these locations. Because of the low injection pressure the direct perturbation of stress

and pore pressure should be low. Thus, it is possible that stress changes which are generated by the occurrence of preceding seismic events are important for the seismogenesis of fluid-induced earthquakes in this case. Can signatures of aftershocks be identified in catalogs of seismicity registered at hydrothermal systems?

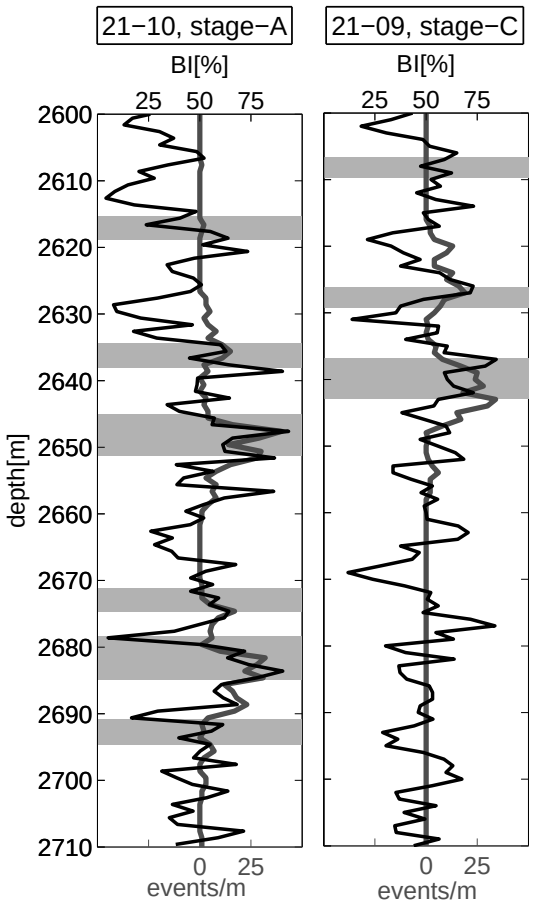

Figure 6.2: Comparison of the density of induced seismic events with depth and the Brittleness Index (BI) along wells 21-10 and 21-09 at the Cotton Valley gas field. The BI is plotted in black, event density in grey. The grey shaded areas mark the perforations along the well. Because fluid injection induced pore pressure and stress change can only occur along the perforated zones along the wells, a comparison between elastic rock properties and density of induced events is only feasible in the perforated depth intervals. Higher values of the BI along a perforation results in a higher density of seismic events. For a detailed discussion see Langenbruch and Shapiro (2014b)

Further research questions are raised by the investigation of the impact of elastic rock heterogeneity on the distribution of stress in the Earth's crust. The results presented in chapter 5 suggest that the occurrence probability of brittle rock failure and associated seismic events is controlled by fluctuations of elastic properties in rocks. However, observations which substantiate this suggestion are still missing. Fluctuations of elastic properties at fluid injection sites can be measured along existing boreholes. The measured fluctuations can then be compared to the distribution of registered and located seismic events which occur during hydraulic reservoir stimulation. A first study [Langenbruch and Shapiro (2014b)] indicates

that the density of seismic events caused by hydraulic fracturing treatments at hydrocarbon reservoirs is directly related to fluctuations of elastic properties. Figure 6.2 shows the example of a hydraulic fracturing treatment of the Carthage Cotton Valley sandstone gas reservoir. An overview about the hydraulic fracturing treatment is given in Rutledge and Phillips (2003). In Figure 6.2 the density of induced seismic events with depth is compared to the brittleness index (BI) of the reservoir rock. This index is defined as a direct combination of Poisson's ratio and Young's modulus measured along boreholes. The BI is defined as [Grieser and Bray (2007)]

$$BI = \left[\frac{E - E_{min}}{E_{max} - E_{min}} + \frac{\nu - \nu_{max}}{\nu_{min} - \nu_{max}} \right] * \frac{100}{2}. \tag{6.1}$$

E_{min}, ν_{min}, E_{max} and ν_{max} are minimum and maximum Young's modulus and Poisson's ratio in the analyzed rock section. The positive relation between the BI and the density of the seismic events with depth (see Fig. 6.2) suggests that elastic rock heterogeneity controls brittle rock failure during hydraulic reservoir stimulation. Langenbruch and Shapiro (2014b) demonstrate that the stress change needed to open new and reactivate pre-existing fractures in a reservoir rock is decreasing with increasing BI in the rock. This demonstration is performed for the special case of the Cotton Valley formation and isotropic elastic properties. However, to finally clarify the relation between elastic rock heterogeneity and the occurrence probability of seismic events in general analytic solution have to be developed to quantify stress fluctuations caused by elastic rock heterogeneity. These solutions should also take into account elastic anisotropy and stratification of rocks.

Finally, it is of interest to study the implications of the universality issue of elastic rock heterogeneity in the Earth's crust. Its impact on seismic wave propagation, attenuation and scattering in fractal elastic media could be topics of further research. This is relevant for interpretation of the frequency content of registered seismic waves. Moreover, a detailed investigation of the differences between scaling exponents resulting at critical points, for instance the percolation threshold discussed in chapter 5, and scaling exponents resulting from the universal fractal nature of elastic rock heterogeneity should be performed.

Bibliography

Abercrombie, R. E. and Brune, J. N. (1994). Evidence for a constant b-value above magnitude 0 in the southern San Andreas, San Jacinto and San Miguel fault zones, and at the Long Valley Caldera, California. *Geophysical Research Letters*, 21, doi: 10.1029/94GL01138.

Aki, K. (1967). Scaling law of seismic spectrum. *Journal of Geophysical Research*, 72, doi: 10.1029/JZ072i004p01217.

Aki, K. (1981). A probabilistic synthesis of precursory phenomena, in earthquake prediction: An international review. *Maurice Ewing Series*, 4, doi: 10.1029/ME004p0566.

Amitrano, D. (2003). Brittle-ductile transition and associated seismicity: Experimental and numerical studies and relationship with the b-value. *Journal of Geophysical Research*, 108(B1), doi: 10.1029/2001JB000680.

Amitrano, D., Grasso, J.-R., and Hantz, D. (1999). From diffuse to localised damage through elastic interaction. *Geophysical Review Letters*, 26, doi: 10.1029/1999GL900388.

Amitrano, D., Grasso, J.-R., and Senfaute, G. (2005). Seismic precursory patterns before a cliff collapse and critical point phenomena. *Geophysical Research Letters*, 32, doi: 10.1029/2004GL022270.

Bachmann, C. E., Wiemer, S., Woessner, J., and Hainzl, S. (2011). Statistical analysis of the induced Basel 2006 earthquake sequence: Introducing a probability-based monitoring approach for Enhanced Geothermal Systems. *Geophysical Journal International*, 186, doi: 10.1111/j.1365-246X.2011.05068.x.

Baisch, S., Bohnhoff, M., Ceranna, L., Tu, Y., and Harjes, H.-P. (2002). Probing the crust to 9-km depth: Fluid-injection experiments and induced seismicity at the KTB superdeep drilling hole, Germany. *Bulletin of the Seismological Society of America*, 92, doi: 10.1785/0120010236.

Bak, P., Christensen, K., Danon, L., and Scanlon, T. (2002). Unified scaling law for earthquakes. *Physical Review Letters*, 88, doi: 10.1103/PhysRevLett.88.178501.

Bak, P. and Tang, C. (1989). Earthquakes as a self-organized critical phenomenon. *Journal of Geophysical Research*, 34, doi: 10.1029/JB094iB11p15635.

Barenblatt, G. I. (1996). Scaling, self-similarity, and intermediate asymptotics. *Cambridge University Press, NY*, 99, ISBN-10.

Baria, R., Baumgärtner, J., Gerard, A., Jung, R., and Garnish, J. (1999). European HDR research programme at Soultz-sous-Forêts (France) 1987-1996. *Geothermics*, 28, doi: 10.1016/S0375-6505(99)00036-X.

Barth, A., Wenzel, F., and Langenbruch, C. (2013). Probability of earthquake occurrence and magnitude estimation in the post shut-in phase of geothermal projects. *Journal of Seismology*, 17, doi: 10.1007/s10950-011-9260-9.

Bohnhoff, M. and Zoback, M. (2010). Oscillation of fluid-filled cracks triggered by degassing of co2 due to leakage along wellbores. *Journal of Geophysical Research*, 115, doi: 10.1029/2010JB000848.

Bosl, W. J. and Nur, A. (2002). Aftershocks and pore fluid diffusion following the 1992 Landers earthquake. *Journal of Geophysical Research*, 107,doi: 10.1029/2001JB000155.

Brudy, M., Zoback, M., Fuchs, K., Rummel, F., and Baumgärtner, J. (1997). Estimation of the complete stress tensor to 8 km depth in the KTB scientific drill holes: Implications for crustal strength. *Journal of Geophysical Research*, 10, doi: 10.1029/96JB029422.

Brune, J. N. (1970). Tectonic stress and the spectra of seismic shear waves from earthquakes. *Journal of Geophysical Research*, 75, doi: 10.1029/JB075i026p04997.

Carslaw, H. and Jaeger, J. (1959). Conduction of heat in solids. *Oxford Univ. Press*, pages 255–281.

Catalli, F., Meier, M.-A., and Wiemer, S. (2013). The role of Coulomb stress changes for injection-induced seismicity: The Basel enhanced geothermal system. *Geophysical Research Letters*, 40, doi: 10.1029/2012GL054147.

Corral, A. (2006). Dependence of earthquake recurrence times and independence of magnitudes on seismicity history. *Tectonophysics*, 424, doi: 10.1016/j.tecto.2006.03.035.

Dahlheim, H., Gebrande, H., Schmedes, E., and Soffel, H. (1997). Seismicity and stress field in the vincinity of the KTB location. *Journal of Geophysical Research*, 102, doi: 10.1029/96JB02812.

Day-Lewis, A., Zoback, M., and Hickman, S. (2010). Scale-invariant stress orientations and seismicity rates near the San Andreas Fault. *Geophysical Research Letters*, 37, doi: 10.1029/2010GL045025.

Delèpine, N., Cuenot, N., Rothert, E., Parotidis, M., Rentsch, S., and Shapiro, S. A. (2004). Characterization of fluid transport properties of the Hot Dry Rock reservoir Soultz-2000 using induced microseismicity. *Journal of Geophysics and Engineering*, 1, doi: 10.1088/1742-2132/1/1/010.

Dieterich, J. (1994). A constitutive law for rate of earthquake production and its application to earthquake clustering. *Journal of Geophysical Research*, 99, doi: 10.1029/93JB02581.

Dinske, C., Shapiro, S., and Rutledge, J. (2010). Interpretation of microseismicity resulting from gel and water fracturing of tight gas reservoirs. *Pure and Applied Geophysics*, 167, doi: 10.1007/s00024-009-0003-6.

Dinske, C. and Shapiro, S. A. (2013). Seismotectonic state of reservoirs inferred from magnitude distributions of fluid-induced seismicity. *Journal of Seismology*, 17, doi: 10.1007/s10950-012-9292-9.

Dolan, S., Bean, C., and Riollet, B. (1998). The broad-band fractal nature of heterogeneity in the upper crust from petrophysical logs. *Geophysical Journal International*, 132, doi: 10.1046/j.1365-246X.1998.00410.x.

Dyer, B. C. (2001). Soultz GPK2 stimulation June/July 2000. *Seismic monitoring report, Semore Seismic Report*.

Eshelby, J. (1957). The determination of the elastic field of an ellipsoidal inclusion, and related problems. *Proceedings of the Royal Society of London*, A 241 (1226), pp. 376-396.

Eshelby, J. (1959). The elastic field outside an ellipsoidal inclusion. *Proceedings of the Royal Society of London*, A 252 (1271), 561-569.

Evans, K. F., Cornet, F. H., Hashida, T., Hayashi, K., Ito, T., Matsuki, K., and Wallroth, T. (1999). Stress and rock mechanics issues of relevance to HDR/HWR engineered geothermal systems: Review of developments during the past 15 years. *Geothermics*, 28, pp. 455-474.

Fehler, M. C. (1989). Stress control of seismicity patterns observed during hydraulic fracturing experiments at the Fenton Hill hot dry rock geothermal energy site, New Mexico. *International Journal of Rock Mechanics and Mining Science*, 26, doi: 10.1016/0148-9062(89)91971-2.

Frohlich, C. and Davis, S. D. (1993). Teleseismic b values; or, much ado about 1.0. *Journal of Geophysical Research*, 98, doi: 10.1029/92JB01891.

Gavrilenko, P. (2005). Hydromechanical coupling in response to earthquakes: On the possible consequences for aftershocks. *Geophysical Journal International*, 161, doi: 10.1111/j.1365-246X.2005.02538.x.

Gibowicz, S. J. and Kijko, A. (1994). An introduction to mining seismology. *Academic Press San Diego*.

Girard, L., Weiss, J., and Amitrano, D. (2012). Damage-cluster distributions and size effect on strength in compressive failure. *Physical Review Letters*, 26, doi: 10.1029/1999GL900388.

Goebel, T. H., Schorlemmer, D., Becker, T. W., Dresen, G., and Sammis, C. G. (2013). Acoustic emissions document stress changes over many seismic cycles in stick-slip experiments. *Geophysical Research Letters*, 40, doi: 10.1002/grl.50507.

Goertz-Allmann, B. P., Goertz, A., and Wiemer, S. (2011). Stress drop variations of induced earthquakes at the Basel geothermal site. *Geophysical Research Letters*, 38, doi: 10.1029/2011GL047498.

Goff, J. and Holliger, K. (1999). Nature and origin of upper crustal seismic velocity fluctuations and associated scaling properties - combined stochastic analyses of KTB velocity and lithology form, chance, and dimensions. *W. H. Freeman and Company*, 104.

Gomberg, J. and Johnson, P. (2005). Seismology: Dynamic triggering of earthquakes. *Nature*, 437, doi: 10.1038/437830a.

Grieser, B. and Bray, J. (2007). Identification of production potential in unconventional reservoirs. *SPE Production and Operations Symposium*, page SPE 106623.

Gutenberg, B. and Richter, C. F. (1954). Seismicity of earth and associated phenomenon, 2nd ed. *Princton Univ. Press, Princton, N. J.*

Hainzl, S., Kraft, T., Wassermann, J., Igel, H., and Schmedes, E. (2006). Evidence for rainfall-triggered earthquake activity. *Geophysical Research Letters*, 33, doi: 10.1029/2006GL027642.

Häring, M. O., Schanz, U., Ladner, F., and Dyer, B. C. (2008). Characterisation of the Basel-1 enhanced geothermal system. *Geothermics*, 37, doi: 10.1016/j.geothermics.2008.06.002.

Helmstetter, A. and Sornette, D. (2002). Diffusion of epicenters of earthquake aftershocks, Omori's law, and generalized continuous-time random walk models. *Physical Review Edition*, 66, doi: 10.1103/PhysRevE.66.061104.

Hickman, S. and Zoback, M. (2004). Stress orientations and magnitudes in the SAFOD pilot hole. *Geophysical Review Letters*, 31, doi: 10.1029/2004GL020043.

Hickman, S., Zoback, M., Ellsworth, W., Boness, N., Malin, P., Roecker, S., and Thurber, C. (2007). Structure and properties of the San Andreas Fault in central California: Recent results from the SAFOD experiment. *Scientific Drilling*, doi: 10.2204/iodp.sd.s01.39.2007.

Hirata, T. (1987). Omori's Power Law aftershock sequences of microfracturing in rock fracture experiment. *Journal of Geophysical Research*, 92, doi: 10.1029/JB092iB07p06215.

Horton, S. (2012). Disposal of hydrofracking waste fluid by injection into subsurface aquifers triggers earthquake swarm in central Arkansas with potential for damaging earthquake. *Seismological Research Letters*, 83, doi: 10.1785/gssrl.83.2.250.

House, L. (1987). Locating microearthquakes induced by hydraulic fracturing in crystalline rock. *Geophysical Research Letters*, 14, doi: 10.1029/GL014i009p00919(9).

Huang, J. and Turcotte, D. (1988). Fractal distributions of stress and strength and variations of b-value. *Earth and Planetary Science Letters*, 91, doi: 10.1016/0012-821X(88)90164-1.

Hudson, J. A., Cornet, F. H., and Christiansson, R. (2003). ISRM suggested methods for rock stress estimation — Part 1: Strategy for rock stress estimation. *International Journal of Rock Mechanics and Mining Science*, 40, doi: 10.1016/j.ijrmms.2003.07.011.

Huenges, E., Erzinger, J., Kück, J., Engeser, B., and Kessels, W. (1997). The permeable crust: Geohydraulic properties down to 9101 m depth. *Journal of Geophysical Research*, 102, doi: 10.1029/96JB03442.

Hummel, N. and Müller, T. M. (2009). Microseismic signatures of non-linear pore-fluid pressure diffusion. *Geophysical Journal International*, 179, doi: 10.1111/j.1365-246X.2009.04373.x.

Hummel, N. and Shapiro, S. A. (2012). Microseismic estimates of hydraulic diffusivity in case of non-linear fluid-rock interaction. *Geophysical Journal International*, 188, doi: 10.1111/j.1365-246X.2011.05346.x.

Isichenko, M. (1992). Percolation, statistical topography, and transport in random media. *Reviews of Modern Physics*, 64, doi: 10.1103/RevModPhys.64.961.

Ito, T. and Zoback, M. (2000). Fracture permeability and in situ stress to 7 km depth in the KTB scientific drillhole. *Geophysical Research Letters*, 27, doi: 10.1029/1999GL011068.

Jaeger, J., Cook, N., and Zimmerman, R. (2007). Fundamentals of rock mechanics 4th edition. *Blackwell Publishing*.

Kagan, Y. Y. (1999). Universality of the seismic moment-frequency relation. *Pure Appl. Geophys.*, 155, doi: 10.1007/978-3-0348-8677-2_16.

Kanamori, H. (1977). The energy release in great earthquakes. *Journal of Geophysical Research*, 82, pp. 2981-2987.

Kanamori, H. and Anderson, D. (1975). Theoretical basis of some empirical relations in seismology. *Bulletin of the Seismological Society of America*, 65, 1073-1095.

Kilb, D., Gomberg, J., and Bodin, P. (2002). Aftershock triggering by complete coulomb stress changes. *Journal of Geophysical Research*, 107, doi: 10.1029/2001JB000202.

King, G. C. P., Stein, R. S., and Lin, J. (1994). Static stress changes and the triggering of earthquakes. *Bulletin of the Seismological Society of America*, 84, http://www.bssaonline.org/content/84/3/935.full.pdf+html.

Langenbruch, C., Dinske, C., and Shapiro, S. (2011). Inter event times of fluid induced earthquakes suggest their Poisson nature. *Geophysical Research Letters*, 38, doi: 10.1029/2011GL049474.

Langenbruch, C. and Shapiro, S. (2010). Decay rate of fluid-induced seismicity after termination of reservoir stimulations. *Geophysics*, 75, doi: 10.1190/1.3506005(6).

Langenbruch, C. and Shapiro, S. (2014a). Gutenberg-Richter relation originates from Coulomb stress fluctuations caused by elastic rock heterogeneity. *Journal of Geophysical Research: Solid Earth*, doi: 10.1002/2013JB010282.

Langenbruch, C. and Shapiro, S. A. (2014b). Elastic rock heterogeneity controls brittle rock failure during hydraulic reservoir stimulation. *76nd EAGE Conference & Exhibition, Extended abstract*, doi: 10.3997/2214-4609.20141079.

Leary, P. C. (1997). Rock as a critical-point system and the inherent implausibility of reliable earthquake prediction. *Geophysical Journal International*, 131, doi: 10.1111/j.1365-246X.1997.tb06589.x.

Lindman, M., Lund, B., Roberts, R., and Jonsdottir, K. (2006). Physics of the Omori law: Inferences from interevent time distributions and pore pressure diffusion modeling. *Tectonophysics*, 424, doi: 10.1016/j.tecto.2006.03.045.

Lockner, D. (1993). The role of acoustic emission in the study of rock fracture. *International Journal of Rock Mechanics and Mining Sciences & Geomechanics Abstracts*, 30, http://dx.doi.org/10.1016/0148-9062(93)90041-B.

Lockner, D. and Byerlee, J. (1977). Acoustic emission and creep in rock at high confining pressure and differential stress. *Bulletin of the Seismological Society of America*, 67, pp. 247-258.

Lorenz, D. and Ziff, R. (1998). Universality of the excess number of clusters and the crossing probability function in three-dimensional percolation. *Journal of Physics A: Mathematical and General*, 31, doi: 10.1088/0305-4470/31/40/009.

Main, I. (1996). Statistical physics, seismogenesis, and seismic hazard. *Reviews of Geophysics*, 34, doi: 10.1029/96RG02808.

Majer, E. L., Baria, R., Stark, M., Oates, S., Bommer, J., Smith, B., and Asanuma, H. (2007). Induced seismicity associated with enhanced geothermal systems. *Geothermics*, 489, doi: http://dx.doi.org/10.1016/j.geothermics.2007.03.003,.

Mandelbrot, B. B. (1977). The fractal geometry of nature. *San Francisco: WH Freeman*.

Mayr, S., Stanchits, S., Langenbruch, C., Dresen, G., and Shapiro, S. (2011). Acoustic emission induced by pore-pressure changes in sandstone samples. *Geophysics*, 76, doi: 10.1190/1.3569579.

Miller, A. D., Foulger, G. R., and Julian, B. R. (1998). Non-double-couple earthquakes 2. observations. *Reviews of Geophysics*, 36, doi: 10.1029/98RG00717.

Mogi, K. (1962). Magnitude-frequency relation for elastic shocks accompanying fractures of various materials and some related problems in earthquakes (2nd paper). *Bulletin of the Earthquake Research Institute*, 40.

Mukuhira, Y., Asanuma, H., Niitsuma, H., and Häring, M. O. (2013). Characteristics of large-magnitude microseismic events recorded during and after stimulation of a geothermal reservoir at Basel, Switzerland. *Pure and Applied Geophysics*, 45, doi: 10.1016/j.geothermics.2012.07.005.

Narteau, C., Byrdina, S., Shebalin, P., and Schorlemmer, D. (2009). Common dependence on stress for the two fundamental laws of statistical seismology. *Nature*, 462, doi: 10.1038/nature08553.

Nur, A. and Booker, J. R. (1972). Aftershocks caused by pore fluid flow? *Science*, 175, (4024), 885-887.

Ogata, Y. (1998). Space-time point-process models for earthquake occurrences. *Annals of the Institute of Statistical Mathematics*, 50, doi: 10.1023/A:1003403601725.

Ojala, I. O., Main, I. G., and Ngwenya, B. T. (2004). Strain rate and temperature dependence of Omori law scaling constants of AE data: Implications for earthquake foreshock-aftershock sequences. *Geophysical Research Letters*, 31, doi: 10.1029/2004GL020781.

Omori, F. (1894). On the aftershocks of earthquakes. *Journal of Colloid Science*.

Pacheco, J., Scholz, C., and Sykes, L. (1992). Changes in frequency-–size relationship from small to large earthquakes. *Nature*, 355, doi: 10.1038/355071a0.

Parotidis, M., Rothert, E., and Shapiro, S. A. (2003). Pore-pressure diffusion: A possible triggering mechanism for the earthquake swarms 2000 in Vogtland/NW-Bohemia, central Europe. *Geophysical Research Letters*, 30, doi: 10.1029/2003GL018110.

Parotidis, M. and Shapiro, S. A. (2004). A statistical model for the seismicity rate of fluid-injection-induced earthquakes. *Geophysical Research Letters*, 31, doi: 10.1029/2004GL020421.

Parotidis, M., Shapiro, S. A., and Rothert, E. (2004). Back front of seismicity induced after termination of borehole fluid injection. *Geophysical Research Letters*, 31, doi: 10.1029/2003GL018987.

Pearson, C. (1981). Pore pressure diffusion and the mechanism of reservoir-induced seismicity. *Journal of Geophysical Research*, 86, doi: 10.1029/JB086iB09p07855.

Pearson, C. (1982). Parameters and a magnitude moment relationship from small earthquakes observed during hydraulic fracturing experiments in crystalline rocks. *Geophysical Research Letters*, 9, doi: 10.1029/GL009i004p00404.

Pechnig, R., Haverkamp, S., Wohlenberg, J., Zimmermann, G., and Burkhardt, H. (1997). Integrated log interpretation in the German Continental Deep Drilling Program: Lithology, porosity, and fracture zones. *Journal of Geophysical Research*, 102, doi: 10.1029/96JB03802.

Rivera, L. and Kanamori, H. (2002). Spatial heterogeneity of tectonic stress and friction in the crust. *Geophysical Review Letters*, 29, doi: 10.1029/2001GL013803.

Rothert, E. and Shapiro, S. A. (2003). Microseismic monitoring of borehole fluid injections: Data modeling and inversion for hydraulic properties of rocks. *Geophysics*, 68, doi: 10.1190/1.1567239.

Rothert, E. and Shapiro, S. A. (2007). Statistics of fracture strength and fluid-induced microseismicity. *Journal of Geophysical Research*, 112, doi: 10.1029/2005JB003959.

Rundle, J. B. (1989). Derivation of the complete Gutenberg-Richter magnitude-frequency relation using the principle of scale invariance. *Journal of Geophysical Research*, 94, doi: 10.1029/JB094iB09p12337.

Rutledge, J. T. and Phillips, W. S. (2003). Hydraulic stimulation of natural fractures as revealed by induced microearthquakes, Carthage Cotton Valley gas field, East Texas. *Geophysics*, 68, doi: 10.1190/1.1567214.

Schoenball, M., Baujard, C., Kohl, T., and Dorbath, L. (2012). The role of triggering by static stress transfer during geothermal reservoir stimulation. *Journal of Geophysical Research*, 117, doi: 10.1029/2012JB009304.

Scholz, C. (1962). The frequency-magnitude relation of microfracturing in rock and its relation to earthquakes. *Bulletin of the Seismological Society of America*, 58, 399-415.

Scholz, C. H. (2002). The mechanics of earthquakes and faulting,2nd Edn. *Cambridge University Press, Cambridge*.

Schorlemmer, D., Wiemer, S., and Wyss, M. (2005). Variations in earthquake-size distribution across different stress regimes. *Nature*, 437, doi: 10.1038/nature04094.

Sellers, E. J., Kataka, M. O., and Linzer, L. M. (2003). Source parameters of acoustic emission events and scaling with mining-induced seismicity. *Journal of Geophysical Research*, 108, doi: 10.1029/2001JB000670.

Shapiro, S., Krueger, O., Dinske, C., and Langenbruch, C. (2011). Magnitudes of induced earthquakes and geometric scales of fluid-stimulated rock volumes. *Geophysics*, 76, doi: 10.1190/geo2010-0349.1.

Shapiro, S. A. and Dinske, C. (2009). Scaling of seismicity induced by nonlinear fluid-rock interaction. *Journal of Geophysical Research*, 114, doi: 10.1029/2008JB006145.

Shapiro, S. A., Dinske, C., and Kummerow, J. (2007). Probability of a given-magnitude earthquake induced by a fluid injection. *Geophysical Research Letters*, 34, doi: 10.1029/2007GL031615.

Shapiro, S. A., Dinske, C., Langenbruch, C., and Wenzel, F. (2010). Seismogenic index and magnitude probability of earthquakes induced during reservoir fluid stimulations. *The Leading Edge*, 29, doi: 10.1190/1.3353727.

Shapiro, S. A., Huenges, E., and Borm, G. (1997). Estimating the crust permability from fluid-injection-induced seismic emission at the KTB site. *Geophysical Journal International*, 13, doi: 10.1111/j.1365-246X.1997.tb01215.x1.

Shapiro, S. A., Krüger, O. S., and Dinske, C. (2013). Probability of inducing given-magnitude earthquakes by perturbing finite volumes of rocks. *Journal of Geophysical Research*, 118, doi: 10.1002/jgrb.50264.

Shapiro, S. A., Patzig, R., Rothert, E., and Rindschwenter, J. (2003). Triggering of microseismicity due to pore-pressure pertubation: Permeability related signatures of the phenomenon. *Pure and Applied Geophysics*, 160, doi: 10.1007/978-3-0348-8083-1-16.

Shapiro, S. A., Rothert, E., Rath, V., and Rindschwentner, J. (2002). Characterization of fluid transport properties of reservoirs using induced microseismicity. *Geophysics*, 67, doi: 10.1190/1.1451597.

Shcherbakov, R., Yacolev, G., Turcotte, D. L., and Rundle, J. B. (2005). Model for distribution of aftershocks interoccurence times. *Physical Review Letters*, 95, doi: 10.1103/PhysRevLett.95.218501.

Talwani, P. (1997). On the nature of reservoir-induced seismicity. *Pure and Applied Geophysics*, 150, 473-492.

Talwani, P. and Acree, S. (1984). Pore pressure diffusion and the mechanism of reservoir-induced seismicity. *Pure and Applied Geophysics*, http://dx.doi.org/10.1007/BF00876395.

Toda, S., Stein, R. S., Reasenberg, P. A., Dieterich, J. H., and Yoshida, A. (1998). Stress transferred by the 1995 m_w = 6.9 Kobe, Japan, shock: Effect on aftershocks and future earthquake probabilities. *Journal of Geophysical Research*, 103, doi: 10.1029/98JB00765.

Toda, S., Stein, R. S., and Sagiya, T. (2002). Evidence from the ad 2000 Izu islands earthquake swarm that stressing rate governs seismicity. *Nature*, 419, doi: 10.1038/nature00997.

Touati, S., Naylor, M., Main, I. G., and Christie, M. (2011). Masking of earthquake triggering behavior by a high background rate and implications for Epidemic-Type Aftershock Sequence inversions. *Journal of Geophysical Research*, 116, doi: 10.1029/2010JB007544.

Turcotte, D. L. (1997). Fractals and chaos in geology and geophysics. *Cambridge university press*.

Utsu, T., Ogata, Y., and Matsu'ura, R. S. (1995). The centenary of Omori formula for decay law of aftershock activity. *Journal of Physics of the Earth*, 43, 1-33.

Vidale, J. E., Agnew, D. C., Johnston, M. J. S., and Oppenheimer, D. H. (1998). Absence of earthquake correlation with earth tides: An indication of high preseismic fault stress rate. *Journal of Geophysical Research*, 113, doi: 10.1029/98JB00594.

Zaliapin, I., Gabrielov, A., Keilis-Borok, V., and Wong, H. (2008). Clustering analysis of seismicity and aftershock identification. *Physical Review Letters*, 101, doi: 10.1103/PhysRevLett.101.018501.

Zhao, P., Kühn, D., Oye, V., and Cesca, S. (2014). Evidence for tensile faulting deduced from full waveform moment tensor inversion during the stimulation of the Basel enhanced geothermal system. *Geothermics*, http://dx.doi.org/10.1016/j.geothermics.2014.01.003.

Zoback, M. and Harjes, H. P. (1997). Injection-induced earthquakes and crustal stress at 9 km depth at the KTB deep drill site, Germany. *Journal of Geophysical Research*, 102, doi: 10.1029/96JB02814.

Zoback, M. D. (2010). Reservoir geomechanics. *Cambridge University Press*.

Zoback, M. D. and Gorelick, S. M. (2012). Earthquake triggering and large-scale geologic storage of carbon dioxide. *PNAS*, 109, doi: 10.1073/pnas.1202473109.

List of publications

Journal publications:

Langenbruch, C. and Shapiro S. A. (2014), *Gutenberg-Richter relation originates from Coulomb stress fluctuations caused by elastic rock heterogeneity*. **Journal of Geophysical Research: Solid Earth**, 119, doi:10.1002/2013JB010282.

Barth, A., Wenzel, F. and **Langenbruch, C.** (2013), *Probability of earthquake occurrence and magnitude estimation in the post shut-in phase of geothermal projects*. **Journal of Seismology**, 17, doi: 10.1007/s10950-011-9260-9.

Langenbruch, C., Dinske, C. and Shapiro, S. A. (2011), *Inter event times of fluid induced earthquakes suggest their Poisson nature*. **Geophysical Research Letters**, 38, doi: 10.1029/2011GL049474.

Mayr, S., Stanchits, S., **Langenbruch, C.**, Dresen, G. and Shapiro, S. A. (2011), *Acoustic emission induced by pore-pressure changes in sandstone samples*. **Geophysics**, 76, doi: 10.1190/1.3569579.

Shapiro, S. A., Krüger, O. S., Dinske, C. and **Langenbruch, C.** (2011), *Magnitudes of induced earthquakes and geometric scales of fluid-stimulated rock volumes*. **Geophysics**, 76, doi: 10.1190/geo2010-0349.1.

Haney, F., Kummerow, J., **Langenbruch, C.**, Dinske, C., Shapiro, S. A. and Scherbaum, F. (2011), *Magnitude estimation for microseismicity induced during the KTB 2004/2005 injection experiment*. **Geophysics**, 76, doi: 10.1190/geo2011-0020.1.

Shapiro, S. A., Dinske, C., **Langenbruch, C.** and Wenzel, F. (2010), *Seismogenic index and magnitude probability of earthquakes induced during reservoir fluid stimulations*, **The Leading Edge**; March 2010; v. 29; no. 3; p. 304-309; doi: 10.1190/1.3353727.

Langenbruch, C. and Shapiro, S. A. (2010), *Decay Rate of Fluid Induced Seismicity after Termination of Reservoir Stimulations.* **Geophysics**, 75, doi: 10.1190/1.3506005.

Extended abstracts:

Langenbruch, C. and Shapiro, S. A. (2014), *Elastic Rock Heterogeneity Controls Brittle Rock Failure during Hydraulic Reservoir Stimulation*. Extended abstract, 76nd EAGE Conference & Exhibition.

Langenbruch, C. and Shapiro, S. A. (2013), *Relation between Elastic Heterogeneity, Stress and the Gutenberg Richter b-value: A b-value Estimation using Sonic Logs*. 4th EAGE Passive Seismic Workshop.

Galindo Guerreros, J. C., Dinske, C., **Langenbruch, C.** and Shapiro, S. A. (2013), *Numerical Simulations of Fluid Induced Seismicity in Hydraulically Heterogeneous Media.* 75th EAGE Conference & Exhibition incorporating SPE EUROPEC 2013, doi: 10.3997/2214-4609.20131125.

Dinske, C., **Langenbruch, C.**, Galindo Guerreros, J. C. and Shapiro, S. A. (2013), *Influence of Hydraulic Heterogeneity of Rocks on Pore Pressure Changes Induced by Reservoir Stimulations.* 75th EAGE Conference & Exhibition incorporating SPE EUROPEC 2013, doi: 10.3997/2214-4609.20130174.

Langenbruch, C. and Shapiro, S. A. (2012), *Modelling of Fracture Strength Distribution in Elastically Heterogeneous Rocks*. Extended abstract, 74nd EAGE Conference & Exhibition.

Langenbruch, C. and Shapiro, S. A. (2012), *Influence of elastic heterogeneity on fracture strength distribution in rocks*. SEG Technical Program Expanded Abstracts 2012. Society of Exploration Geophysicists, 2012, doi: 10.1190/segam2012-0179.1.

Langenbruch, C. and Shapiro, S. A. (2011), *Geomechanical Interpretation of Pore Pressures Triggering Microseismicity.* Extended abstract, 73nd EAGE Conference & Exhibition.

Langenbruch, C., Dinske, C. and Shapiro, S. A. (2011), *Inter Event Times of Fluid Induced Earthquakes*. Extended abstract, Third EAGE Passive Seismic Workshop - Actively Passive!

Shapiro, S. A., Krüger, O. S., **Langenbruch, C.** and Dinske, C. (2011) *Geometric control of earthquake magnitudes by fluid injections in rocks*. SEG Technical Program Expanded Abstracts 2011: pp. 1539-1543. doi: 10.1190/1.3627496

Shapiro, S. A., Dinske, C. and **Langenbruch, C.** (2011), *Quantification of fluid-induced microseismic activity using seismogenic index*. Extended abstract, Third EAGE Passive Seismic Workshop - Actively Passive!

Langenbruch, C. and Shapiro, S. A. (2010), *Inter Event Times of Fluid Induced Seismicity*. Extended abstract, 72nd EAGE Conference & Exhibition.

Langenbruch, C. and Shapiro, S. A. (2009), *Induced seismicity after termination of rock stimulations: Possibilities for reservoir characterization*. SEG Expanded Abstracts 28, 1855 (2009); doi:10.1190/1.3255216.

Langenbruch, C. and Shapiro, S. A. (2009), *Omori Law for Fluid Induced Microseismicity and Its Dependency on Parameters of Reservoir and Source*. Extended abstract, 71st EAGE Conference & Exhibition.

Langenbruch, C. and Shapiro, S. A. (2008), *How Long Should We Observe Microseismicity after Finishing a Borehole Fluid Stimulation?* Extended abstract, 70th EAGE Conference & Exhibition.

Abtracts:

Langenbruch, C. and Shapiro, S. A. (2013), *Gutenberg-Richter relation originates from stress fluctuations caused by elastic rock heterogeneity*. Geiser Final Conference, abstracts.

Langenbruch, C. and Shapiro, S. A. (2013), *Relations between elastic rock heterogeneity, stress and the Gutenberg Richter law*. Rock Stress Symposium, Sendai

Langenbruch, C. and Shapiro, S. A. (2012), *Relation between the fractal distribution of elastic parameters in the earth crust and the Gutenberg-Richter b-value of earthquakes: A method to estimate b-values from sonic well logs*. AGU Fall Meeting 2012, abstracts

Langenbruch, C. and Shapiro, S. A. (2012), *Modelling of Fracture Strength in Elastically Heterogeneous Rocks*. ESC 33rd General Assembly, abstract.

Langenbruch, C. and Shapiro, S. A. (2012), *Geomechanical interpretation of pore pressures triggering seismicity*. Jahrestagung der Deutschen Geophysikalischen Gesellschaft.

Langenbruch, C. and Shapiro, S. A. (2011), *Geomechanical Interpretation of Pore Pressures Triggering Microseismicity*. AGU Fall Meeting 2011, Abstracts

Langenbruch, C. and Shapiro, S. A. (2011), *Inter Event Times of Fluid Induced Earthquakes*. 71. Jahrestagung der Deutschen Geophysikalischen Gesellschaft, abstract.

Langenbruch, C. and Shapiro, S. A. (2010), *Induced seismicity after borehole fluid injections*. Geophysical Research Abstracts, Vol. 12, EGU2010-13309, EGU General Assembly 2010

Langenbruch, C. and Shapiro, S. A. (2010), *Inter Event Times of Fluid Induced Seismicity*. ESC 32nd General Assembly, abstract.

Langenbruch, C. and Shapiro, S. A. (2009), *Omori Law for Fluid Induced Microseismicity and its Dependency on Parameters of Reservoir and Source*. 69. Jahrestagung der Deutschen Geophysikalischen Gesellschaft, abstract.

Langenbruch, C. and Shapiro, S. A. (2008), *Seismicity Rate and Omori Law of Fluid Induced Microseismicity*. 68. Jahrestagung der Deutschen Geophysikalischen Gesellschaft, abstract.

Langenbruch, C. and Shapiro, S. A. (2008), *How Long Should We Observe Microseismicity After Finishing a Borehole Fluid Stimulation?* ESC 31st General Assembly, abstract.

Acknowledgments - Danksagung

An erster Stelle gilt mein Dank Prof. Dr. Serge A. Shapiro, der durch seine großartige Betreuung maßgeblich zum Erfolg dieser Arbeit beigetragen hat. Seine breite wissenschaftliche Expertise, stetige Bereitschaft zur Diskussion, ausnahmslose Unterstützung und sein Ideenreichtum haben mich immer inspiriert und mir den Weg in die internationale wissenschaftliche Welt aufgezeigt.

Ich bedanke mich bei Prof. Dr. Frederik Tilmann für die Übernahme des Korreferats. Auch danke ich den weiteren Mitgliedern der Promotionskommission, Prof. Dr. Timm John, Dr. Carsten Dinske und Prof. Dr. Marco Bohnhoff als deren Vorsitzender.

Vielen Dank an alle Kolleginnen und Kollegen der Fachrichtung Geophysik, die ein sehr angenehmes Arbeitsklima geschaffen haben. Béatrice Cailleau danke ich für die Einführung in Abaqus. Ich danke Dr. Jörn Kummerow, Dr. Anton Reshetnikov, Dr. Nicolas Hummel, Antonia Oelke und Karsten Stürmer mit denen ich zahlreiche angenehme Dienstreisen erlebt habe. Ein persönlicher Dank geht hier an Dr. Carsten Dinske der mein Leben nicht nur beruflich sondern auch privat bereichert hat. Ich danke allen Menschen die mich in den zurückliegenden Jahren begleitet und diese zu einer wunderbaren Zeit gemacht haben.

Ganz herzlich bedanke ich mich bei meiner ganzen Familie die mich immer bei allen meinen Vorhaben unterstützt hat. Ein ganz besonderer Dank gilt meinen Eltern Dr. Paul-Friedrich und Adelheid Langenbruch.

Abschließend danke ich Tanja, die mich immer daran erinnert, dass es ein sehr interessantes und schönes Leben abseits der Geophysik gibt.